Aachener Verfahrenstechnik Series
AVT.CVT – Chemical Process Engineering
Volume 54 (2025)

Jonas Frederik Bäßler

Selective Methanol Oxidation for Paired Electrolysis

Selective Methanol Oxidation for Paired Electrolysis

Selektive Methanoloxidation für die gepaarte Elektrolyse

Von der Fakultät für Maschinenwesen
der Rheinisch-Westfälischen Technischen Hochschule Aachen
zur Erlangung des akademischen Grades
eines Doktors der Ingenieurwissenschaften
genehmigte Dissertation

vorgelegt von

Jonas Frederik Bäßler

Berichter:
Univ.-Prof. Dr.-Ing. Matthias Wessling
Prof. Carlos Ponce De Leon Albarran, PhD

Tag der mündlichen Prüfung: 21.05.2025

Diese Dissertation ist auf den Internetseiten der Universitätsbibliothek online verfügbar.

Parts of this dissertation have been published. Reproduced with permission from:

Jonas Baessler, Tamara Oliveira, Robert Keller, and Matthias Wessling
Paired electrosynthesis of formic acid from CO_2 and formaldehyde from methanol
ACS Sustainable Chemistry & Engineering, 2023
DOI: 10.1021/acssuschemeng.2c07523

Jonas Baessler, Niklas Vollmert, Jan Vehrenberg, Miriam Mineur, Sophia Schenke, Lukas Griesberg, Paulina Montero Pineda, and Robert Keller
Reaction engineering for high yield electrosynthesis:
Unraveling the impact of reaction conditions and conversion on methanol oxidation to formate
Chemical Engineering Journal, 2024
DOI: 10.1016/j.cej.2024.153000

Jonas Baessler, Malte Wehner, Mojtaba Mohseni, Julian Neumann, Matthias Wessling, and Robert Keller
Feed and bleed operating mode for electrochemical flow cells:
Challenges, solutions and practical insights
ChemElectroChem, 2025
DOI: 10.1002/celc.202500034

Titel: Selective Methanol Oxidation for Paired Electrolysis

Selektive Methanoloxidation für die gepaarte Elektrolyse

Autor: Jonas Frederik Bäßler

Reihe: Aachener Verfahrenstechnik Series
AVT.CVT - Chemical Process Engineering
Volume: 54 (2025)

Herausgeber: Aachener Verfahrenstechnik
Forckenbeckstraße 51
52074 Aachen
Tel.: +49 (0)241 8095470
Fax.: +49 (0)241 8092252
E-Mail: secretary.cvt@avt.rwth-aachen.de
http://www.avt.rwth-aachen.de/AVT

Volltext verfügbar: 10.18154/RWTH-2025-04916

Danksagung

Während meiner Promotion am Lehrstuhl für Chemische Verfahrenstechnik habe ich fachlich und persönlich viel gelernt - und eine Menge Spaß gehabt. Mein herzlicher Dank gilt allen, die mich über die Jahre hinweg immer wieder unterstützend begleitet haben und deren Beiträge meine Arbeit und Promotionszeit geprägt und sehr bereichert haben.

Zunächst möchte ich meinem Doktorvater, Prof. Matthias Wessling, für seine stetige Unterstützung und die wissenschaftliche Betreuung meiner Arbeit danken. Vielen Dank für deinen Input, deine Beratung und die Möglichkeit, vielen spannenden Fragen und verschiedenen Aufgaben nachzugehen. I would also like to express my sincere gratitude to Prof. Carlos Ponce De Leon Albarran for being the second examiner of my dissertation and for his valuable feedback on my thesis. Weiterhin möchte ich Prof. Niklas von der Aßen für die Übernahme des Prüfungsvorsitzes im Rahmen meines Promotionsverfahrens danken.

Mein herzlicher Dank gilt Robert Keller für den hilfreichen fachlichen Austausch und seine kontinuierliche Unterstützung über meine gesamte Promotionszeit hinweg, zuerst im Covestro-Projekt und anschließend als Gruppenleiter. Weiterhin möchte ich dem Projektteam bei Covestro für die gute Zusammenarbeit in unserem bilateralen Projekt zu Beginn meiner Promotion danken. Der gemeinsame Austausch und die Einblicke in die industrielle Perspektive auf elektrochemische Prozesse haben meine Promotion bereichert.

Meine Kolleginnen und Kollegen haben meine Promotionszeit maßgeblich geprägt - nicht nur durch gelungene und spannende Zusammenarbeit, sondern auch durch ihren Teamgeist und die vielen gemeinsamen Erlebnisse. Ob bei der Summer- oder Winterschool, in der Mensa oder im Forckenbeck, bei diversen Feiern, bei kurzen oder ausgedehnten Kaffeepausen, Spaziergängen oder beim gemütlichen Borreln am Freitag - diese Momente mit euch bleiben mir in sehr schöner Erinnerung. Ich möchte besonders meinen wunderbaren Bürokollegen danken, die mich über viele Jahre begleitet und unterstützt haben: Kristina Baitalow, Jan Vehrenberg, Matthias Hesselmann und später auch Stephan Zimmer, Maria Padligur und Mojtaba Mohseni. Vielen Dank für die schöne Zeit im Büro und außerhalb, es hat wirklich viel Spaß mit euch gemacht. Über die Zeit konnte ich mit vielen tollen Menschen zusammenarbeiten, bei Papern, Projekten und gemeinsamen Studiarbeiten - Jan Vehrenberg, Matthias Hesselmann, Maren Großeheide, Niklas Vollmert, Miriam Mineur, Mojtaba Mohseni, Maria Padligur,

Jannik Mehlis, Malte Wehner, Wibke Zängler und Julian Neumann. Vielen Dank für die schöne Zusammenarbeit, ich habe sehr gerne mit euch gearbeitet und Einiges von und mit euch lernen können. Liebe Muco-Gruppe, vielen Dank für die guten, witzigen und hilfreichen Treffen, eure Ratschläge und Erfahrungen haben mir sehr weitergeholfen. Liebes FXC-Team - Maria Padligur, Christian Linnartz, Nicolas Mulandi, Igor Samoylenko, Markus Wessling und Miriam Mineur. Ich bin froh, dass wir die Gründung gemeinsam angegangen sind. Ihr seid ein großartiges Team und ich freue mich darauf, nach der Promotion weiter mit euch zu arbeiten. Vielen Dank, Susanne Offermann, für deinen Einsatz für das Institut und deine Unterstützung rund um meine Promotion. Danke Karin Faensen, Heike Zander und Caroline Schmitz für eure Hilfe bei Laborfragen, bei Messungen und beim 3D-Druck. Weiterhin ein herzliches Dankeschön an die mechanische Werkstatt und das ZAL für eure Beratung und die tatkräftige Unterstützung, sowie an die Buchhaltung und IT für euren engagierten Einsatz.

Neben den Kolleginnen und Kollegen möchte ich auch all den Studierenden danken, die mit mir zusammengearbeitet und geforscht haben: Szymon Herdzik, Miriam Mineur, Hexin Zhu, Florian Schwarz, Tamara Oliveira, Niklas Vollmert, Markus Wessling, Jannik Mehlis, Alexander Kohushölter, Florian Frick, Paulina Montero, Lukas Griesberg, Sophia Schenke und Nicolas Mulandi. Ich bin sehr dankbar für eure tolle Arbeit, ohne euch wäre vieles so nicht möglich gewesen und meine Promotion hätte auch nicht so viel Spaß gemacht.

Außerhalb meines Arbeitsumfeldes möchte ich meinen Freunden danken, insbesondere der wunderbaren Grill-&Chill-Gruppe, die mich nicht nur durch das Studium, sondern auch durch die gesamte Promotion begleitet hat.

Einen ganz besonderen Dank an meine Eltern für eure jahrelange Unterstützung, Beratung und euren Einsatz. Man kann sich immer auf euch verlassen und ihr habt einen großen Beitrag daran, dass ich mich für wissenschaftliche und technische Fragenstellungen begeistern kann. Chrissy, ich danke dir sehr für deine Unterstützung und deine Ratschläge über meine ganze Promotionszeit hinweg. Ohne dich hätte das Studium und auch die Promotionszeit nicht halb so viel Spaß gemacht. Ich bin froh, dass wir das alles zusammen machen. Und zuletzt, ein besonderer Dank an meinen Sohn Felix, du hast mich erfolgreich abgelenkt, aber mich auch gut motiviert, fertig zu werden, damit ich mehr Zeit für andere Dinge habe.

Contents

Abstract

Electrochemical processes offer promising routes to defossilize the chemical industry by integrating low-carbon electricity. Industrial application is still hindered by high costs and the challenging transition from lab-scale research to industrial maturity. Key processes, such as cathodic hydrogen evolution and CO_2 reduction, are typically paired with the anodic oxygen evolution reaction (OER). However, the generated oxygen holds little value, and the electrical costs associated with energy-intensive OER pose a significant economic barrier.

This thesis explores selective methanol oxidation as a less energy-intensive alternative to OER for paired electrolysis, which yield value-added products from both anodic and cathodic reactions. Two paired processes were studied in electrochemical flow cells: Methanol oxidation to formaldehyde at platinum paired with CO_2 reduction, and methanol oxidation to formate at hierarchically structured copper oxide paired with hydrogen evolution. Investigating both processes at conditions significantly exceeding previous studies in terms of electrode area, current density, and product concentration allowed novel insights into selective methanol oxidation and revealed crucial interactions within the paired systems. Furthermore, methanol oxidation was employed to introduce 'feed and bleed' as a versatile alternative to conventional batch and single-pass operation of electrochemical flow cells.

Methanol oxidation to formaldehyde was strongly influenced by the oxidation state of the electrode with a higher Faraday efficiency for oxidized platinum (up to 58%), but a lower anodic potential for metallic platinum. Methanol oxidation to formate at optimized conditions achieved nearly 100% Faraday efficiency and up to 70% yield. The reaction conditions, in particular the conversion, had a critical impact on the selectivity for formate. In both paired processes, methanol oxidation required less electrical energy than conventional OER and provided value-added products with substantial yields. Interactions between the anode and cathode side, such as ion transfer and the crossover of water and reactants were found to be crucial for the stability of the paired processes, especially at high product concentrations. Building on the findings on methanol oxidation, the 'feed and bleed' operating mode was established enabling the investigation of reactions in steady state at high product concentration.

The present work highlights the benefits of paired electrolysis and provides valuable insights on selective methanol oxidation to formaldehyde and formate with yields and product concentrations exceeding the previous state of the art. Challenges arising from high product concentration and adverse interactions within the paired process were identified and discussed. The methodological aspects of this work can be applied to the investigation of other electrochemical processes under industrially relevant conditions and thus contribute to the overarching goal of bringing sustainable processes to industrial application.

Zusammenfassung

Elektrochemische Prozesse bieten vielversprechende Routen zur Defossilisierung der chemischen Industrie durch die Integration von emissionsarmer Elektrizität. Die industrielle Anwendung wird durch hohe Kosten und durch Herausforderungen beim Transfer von der Forschung zur industriellen Reife behindert. Schlüsselprozesse wie die kathodische Wasserstoffentwicklung und die CO_2-Reduktion werden in der Regel mit der anodischen Sauerstoffentwicklung (Oxygen Evolution Reaction, OER) gekoppelt. Der erzeugte Sauerstoff hat jedoch nur einen geringen Wert und der hohe Energiebedarf von OER stellt ein erhebliches wirtschaftliches Hindernis dar. In der vorliegenden Arbeit wird die selektive Methanoloxidation als energiesparende Alternative zu OER für die gepaarte Elektrolyse untersucht, die wertschöpfende Produkte aus der anodischen und kathodischen Reaktion gewinnt. Zwei gepaarte Prozesse wurden in elektrochemischen Flusszellen untersucht: Methanoloxidation zu Formaldehyd an Platin gepaart mit CO_2-Reduktion, und Methanoloxidation zu Formiat an Kupferoxid gepaart mit Wasserstoffentwicklung. Beide Prozesse wurden unter Bedingungen untersucht, die in Bezug auf die Elektrodenfläche, die Stromdichte und die Produktkonzentration deutlich über bisherige Studien hinausgingen. Dadurch wurden neue Erkenntnisse zur Methanoloxidation gewonnen und entscheidende Wechselwirkungen innerhalb der gepaarten Systeme identifiziert. Weiterhin wurde die Methanoloxidation genutzt, um den 'Feed and Bleed' Betriebsmodus als vielseitige Alternative zu konventionellen Betriebsarten von elektrochemischen Flusszellen zu etablieren. Die Methanoloxidation zu Formaldehyd wurde stark vom Oxidationszustand der Elektrode beeinflusst. Die Faraday-Effizienz war höher für oxidiertes Platin (bis zu 58%), aber das Anodenpotential was niedriger mit metallischem Platin. Die Methanoloxidation zu Formiat erreichte unter optimierten Bedingungen eine Faraday-Effizienz von nahezu 100% und eine Ausbeute von bis zu 70%. Die Reaktionsbedingungen und der Umsatz hatten einen entscheidenden Einfluss auf die Selektivität. In beiden gepaarten Prozessen erforderte die Methanoloxidation weniger elektrische Energie als OER und lieferte wertsteigernde Produkte mit erheblichen Ausbeuten. Wechselwirkungen zwischen der Anoden- und der Kathodenseite waren entscheidend für die Stabilität der gepaarten Prozesse, insbesondere bei hoher Produktkonzentration. Aufbauend auf den Erkenntnissen zur Methanoloxidation wurde der 'Feed and Bleed' Betriebsmodus eingeführt, um Reaktionen im stationären Zustand und bei hoher Produktkonzentration zu untersuchen. Die vorliegende Arbeit unterstreicht die Vorteile der gepaarten Elektrolyse und liefert wertvolle Erkenntnisse zur selektiven Methanoloxidation mit Ausbeuten und Produktkonzentrationen über dem bisherigen Stand der Technik. Die Herausforderungen durch hohe Ausbeuten und nachteilige Wechselwirkungen innerhalb der gepaarten Prozesse wurden identifiziert und diskutiert. Die Methoden dieser Arbeit können für die Untersuchung anderer elektrochemischer Prozesse unter industriell relevanten Bedingungen genutzt werden und damit dazu beitragen nachhaltige Verfahren zur industriellen Anwendung zu bringen.

1. Introduction

Anthropogenic carbon dioxide (CO_2) emissions are causing global warming, which severely impacts human life and the ecosystems, if not mitigated [Port2022]. To reduce CO_2 emissions, ongoing efforts are being made to develop sustainable technologies to replace fossil fuels and feedstocks [Riss2020]. Electrochemical processes offer promising approaches for the production of chemicals from renewable feedstocks [Wynd2021; Luna2019]. Especially water electrolysis and electrochemical CO_2 reduction (CO2R) have emerged as focal points of extensive research and industrial interest. However, the high cost compared to fossil-based routes presents a major hurdle for both processes [Grig2020; Luna2019; Joun2018].

Typically, only one half-cell reaction of electrochemical reactors is exploited for the synthesis of value-added chemicals [Vass2021; Xu2019]. The value-adding reaction of water electrolysis, CO2R, and various other electrochemical processes is a reduction reaction at the cathode side of the cell. The cathodic reactions typically exhibit low standard potentials, specifically E^0 = 0 V vs. standard hydrogen electrode (SHE) for the hydrogen evolution reaction (HER) [Shih2022] and E^0 = -0.1 - 0.2 V vs. SHE for the CO_2 reduction reaction (CO2RR) to most products [Na2019]. These cathodic reactions are commonly paired with the energy-intensive oxygen evolution reaction (OER) at the anode side [Vass2021; Xu2019], which exhibits a high standard potential of E^0 = 1.23 V vs. SHE [Shih2022]. Consequently, OER accounts for the majority of the electrical energy demand, while the generated oxygen holds little value and does not contribute to economic viability. The cost of electrical energy is the main contributor to the overall production costs for both water electrolysis and CO2R [Grig2020; Luna2019]. To

reduce the electrical energy demand and enhance economic viability, recent literature has explored replacing the energy-intensive OER with organic oxidation reactions, which can reduce electricity consumption while providing additional value-added products [Na2019; Verm2019; Vass2021; Vehr2023; Xu2019; Jack2021; Chen2022].

The selective oxidation of methanol to formaldehyde or formic acid (including corresponding formate salts) is a promising alternative anode reaction to replace OER. Selective methanol oxidation exhibits a low standard potential which allows to reduce electricity consumption compared to OER while providing additional value-added products. Both formaldehyde and formic acid have a higher market price than the starting material methanol [Reus2010; ICIS2007; Joun2018; Intr2018a; Intr2018b]. Methanol oxidation to formaldehyde was previously only investigated in mechanistic studies in the context of direct methanol fuel cells and was not applied for the targeted synthesis of formaldehyde yet [Ota1984; Chil1999; Bati2003]. On the other hand, methanol oxidation to formate was extensively studied and a range of promising catalysts were developed [Wei2021; Wu2021; Li2020a; Li2020b; Xian2020; Xian2021; Du2023]. However, there is still a lack of studies addressing the paired process and the interactions between anode and cathode side such as the crossover of ions, water and reactants. Furthermore, the formate concentration obtained in previous studies was either low or not reported, even though product concentration and yield are crucial parameters for any chemical synthesis. Also, in electrosynthesis in general, there is a critical need for research and techniques that study processes under industrially relevant conditions including scale, current density, temperature, product concentration, conversion, and yield [Burd2019; Zhou2023; This2024].

The present thesis investigates selective methanol oxidation as anode reaction for paired electrolysis. Two products and reaction systems are considered: Methanol oxidation to formaldehyde at platinum electrodes and the oxidation of methanol to formate at hierarchically structured copper oxide. Studying both reaction systems at conditions significantly exceeding previous mechanistic and catalytic studies in terms of electrode area,

current density, temperature, and product concentration provides novel insights into selective methanol oxidation and into crucial interactions within the paired process. Furthermore, this thesis employs methanol oxidation on a methodological level to introduce the feed and bleed operation mode for electrochemical flow cells. The unique characteristics of the feed and bleed mode allow to operate electrochemical reactions simultaneously at high product concentration and steady state. From a broader perspective, the present thesis addresses three key challenges for the transition of electrochemical processes from laboratory-scale research to a viable industrial application: (i) The high energy and operational costs of electrochemical processes, (ii) the need for research at industrially relevant conditions and (iii) the required process stability over time. An overview is shown in Figure 1.1 which highlights the key challenges addressed by each chapter. The scope of the thesis is further outlined in the following paragraphs.

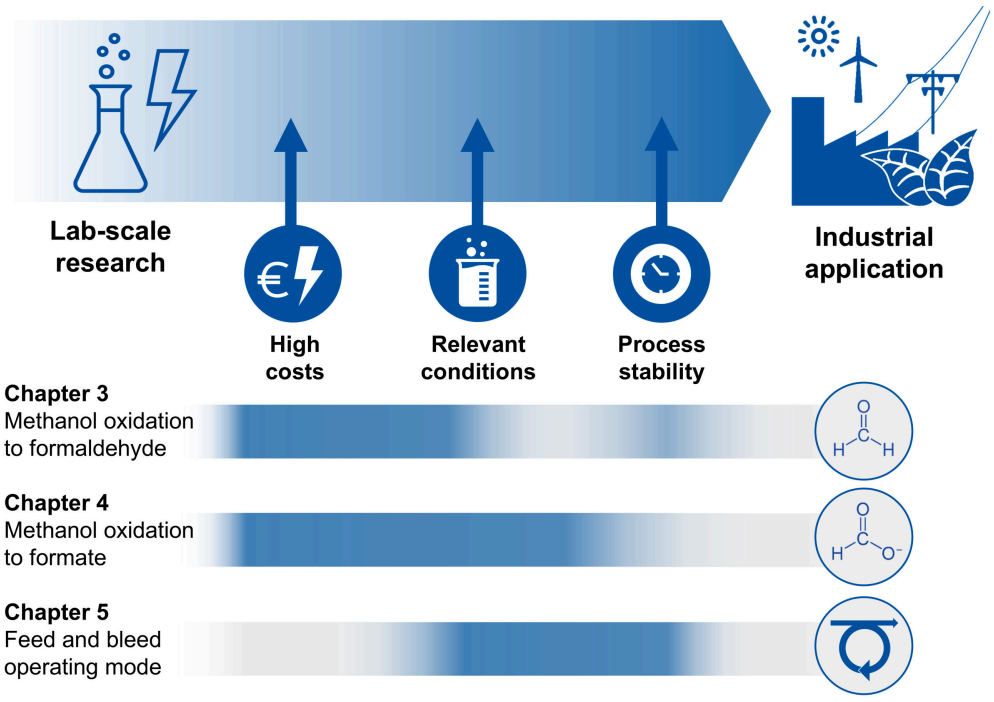

Figure 1.1.: Overview of the thesis presenting three key challenges for the transition of electrochemical processes from laboratory-scale research to a viable industrial application. The key challenges addressed by each chapter are highlighted in blue.

Fundamentals of electrolysis, paired electrolysis, selective methanol oxidation, and key figures are presented in **Chapter 2** with an overview of previous works and the state of the art.

Methanol oxidation to formaldehyde exhibits beneficial characteristics as anode reaction for paired synthesis. However, targeted synthesis was not investigated before. The synthesis of formaldehyde by methanol oxidation in an electrochemical flow cell is presented in **Chapter 3**. Metallic and oxidized platinum electrodes are investigated within a current density range of 25 - 100 mA/cm^2 and compared with respect to selectivity and required potential. Furthermore, anodic methanol oxidation to formaldehyde is paired with cathodic CO_2 reduction to formate, examining both sides of the process and their interactions.

In contrast to formaldehyde, considerable research focused on selective methanol oxidation to formate. While high Faraday efficiency (FE) for formate was reported, neither reaction conditions nor conversion and product yield were considered. **Chapter 4** investigates the selectivity of methanol oxidation to formate with progressing conversion on hierarchically structured copper(II) oxide electrodes using a flow cell with current densities up to 200 mA/cm^2. The impact of the reaction conditions is analyzed, including current density, temperature, flow rate, electrolyte composition, and membrane type. Optimized reaction conditions are applied to achieve high formate yields. Furthermore, interactions in the paired process of anodic methanol oxidation and cathodic hydrogen evolution are examined, including the transfer of ions, reactants and water.

Chapter 5 introduces the feed and bleed operating mode for electrosynthesis in flow cells, which enables versatile steady-state operation of electrochemical processes. The 'feed and bleed' mode is compared to batch and single-pass operation. Batch, single-pass, and feed and bleed operation is demonstrated by methanol oxidation to formate at 200 mA/cm^2 in flow cell, providing an experimental comparison concerning product/reactant concentration, conversion, and FE. The comparison highlights the characteristics of each operation mode for the electrosynthesis of chemicals, showcasing the unique characteristics of the feed and bleed mode,

which enables steady-state operation at industrially-relevant conditions with high product concentration.

The findings of the thesis are summarized in **Chapter 6** highlighting the main results and their implications. Finally, challenges and opportunities for future work are discussed.

Previous Publications in Student Theses

This thesis's content and results emanate from research conducted under the affiliation and position of the author as research fellow and PhD candidate at RWTH Aachen University. The position is associated with the Chair of Chemical Process Engineering. The work comprises data based on the following student theses:

- Tamara Oliveira, Master's thesis, 01.12.2020, *Coupled electrochemical synthesis: Investigation of concurrent alcohol oxidation and CO_2 reduction*
- Paulina Montero, Bachelor's thesis, 29.07.2022, *Methanol oxidation paired with CO_2 reduction: 200% electrochemical synthesis of formate*
- Sophia Schenke, Bachelor's thesis, 10.06.2023, *200% electrochemical synthesis of formate: Paired methanol oxidation and CO_2 reduction*

While working at the Chair of Chemical Process Engineering, the author further supervised the student theses listed below. The findings, methods and devices from these works contributed to this thesis and other publications of the author. The work of all students is gratefully acknowledged.

- Szymon Herdzik, Master's thesis, 26.09.2019, *Carbon dioxide as a resource: Electrochemical synthesis of basic chemicals*
- Miriam Mineur, Bachelor's thesis, 08.04.2020, *Rapid manufacturing for electrosynthesis: Design of a modular and scalable electrochemical cell*

- Hexin Zhu, Bachelor's thesis, 30.04.2020, *Model-based design and construction of a temperature control system in a parallelized experimental set-up for electrochemical synthesis*
- Florian Schwarz, Master's thesis, 29.05.2020, *Electrochemical Dehydrogenation of Methanol to Formaldehyde as the Anode Reaction for the Reduction of CO_2*
- Niklas Vollmert, Master's thesis, 24.12.2021, *Synthesis of formic acid by concurrent methanol oxidation and CO_2 reduction in an electrochemical flow cell*
- Markus Wessling, Bachelor's thesis, 17.02.2022, *Rapid Manufacturing for electrosynthesis: Design and optimization of a modular and scalable electrochemical cell*
- Jannik Mehlis, Master's thesis, 11.06.2022, *Experimental and simulative investigation of mass transport limitation in the electrochemical flow-cell flex-E-cell*
- Alexander Kohushölter, Master's thesis, 22.07.2022, *Tunable anode reactions for CO_2 reduction: Experimental investigation for strategies towards flexible energy demand in electrosynthesis*
- Florian Frick, Bachelor's thesis, 29.07.2022, *Design and implementation of an experimental setup for electrochemical CO_2 reduction to carbon monoxide at industrially relevant conditions*
- Lukas Griesberg, Bachelor's thesis, 09.09.2022, *200% electrochemical synthesis of formate: CO_2 reduction paired with methanol oxidation*
- Nicolas Mulandi, Master's thesis, 11.09.2023, *Spiral wound electrochemistry: Design of a modular flow cell and its application in alkaline water electrolysis*
- Markus Wessling, Master's thesis, 22.12.2023, *Additive manufacturing of electrochemical cell components: Multi-material structures to improve mass transfer and enable function integration*

2. Fundamentals

2.1. Principles of electrolysis

Electrochemistry is concerned with the mutual conversion of electrical and chemical energy [Bago2006], whereby two different types of electrochemical cells can be distinguished based on the direction of energy conversion [Bard2001; Inze2015]. Galvanic cells convert chemical energy into electrical energy, which allows to draw current from the cell to power an external load [Bard2001; Inze2015]. The present work focuses on electrolysis and electrolytic cells, in which electrical energy is converted to chemical energy by applying an electric potential from an external source to drive electrochemical reactions [Bard2001; Inze2015]. A basic electrolytic cell consists of two electrodes connected by an ionically conductive electrolyte [Schm2004]. Figure 2.1 depicts a simple electrolytic cell with two electrolyte compartments and an ion-permeable separator in between. Electrochemical reactions occur at the electrode-electrolyte interface and involve the transfer of electrons between the electrode and a reactant [Schm2004]. Based on the direction of electron transfer, electrochemical reactions can be classified into oxidation and reduction reactions [Schm2004].

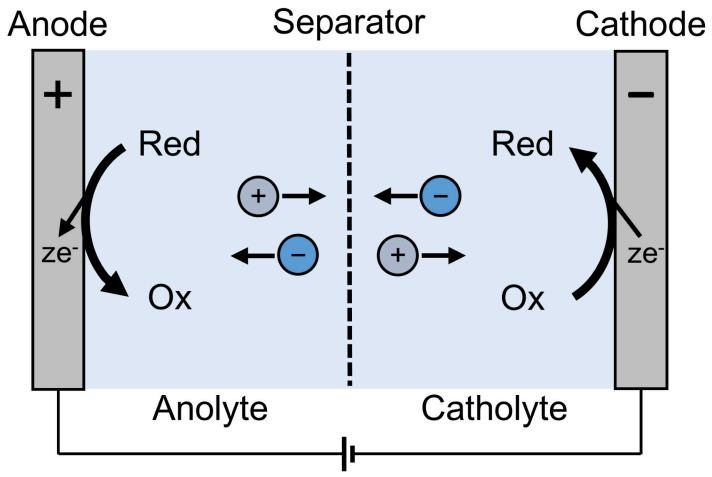

Figure 2.1.: Schematic of an electrolytic cell with two electrolyte compartments (anolyte and catholyte) and an ion-permeable separator in between. The circles with positive and negative signs represent ions migrating in the electric field. Adapted from [Schm2004].

Oxidation is characterized by the release of electrons from a reactant to the electrode (Equation 2.1), leading to an increase in the oxidation state of the reactant. The electrode where an oxidation occurs is defined as anode [Schm2004].

$$Red \longrightarrow Ox + ze^{-} \tag{2.1}$$

with the reduced species *Red*, the oxidized species *Ox* and the number of electrons transferred per reaction z. Reduction involves the uptake of electrons (Equation 2.2), while the oxidation state of the reactant is reduced. The electrode at which a reduction occurs is known as cathode [Schm2004].

$$Ox + ze^{-} \longrightarrow Red \tag{2.2}$$

Electrochemical oxidation and reduction are intrinsically linked in an electrochemical cell, since the same current passes through the anode and cathode [Plet1993; Schm2004]. Thus, the rate of charge transfer at the anode and cathode is identical, but in the opposite direction (oxidation vs.

reduction).

The minimum potential required to drive an electrochemical reaction is defined by thermodynamics. The standard electrode potential E^0 is the minimum potential required at standard conditions and can be calculated from the change of the Gibbs energy ΔG over the reaction, as shown in Equation 2.3 [Elia2019], where F is the Faraday constant and z the number of electrons transferred in the reaction. Standard conditions refer to a temperature of 25 °C, a pressure of 101.325 kPa, and an activity of 1 mol/L for all soluble species [Hayn2017].

$$E^0_{electrode} = \frac{\Delta G^0}{-zF} \tag{2.3}$$

Electrode potentials are reported as the difference in potential relative to a well-defined reference electrode [Ping2020]. The standard electrode potential is typically reported against the standard hydrogen electrode (SHE), which uses the potential of the redox couple of $2H^+ \rightleftharpoons H_2$ at standard conditions as a reference [Bard2001].

The thermodynamic minimum potential required beyond standard conditions, the reversible electrode potential $E^{rev}_{electrode}$, is described by the Nernst equation (Equation 2.4), which considers the influence of the temperature and the activity of the reactants and products [Petr2021; Seeb2015].

$$E^{rev}_{electrode} = E^0_{electrode} - \frac{RT}{zF} \ln Q_r = E^0_{electrode} - \frac{RT}{zF} \ln \frac{a_{Red}}{a_{Ox}} \tag{2.4}$$

with the ideal gas constant R, the temperature T, and the reaction quotient Q_r. For a simple oxidation reaction (Equation 2.1), the reaction quotient equals the quotient of the activities of the reactant a_{Red} and the product a_{Ox} [Seeb2015]. The Nernst equation is only valid for an ideal reaction in equilibrium without electric current passing through the electrode [Chak2018].

Ion exchange membranes are commonly used as separators for electrolytic cells, which selectively allow the passage of positive or negative ions, while blocking ions of the opposite charge [Luo2018]. The reversible membrane potential between the separate electrolyte phases at equilibrium can be calculated analogously to the Nernst equation by Equation 2.5, with

the simplified assumption that one permeating ion species (index *i*) accounts for the entire charge transport [Bard2001; Zosk2007]. The equation has a negative or positive sign for cations and anions as permeating species, due to their opposite direction of migration.

$$E^{rev}_{membrane} = \pm \frac{RT}{zF} \ln \frac{a_i^{catholyte}}{a_i^{anolyte}} \tag{2.5}$$

The actual electrode potential $E_{electrode}$ required to drive an electrochemical reaction beyond equilibrium with an electric current *I* can exceed the reversible potential significantly. The potential required beyond the reversible electrode potential is defined as overpotential $\eta_{electrode}$ (Equation 2.6) [Elia2019].

$$\eta_{electrode} = E_{electrode} - E^{rev}_{electrode} \tag{2.6}$$

The overpotential can be considered as a sum of terms that are associated with different steps of the electrode reaction (Equation 2.7) [Bard2001]. The reaction pathway in Figure 2.2 illustrates multiple steps from reactant to product: Mass transfer from the bulk solution to the electrode surface, electron transfer at the electrode surface, chemical reactions preceding or following the electron transfer, and adsorption/desorption at the electrode surface [Bard2001].

$$\eta_{electrode} = \eta_{mt} + \eta_{rxn} + \eta_{ct} \tag{2.7}$$

with the mass-transfer overpotential η_{mt}, the charge-transfer overpotential η_{ct} (also called activation overpotential [Elia2019]), and η_{rxn} the overpotential caused by preceding chemical reactions [Bard2001].

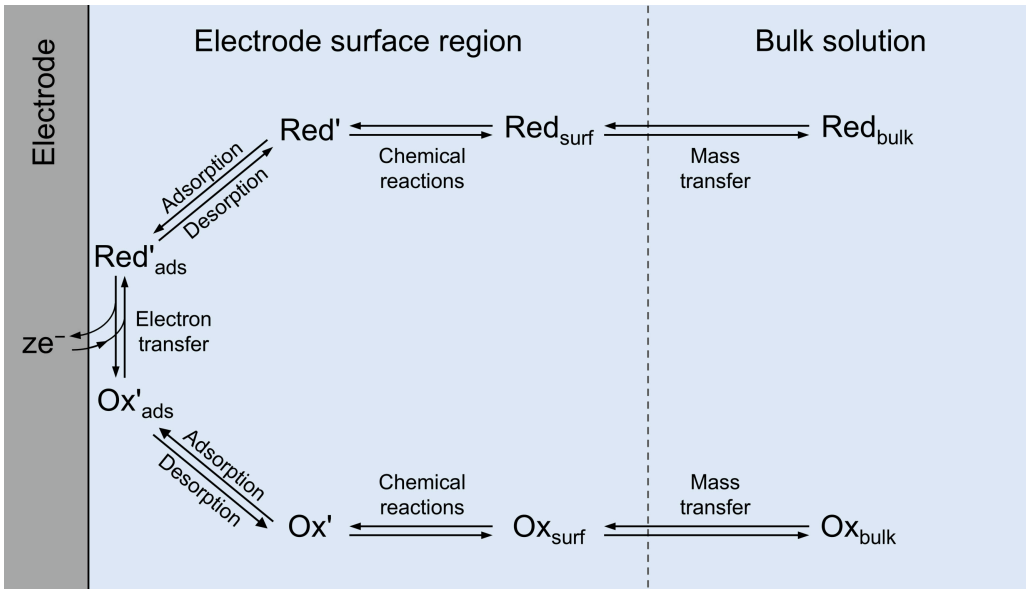

Figure 2.2.: Pathway of electrode reactions illustrating multiple steps from reactant to product. Oxidation and reduction are depicted counterclockwise and clockwise, respectively (compare to Equation 2.1 and 2.2). Adapted from [Bard2001].

Similar to the electrode overpotential, the overpotential at the cell level is also composed of multiple components (Equation 2.8).

$$\eta_{cell} = \eta_{anode} + \eta_{anolyte} + \eta_{membrane} + \eta_{catholyte} + \eta_{cathode} \tag{2.8}$$

Figure 2.3 illustrates the distribution of the overpotential over the distance from the anode to the cathode of a simple two-compartment cell.

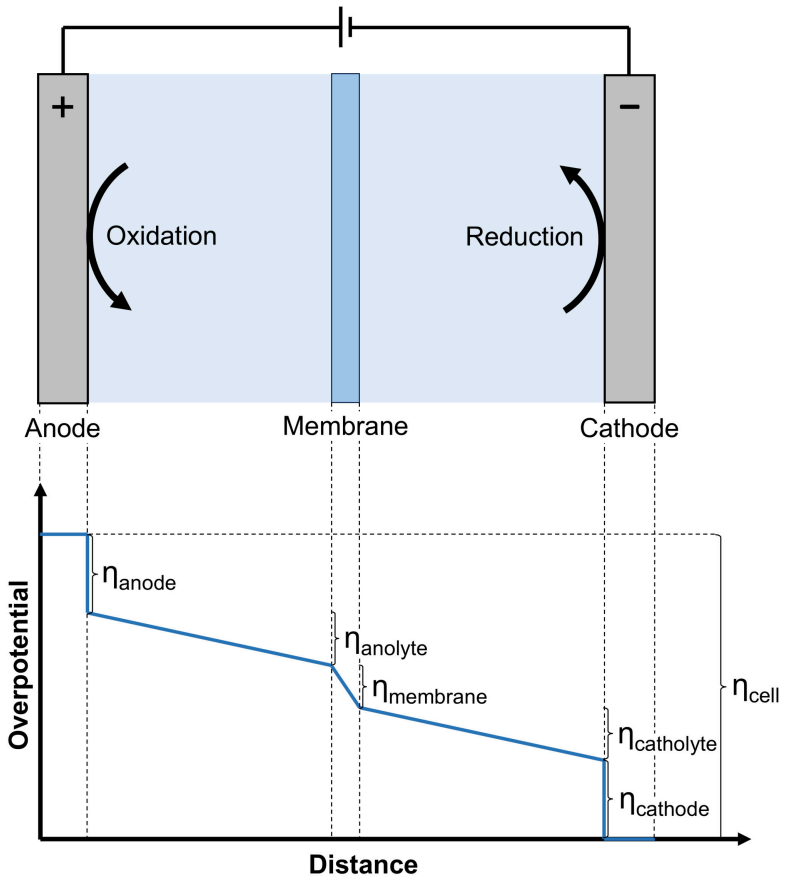

Figure 2.3.: Schematic distribution of the overpotential over the distance from anode to cathode in a simple two-compartment cell. Adapted from [Schm2004].

The overpotentials of the electrolyte and membrane can be described as potential drop over the ohmic resistance of the electrolyte $R_{electrolyte}$ and membrane $R_{membrane}$, respectively (Equation 2.9 and 2.10) [Schm2004; Cost2001].

$$\eta_{electrolyte} = I \cdot R_{electrolyte} \tag{2.9}$$

$$\eta_{membrane} = I \cdot R_{membrane} \tag{2.10}$$

Finally, the overall cell potential is composed of the ideal reversible potentials of the cathode, membrane, and anode, and the overpotential of the cell (Equation 2.11). The reversible potentials describe the minimum potential required at equilibrium without electrical current. The overpotential of the cell increases with increasing current and accounts for the losses in

electric potential due to the components and phenomena discussed in the previous paragraphs.

$$E_{cell} = E^{rev}_{cathode} + E^{rev}_{membrane} - E^{rev}_{anode} - \eta_{cell} \tag{2.11}$$

The general equation for the cell potential yields a negative cell potential for electrolytic cells (potential from an external source must be applied to drive the reactions), while the cell potential is positive for galvanic cells (the reactions can drive electric current to power an external load). However, literature on electrolysis, as well as the present work, omits the negative sign of the cell potential since the direction of energy conversion is clear and the electric potential must be applied.

This section provides an overview of important components and phenomena in electrolysis. However, it should be noted that the representation of the cell components includes simplifications and neglects certain details. For a comprehensive description of the phenomena and components in electrochemical cells, the author would like to refer to existing literature [Brow2018; Elia2019; Bard2001; Schm2004].

2.2. Key figures of electrolysis

Faraday efficiency

The Faraday efficiency (FE) describes how much of the total charge transferred is utilized to form a specific product [Scho2020]. The Faraday efficiency is defined by Equation 2.12 for cumulative calculation [Scho2020], or by Equation 2.13 for discrete calculation based on the difference in charge between two points in time [Bird2020].

$$FE = \frac{Q_{product}}{Q_{total}} \tag{2.12}$$

$$FE = \frac{\Delta Q_{product}}{\Delta Q_{total}} \tag{2.13}$$

$Q_{product}$ is the theoretical charge required to form the measured amount of product and Q_{total} is the total charge that was transferred during electrolysis. The charge of $Q_{product}$ and Q_{total} can be calculated by Equation 2.14 and 2.15 respectively [Scho2020]:

$$Q_{product} = z \cdot n_{product} \cdot F \tag{2.14}$$

$$Q_{total} = \int I\,dt \quad \xrightarrow[\text{current}]{\text{at constant}} \quad Q_{total} = I \cdot t \tag{2.15}$$

where z is the number of electrons transferred per reaction, $n_{product}$ is the molar amount of product formed (e.g., formaldehyde or formate from methanol oxidation), F is the Faraday constant, I the electric current and t the duration of electrolysis.

In this work, the FE is calculated at a constant current based on measured concentrations. Hence, Equation 2.16 can be derived for the FE of a closed system from inserting Equations 2.14 and 2.15 in Equation 2.13.

$$FE_n = \frac{zFV}{I} \cdot \frac{c_n - c_{n-1}}{t_n - t_{n-1}} \tag{2.16}$$

where c is the concentration of the product, V is the electrolyte volume

in the closed system and the indices denote the current data point (index n) and the previous data point (index $n-1$). Please refer to Section 5.3.1 for a comparison of FE calculation for different operation modes of electrochemical flow cells.

Potential

The cell potential is measured between the anode and cathode and comprises all components within the cell, as discussed in Section 2.1. The electrode potential of the anode or cathode is the potential applied to drive the electrochemical reaction at the corresponding electrode (see Section 2.1). This work reports electrode potentials relative to the reversible hydrogen electrode (RHE), which uses the potential of the redox couple of $2H^+ \rightleftharpoons H_2$ in the surrounding electrolyte as reference [Krey2014]. Thus, a positive electrode potential of an oxidation reaction indicates how much more potential is needed than for the oxidation of H_2 to $2H^+$.

Current density

The current density i describes the electric current per electrode area as defined by equation 2.17 [Bard2001]:

$$i = \frac{I}{A} \tag{2.17}$$

with the electric current I and the electrode area A. In the present thesis, the current density is always calculated with the geometric area of the electrode, which is defined by its external dimensions.

Conversion and yield

The conversion indicates how much of a substance has been reacted, while the (fractional) yield provides information on how much of the reacted substance has been converted to a specific product [Leve1999]. The conversion and yield of methanol oxidation can be calculated with the Equations 2.18 and 2.19 [Leve1999]. The indices denote the current concentration (index *n*) and the initial concentration (index 0).

$$conversion = \frac{c_{0,methanol} - c_{n,methanol}}{c_{0,methanol}} \tag{2.18}$$

$$yield = \frac{c_{n,product}}{c_{0,methanol}} \tag{2.19}$$

2.3. Paired electrolysis

In paired electrolysis, the anodic and cathodic reactions are involved in the production of value-added products, utilizing both sides of the electrochemical cell [Iban2017]. Various terms are used in the literature for paired electrolysis (e.g., combined, concurrent, dual, duet, parallel, simultaneous, and synchronous electrochemical processes)[Iban2017]. The present work uses the term 'paired' in accordance with the consistent scheme for nomenclature and classification proposed by Ibanez et al. [Iban2017]. Paired electrochemical processes can be classified by their mode of action, as illustrated in Figure 2.4 [Aust2014; Iban2017]. Divergent paired electrolysis describes the formation of two different products from the same reactant, whereas convergent paired electrolysis describes the formation of the same product from two different reactants (Figure 2.4a-b). The present thesis is focused on parallel paired electrolysis with the anodic and cathodic reaction forming two different products from two different reactants (Figure 2.4c).

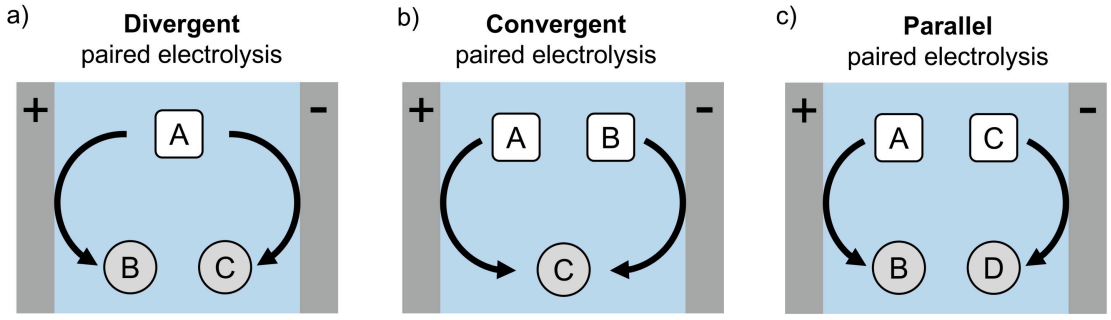

Figure 2.4.: Selected types of paired electrolysis, based on the classification scheme from Ibanez et al. [Iban2017].

The concept of paired electrolysis was already applied in the early years of industrial electrochemistry with the first chlor-alkali electrolysis plants that produced chlorine at the anode and caustic soda and hydrogen at the cathode [Bald1927]. For the current transition from fossil-based processes to the production of chemicals from renewable feedstocks, especially reduction reactions at the cathode are of major interest. Cathodic hydrogen evolution (HER) and CO_2 reduction (CO2R) are regarded as highly promising reactions for the sustainable production of hydrogen, carbon monoxide,

ethylene, and other basic chemicals [Wynd2021; Luna2019]. Hydrogen evolution or CO_2 reduction is typically paired with the anodic oxygen evolution reaction (OER) [Vass2021; Kahl2023]. However, OER has a high energy demand and the oxygen produced has no relevant market value [Kahl2023]. In this context, alternative anode reactions and the strategy of paired electrolysis have come into focus [Vass2021; Kahl2023]. While the simultaneous production of chlorine and caustic soda was a mere result of brine electrolysis, current research is focused on the targeted exploration of useful and compatible anode reactions to substitute oxygen evolution [Vass2021; Kahl2023]. Alternative anode reactions ideally have two advantages over oxygen evolution: A lower anodic potential and the production of value-added products [Vass2021; Kahl2023]. Reducing the anodic potential compared to OER can significantly affect the viability of the overall process, as OER accounts for the majority of the electricity consumption which is the main contributor to the overall production costs for both conventional water electrolysis and CO_2 reduction [Grig2020; Luna2019]. The formation of value-added oxidation products can further improve the overall process by contributing to the overall economic viability [Vass2021; Kahl2023]. Successful pairing of two reactions require compatibility in terms of reaction conditions, as the paired reactions are required to work in the same cell at the same current density. From a macroeconomic perspective, alternative anode reactions that yield products with significantly lower demand than for the cathodic product can only improve a small fraction of the total production. Therefore, the demand for the anodic product should ideally range in the same order of magnitude as that for the cathodic product [Kahl2023].

A broad range of anodic reactions has been considered as an alternative to OER for paired electrolysis. The overview over selected reactions in Figure 2.5 shows feedstocks and products, as well as the reactions standard potential vs. standard hydrogen electrode (SHE). The characteristics and the state of the art of the illustrated reactions are briefly summarized in the following paragraphs.

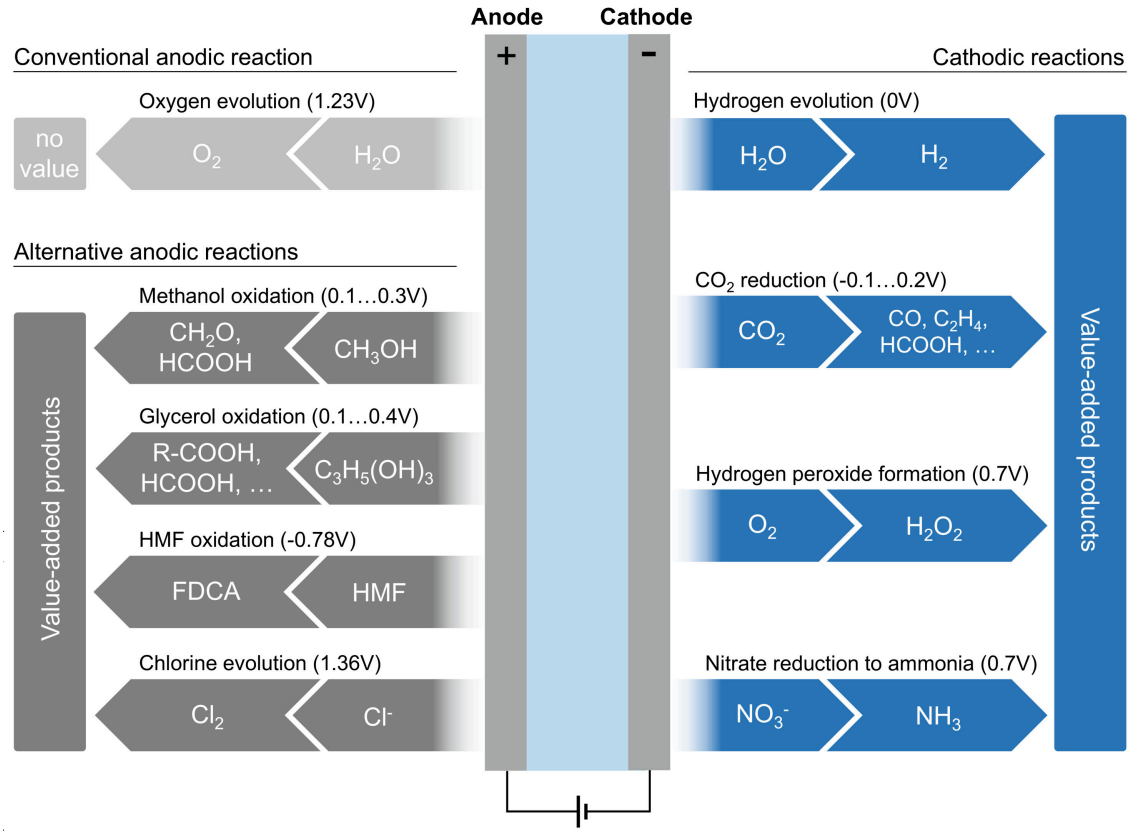

Figure 2.5.: Schematic illustrating the concept of paired electrolysis in which the reactions on both sides of the electrochemical cell are utilized to produce value-added products. Selected anodic and cathodic reactions are presented providing the standard electrode potential vs. SHE in brackets.

Oxygen evolution has a high standard potential of 1.23 V vs. SHE and provides no value-added product [Kahl2023]. Nonetheless, OER is the standard anodic reaction for conventional water electrolysis and CO_2 reduction [Vass2021; Kahl2023]. Water electrolysis utilizes different processes, in particular alkaline electrolysis and proton exchange membrane (PEM) electrolysis, which have different characteristics [Seze2025]. Iridium- and ruthenium-based catalysts are considered as the state of the art for OER in PEM electrolysis and nickel-iron based oxides and (oxy)hydroxides for alkaline electrolysis [Wang2021]. OER is operated in water electrolysis with high current densities, the range differs depending on the process (alkaline electrolysis: 0.2 - 0.7 A/cm^2, PEM electrolysis: 1.0 - 2.2 A/cm^2) [Seze2025]. The sluggish kinetics of OER still causes considerable overpotentials leading to typical anodic potentials of 1.5 - 2.0 V vs. RHE

[Seze2025; Huan2024b].

Selective methanol oxidation offers a low standard potential (0.1...0.3 V vs. SHE) [Wei2021; Hayn2017] and can provide formaldehyde or formic acid/formate as value-added products. Methanol can be produced from renewable feedstock [Olah2018] and its oxidation products are needed on a large scale, especially formaldehyde with a production of 18 Mt/year [Vass2021]. Formaldehyde formation on platinum electrodes occurs at 0.5 - 0.7 vs. RHE and was investigated mainly in mechanistic studies (current density < 10 mA/cm^2) [Chil1999; Bati2003; Ota1984; Jusy2003]. Methanol oxidation to formate typically employs copper, nickel, and cobalt-based catalysts at alkaline conditions with anodic potentials of 1.3 - 1.6 V vs. RHE reaching current densities of 10 - 200 mA/cm^2 [Li2020a; Wei2021; Wu2021; Xian2020]. The reaction mechanism and the state-of-the-art of selective methanol oxidation to formaldehyde and formate are discussed in detail in Chapter 2.4.

Glycerol oxidation exhibits a low standard potential (0.1...0.4 V vs. SHE)[Verm2019; Vehr2023] and forms a wide range of products, such as formic acid, lactic acid, glyceraldehyde, and oxalic acid [Kuma2023]. Typically, several of these products are formed concurrently, which can increase the complexity of downstream processing [Fan2021]. Glycerol is produced from renewable feedstock as a by-product of biodiesel production [Kuma2023]. However, the demand for the glycerol oxidation products (< 1 Mt/year) is significantly lower compared to the demand for formaldehyde [Kahl2023]. Catalysts based on platinum, gold, nickel, or cobalt were frequently used for glycerol oxidation with typical current densities of 10 - 100 mA/cm^2 [Kuma2023]. The corresponding anodic potential is between 0.5 - 1.5 V vs. RHE with the noble metal electrodes being typically at the lower end of the range [Kuma2023].

Hydroxymethylfurfural (HMF) oxidation to 2,5-furandicarboxylic acid (FDCA) exhibits a remarkably low standard potential (-0.78 V vs. SHE) and a significant increase in value from feedstock to product [Kahl2023]. The current annual production of FDCA is rather low (0.5 Mt/year)[Kahl2023], but could increase if FDCA-based polymers gained a larger market share.

HMF oxidation is typically performed on nickel-, cobalt- or copper-based catalysts at anodic potentials of 1.3 - 1.6 V vs. RHE reaching current densities of 10 - 100 mA/cm^2 [Chen2023]. Recent studies demonstrated HMF oxidation to FDCA surpassing the typical current range with current densities of up to 1000 mA/cm^2 [Chen2023].

Chlorine evolution exhibits a high standard potential of 1.36 V vs. SHE [Vass2021] and is an established reaction in industrial chlorine production from chlor-alkali or hydrochloric acid electrolysis [Kint2017; Deng2024]. The yearly production of chlorine is about 100 Mt/year [Vass2021]. Chlorine evolution is performed on dimensionally stable anodes (DSA) which are coated with a mixture of RuO_2 and TiO_2 oxides at current densities of 150 - 700 mA/cm^2 [Deng2024].

Hydrogen evolution has a low standard potential of 0 V vs. SHE and is paired with OER for conventional water electrolysis [Shih2022; Kahl2023]. Hydrogen is an important base chemical with a production of 90 Mt/year, which is expected to increase to 130 Mt/year by 2030 [Inte2022]. As with OER, it should be differentiated between alkaline electrolysis and PEM electrolysis. Platinum-based electrodes are considered as the state of the art for PEM electrolysis, nickel based electrodes for alkaline electrolysis [Chat2022]. HER is operated at high current densities in conventional water electrolysis, the range differs depending on the process (alkaline electrolysis: 0.2 - 0.7 A/cm^2, PEM electrolysis: 1.0 - 2.2 A/cm^2)[Seze2025]. The cathode potential is typically in the range of -0.1...-0.5 V vs. RHE with alkaline HER being at the higher end [Seze2025; Huan2024b; Mahm2018].

Electrochemical CO_2 reduction can produce a wide range of basic chemicals, such as carbon monoxide, formic acid, or ethylene [Chen2018; Joun2018; Gawe2022]. CO_2 reduction is a promising sustainable alternative to conventional processes utilizing electricity from renewable sources and CO_2 instead of fossil feedstock [Wynd2021]. Ethylene and syngas (mixture of hydrogen and carbon monoxide) are produced on a large scale with an annual production of about 150 Mt/year each [Joun2018; Luna2019], the annual production of formic acid is significantly lower at 0.9 Mt/year [Kahl2023]. CO_2 reduction is typically carried out under slightly

alkaline conditions, often with an anion exchange membrane in direct contact with the electrode [Gawe2022]. Depending on the product, different metals are used for catalyst development, such as silver and gold for carbon monoxide, tin for formic acid, and copper for ethylene [Luna2019; Kuma2023]. Typical current densities are 100 - 500 mA/cm^2 for carbon monoxide or formic acid and 200 - 1000 mA/cm^2 for ethylene [Kuma2023] at cathode potentials of -0.5 to -1.5 V vs. RHE [Leon2024; Kuma2023].

While the present work investigates paired electrolysis with hydrogen evolution and CO_2 reduction, it should be noted that alternative anode reactions can be paired with other promising cathodic reactions, such as the electrochemical production of hydrogen peroxide or ammonia. In addition to the examples discussed above, numerous reactions have been proposed and investigated for paired electrolysis [Aust2014; Iban2017; Poll2020; Xue2024; Hilt2024]. For a comprehensive discussion of alternative anodic reactions please refer to existing literature reviews on paired electrolysis [Vass2021; Kahl2023; Cout2016; Xi2024; Xu2019]. Furthermore, Figure 2.6 provides an overview of selected literature on paired electrochemical synthesis in the context of hydrogen evolution and CO_2 reduction.

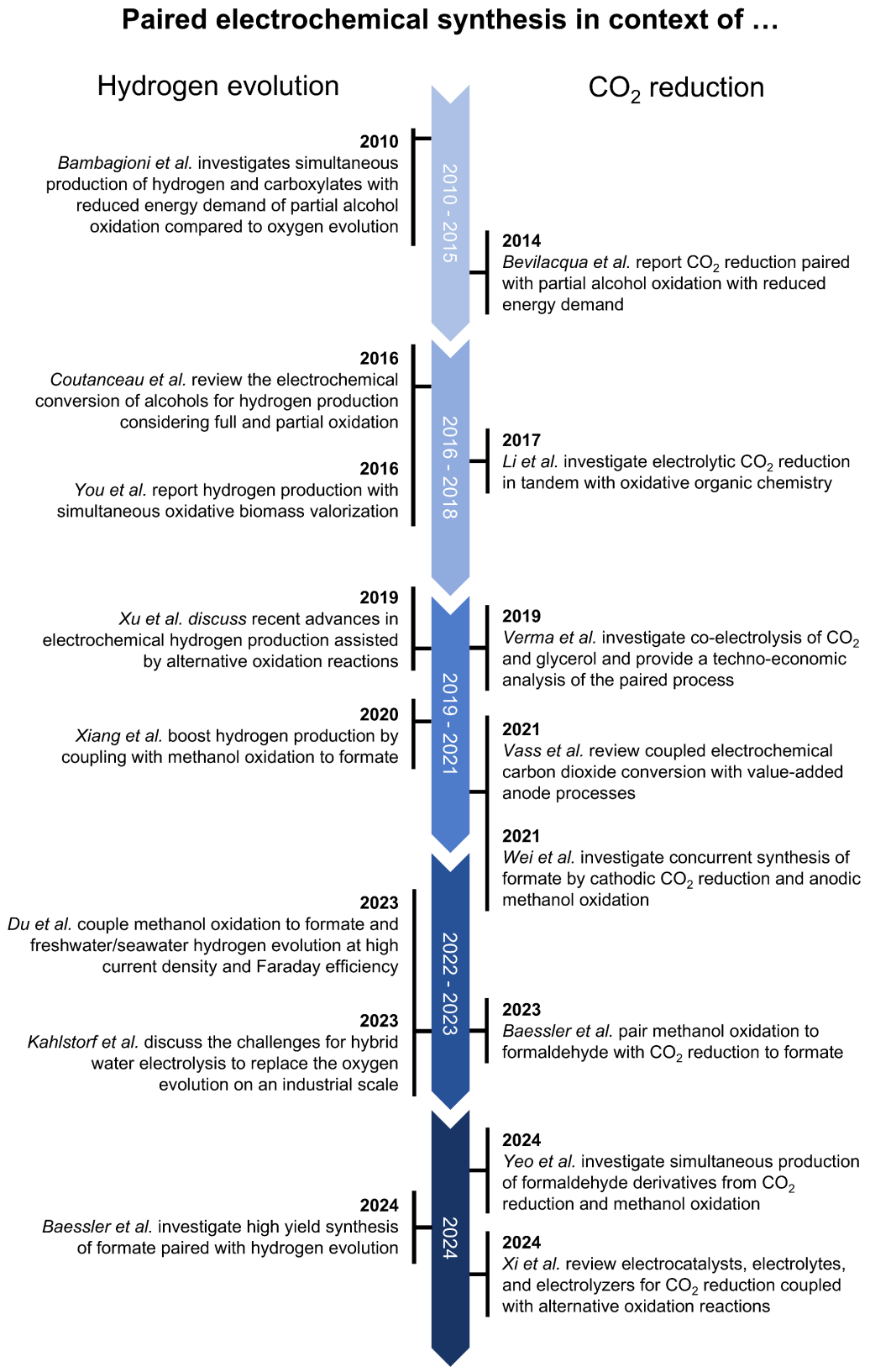

Figure 2.6.: Overview of selected literature on paired electrochemical synthesis in the context of hydrogen evolution and CO_2 reduction [Bamb2010; Cout2016; You2016; Xu2019; Xian2020; Du2023; Kahl2023; Baes2024; Bevi2014; Li2017; Verm2019; Vass2021; Wei2021; Baes2023; Yeo2024; Xi2024].

2.4. Electrochemical oxidation of methanol

Electrochemical methanol oxidation was extensively studied in the context of direct methanol fuel cells (DMFC), aiming for full oxidation to carbon dioxide (CO_2) [Liu2006; Wasm1999; Viel2003]. Formaldehyde and formic acid are known side products formed by undesired partial oxidation of methanol in DMFC studies [Wasm1999]. Figure 2.7 provides an overview of C1 products of methanol oxidation, showing the increasing oxidation state and successive oxidation steps from methanol to CO_2.

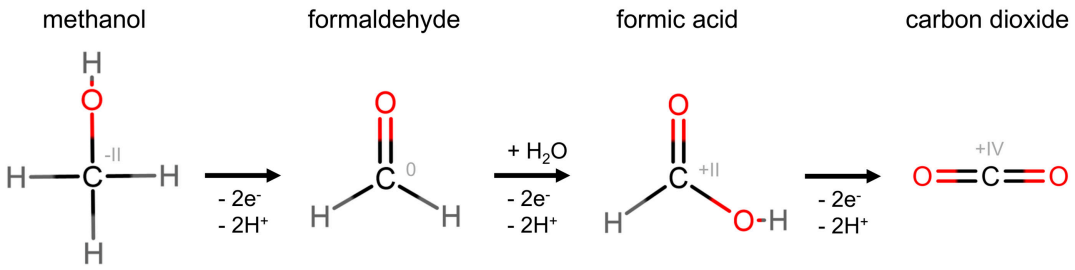

Figure 2.7.: Overview of the C1 products of electrochemical methanol oxidation, showing successive oxidation steps from methanol to carbon dioxide. The small gray number indicates the increasing oxidation state of the carbon atom from left to right.

In the context of paired synthesis, selective partial oxidation of methanol came into focus to produce value-added products. Figure 2.8 provides an overview of selected literature on partial methanol oxidation to formaldehyde or formate. Typical reaction systems, selected studies, and the reaction mechanism are discussed in the following Sections 2.4.1 and 2.4.2.

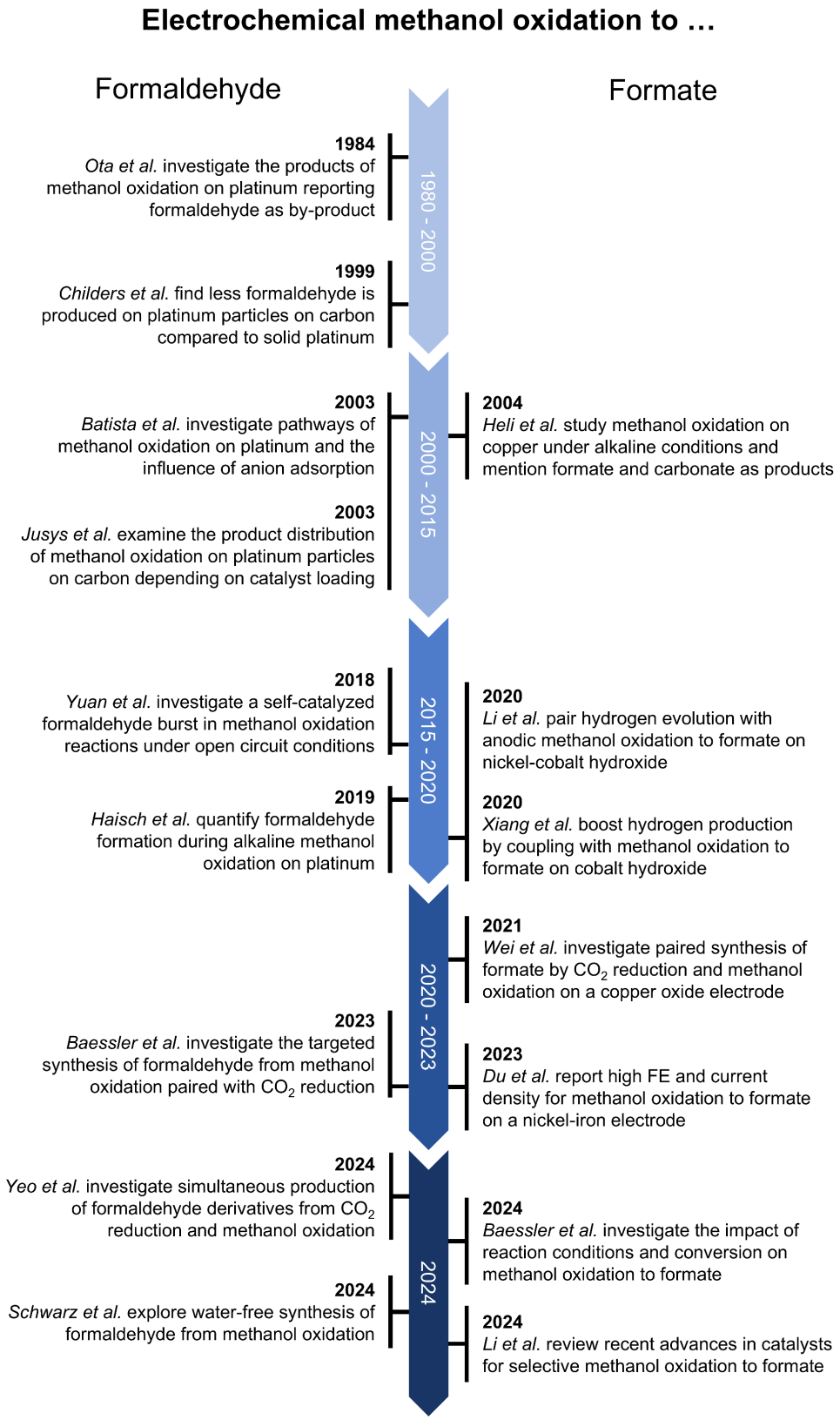

Figure 2.8.: Overview of selected literature on electrochemical methanol oxidation to formaldehyde and formate [Ota1984; Chil1999; Bati2003; Jusy2003; Yuan2018; Hais2019; Baes2023; Yeo2024; Schw2024; Heli2004; Li2020b; Xian2020; Wei2021; Du2023; Baes2024; Li2024].

2.4.1. Partial oxidation to formaldehyde

Electrochemical methanol oxidation to formaldehyde involves the transfer of two electrons (Equation 2.20). Compared to the numerous works on DMFCs and full methanol oxidation, only a few studies investigated the formation of by-products such as formaldehyde explicitly. Formaldehyde formation was mainly investigated in mechanistic studies on methanol oxidation at platinum electrodes under acidic conditions at low current density ($< 10\,mA/cm^2$).

$$CH_3OH \longrightarrow CH_2O + 2H^+ + 2e^- \tag{2.20}$$

Ota et al. studied the products of electrochemical methanol oxidation on platinized platinum electrodes reporting that the product distribution of carbon dioxide, formic acid, and formaldehyde changed depending on the surface roughness of the electrode [Ota1984]. The Faraday efficiency for formaldehyde increased with decreasing surface roughness, while the current density decreased [Ota1984]. With the smoothest electrode tested, the FE for formaldehyde was 53% at 0.6 V vs. RHE with a current density of about $2\,mA/cm^2$ in a solution of 1 mol/L methanol, and 1 mol/L H_2SO_4. Formaldehyde formation decreased over time reaching nearly zero FE after one hour [Ota1984].

Childers et al. investigated formaldehyde formation from methanol oxidation on different platinum-based electrodes [Chil1999]. Almost no formaldehyde was formed with platinum particles supported on carbon black with Nafion [Chil1999]. On a solid polycrystalline platinum electrode, 17% FE was reported at 0.7 V vs. RHE and 36% FE at a lower potential of 0.5 V vs. RHE during an electrolysis time of 2 min, however, the average current density was low for both experiments ($< 0.2\,mA/cm^2$) [Chil1999].

Batista et al. compared methanol oxidation on platinum electrodes in aqueous solutions of 1 mol/L methanol in either 0.5 mol/L sulfuric acid (H_2SO_4) or 0.1 mol/L perchloric acid ($HClO_4$) [Bati2003]. The reported amounts of formaldehyde formed during 15 min electrolysis at 0.6 V vs. RHE correspond to an FE of up to 65% with H_2SO_4 and 18% with $HClO_4$

[Bati2003]. The current density with H_2SO_4 was about four times lower than with $HClO_4$ (0.014 mA/cm^2 vs. 0.056 mA/cm^2), but practically the same amount of formaldehyde was formed [Bati2003]. Batista et al. proposed the hypothesis that the presence of H_2SO_4 inhibits the pathway for methanol oxidation to carbon monoxide by adsorption of a sulfate species on the platinum electrode, while the pathway for formaldehyde formation remains unaffected [Bati2003].

Parallel pathways were proposed for electrochemical methanol oxidation: A pathway involving the formation of adsorbed carbon monoxide (CO), which is further oxidized to CO_2 at sufficient potential and non-CO pathways that involve the formation of soluble by-products such as formaldehyde or formic acid which can be further oxidized to CO_2 as well [Bago1977; Bati2004; Cao2005]. The reaction pathway proposed by Bagotzky et al. is depicted in Figure 2.9 [Bago1977]. For further details on the reaction mechanism of methanol oxidation on platinum, please refer to existing mechanistic studies [Cao2005; Ferr2008; Ande2014; Sako2017].

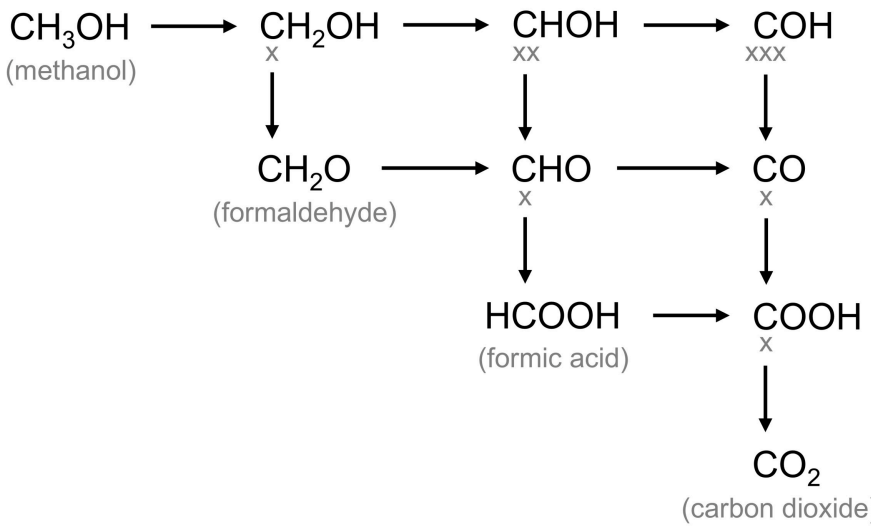

Figure 2.9.: Reaction scheme for methanol oxidation showing intermediates and reaction products (labeled in gray). The gray x indicates the number of valence bonds with the surface. Adapted from [Bago1977; Carr2001].

2.4.2. Partial oxidation to formic acid or formate

Methanol can be oxidized to formic acid under acidic conditions (Equation 2.21) while formate (salt of formic acid) is obtained under alkaline conditions (Equation 2.22).

$$CH_3OH + H_2O \longrightarrow HCOOH + 4H^+ + 4e^- \tag{2.21}$$

$$CH_3OH + 5OH^- \longrightarrow HCOO^- + 4H_2O + 4e^- \tag{2.22}$$

Four electrons are transferred in both reactions, so that the theoretical charge needed for producing the same amount of product is doubled compared to methanol oxidation to formaldehyde with two electrons transferred per reaction (see Equation 2.14 and 2.20). Methanol oxidation to formic acid was reported in mechanistic studies on platinum electrodes (see also Section 2.4.1), but the Faraday efficiency ($<35\%$) and current density ($<10\,\mathrm{mA/cm^2}$) were low [Ota1984; Bati2003]. Alkaline methanol oxidation to formate is typically performed on metal oxide and hydroxide electrodes based on cobalt, nickel, or copper. The electrodes are often fabricated from a 3D-structured substrate (e.g. metal foam), which is modified with a nanostructured surface. Combining a microporous substrate with a nanostructured surface is a common strategy for creating electrodes with a high active surface area [Wals2018]. While previous studies achieved high FE for formate and high current density, the influence of the product concentration and the reaction conditions have not been investigated yet. To provide an overview of the state of the art, selected works are summarized in the following paragraphs.

Li et al. reported methanol oxidation to formate with close to 100% FE for formate at 10 mA/cm^2 at 1.32 V vs. RHE using an electrode of nickel-cobalt-hydroxide ($Ni_{0.33}Co_{0.67}(OH)_2$) nanoneedles on nickel foam [Li2020b]. The electrode had a geometric area of 0.5 cm^2 and was operated in an aqueous solution of 0.5 mol/L methanol and 1 mol/L KOH [Li2020b]. Li et al. further paired anodic methanol oxidation with cathodic hydrogen evolution and highlighted the reduced cell potential compared to conventional hydrogen evolution paired with anodic oxygen evolution [Li2020b].

Xiang et al. used an electrode of cobalt hydroxide@hydroxysulfide nanosheets on carbon paper (geometric area 1 cm^2) and reached nearly 100% FE for formate at 10 mA/cm^2 in a paired electrolysis with hydrogen evolution at a cell potential of 1.5 V [Xian2020]. They found that the electrode potential at 10 mA/cm^2 is decreasing from 1.46 to 1.36 V when increasing the methanol concentration from 0.4 to 6 mol/L in 1 mol/L KOH [Xian2020]. However, the influence of the electrolyte composition on the FE was not investigated [Xian2020].

Wei et al. reached 88% FE for formate at 100mA/cm^2 with 1.47 V vs. RHE using an electrode of copper oxide (CuO) nanosheets on copper foam [Wei2021]. The electrode had a geometric area of 15 cm^2 and was operated in an aqueous solution of 1 mol/L methanol and 1 mol/L KOH [Wei2021]. Wei et al. further demonstrated convergent paired electrolysis producing formate from both anodic methanol oxidation and cathodic CO_2 reduction [Wei2021].

Wu et al. used nickel foam covered with nickel hydroxide nanosheets as electrode (geometric area 1 cm^2) reaching nearly 100% FE for formate at 100 mA/cm^2 at 1.57 V vs. RHE with an electrolyte containing 0.5 mol/L methanol and 1 mol/L KOH [Wu2021]. Their work further investigates the convergent paired synthesis of formate from methanol oxidation and CO_2 reduction, highlighting the reduced electrical energy demand of the paired process compared to conventional CO_2 reduction [Wu2021].

The exact mechanism of methanol oxidation on metal oxides and hydroxides is the focus of ongoing research. In the present work, methanol oxidation to formate is investigated on a copper-based electrode. Heli et al. proposed a generalized mechanism for methanol oxidation on copper in alkaline solution involving a redox reaction forming a Cu^{III} species (Equation 2.23), which catalyzes the oxidation of methanol and its intermediates to a product such as formate or carbonate (Equations 2.24 and 2.25) [Heli2004]. Copper(II) oxide (CuO) or copper(II) hydroxide ($Cu(OH)_2$) were proposed as Cu^{II} species and copper oxyhydroxide (CuOOH) or a radical depicted as $CuOO^{\bullet}H$ as Cu^{III} species [Wang2023; Heli2004; Wels1990].

$$Cu^{II} \longrightarrow Cu^{III} + e^{-} \tag{2.23}$$

$$Cu^{III} + CH_3OH_{ads} \longrightarrow Cu^{II} + intermediate \tag{2.24}$$

$$Cu^{III} + intermediate \longrightarrow Cu^{II} + product \tag{2.25}$$

For further details on the reaction mechanism of methanol oxidation or general alcohol oxidation on metal oxides and hydroxides at alkaline conditions please refer to existing mechanistic studies [Heli2004; Flei1972; Wang2023; Phan2024].

3. Methanol oxidation to formaldehyde

Parts of this chapter have been published as:
Jonas Baessler, Tamara Oliveira, Robert Keller, and Matthias Wessling *Paired electrosynthesis of formic acid from CO_2 and formaldehyde from methanol*
ACS Sustainable Chemistry & Engineering, 2023
DOI: 10.1021/acssuschemeng.2c07523

3.1. Introduction

Electrochemical partial oxidation of methanol to formaldehyde exhibits favorable characteristics as anodic reaction for CO2R: the theoretical energy demand is lower, as the standard potential (0.33 V vs. SHE) is lower than for OER (1.23 V vs. SHE) [Hayn2017] and the reaction provides added value, as the product formaldehyde (1.02 – 2.03 $/kg) [Reus2010] has a higher market price than the feedstock methanol (0.4 $/kg) [ICIS2007]. Additionally, paired electrolysis is feasible only if there is sufficient demand for both the anodic and the cathodic product [Na2019; Vass2021]. The large market size of formaldehyde, with an annual production of over 30 Mt/year [Bahm2016], provides sufficient demand for pairing with large-scale CO2R processes to bulk chemicals (e.g. $CO, C_2H_4, HCOOH$). Furthermore, formaldehyde from methanol is beneficial from a downstream perspective: commercial grade formaldehyde solutions consist of 37-50 wt% formaldehyde in aqueous solution with up to 15 wt% methanol [ICIS2010]. Starting with an aqueous product mixture may facilitate purification compared to other alternative anodic reactions as water and unreacted methanol can remain in the final product. Lastly, methanol is a promising platform chemical, which can be used as liquid fuel or as raw material for synthetic hydrocarbons and their products. Similar to hydrogen, it has the potential of an alternative energy carrier to substitute fossil feedstocks, if produced with renewable resources [Olah2018].

The electrochemical methanol oxidation reaction (MOR) on platinum (Pt) was extensively studied in the past decades, almost exclusively in the context of fuel cell applications aiming at efficient full oxidation of methanol to CO_2 [Wasm1999; Iwas2002; Liu2006]. Both formaldehyde and formic acid have been identified as intermediates of aqueous methanol oxidation on platinum electrodes [Ota1984; Iwas2002]. However, partial oxidation of methanol has received far less attention than its full oxidation. Up to date, studies analyzing methanol oxidation to formaldehyde on platinum are driven by a mechanistic understanding, disregarding the targeted synthesis of formaldehyde from methanol [Ota1984; Chil1999; Bati2003]. The

Faraday efficiency (FE) of formaldehyde formation was reported to decline to nearly zero within an hour [Ota1984] limiting technical applicability. In other cases, high Faraday efficiencies were reported at low current density for a short electrolysis duration of minutes [Chil1999; Bati2003].

To the best knowledge of the author, Batista et al. [Bati2003] report the highest FE of partial methanol oxidation to formaldehyde with up to 65% at an average current density of 0.014 $mA\,cm^{-2}$. Higher current densities of up to 40 $mA\,cm^{-2}$ were reported only at significantly lower FE < 7% of formaldehyde formation [Ota1984; Chil1999]. If not reported in the original work cited above, the current density and FE was calculated from the reported charge, experiment duration, electrode area, and amount of formaldehyde.

This work studies methanol oxidation to formaldehyde on platinum-coated titanium sheets in a flow cell within a current density range of 25 to 100 $mA\,cm^{-2}$. Formaldehyde formation was observed on both metallic (Pt) and oxidized platinum (Pt_{Ox}). Comparing MOR on both electrodes, Pt_{Ox} reached a higher FE for formaldehyde, while Pt required a lower potential. Finally, the viability of MOR to formaldehyde as anodic reaction paired with CO2R was investigated and compared to OER in terms of cell potential, FE, and the amount of products formed per energy input. It was found that both paired processes with methanol oxidation on Pt and Pt_{Ox} used electrical energy more efficiently than CO2R paired with OER. The results of this work provide the basis for further research on paired processes with improved stability, lower overpotential, and a higher selectivity for partial methanol oxidation.

3.2. Material and methods

3.2.1. Materials

Methanol (CH_3OH, EMSURE, Supelco, $\geq$99.9%), sulfuric acid (H_2SO_4, AVS TITRINORM, 2.5 mol/L), potassium hydrogencarbonate ($KHCO_3$, AnalaR NORMAPUR, $\geq$99.5%) and perchloric acid ($HClO_4$, Bernd Kraft, 1 mol/L) were purchased from VWR. All chemicals were used without further purification and were diluted to the desired concentrations with deionized water. The cation exchange membrane (F-14100) were bought from Fumatech. The platinum and iridium oxide (IrO_2) plate electrodes were purchased from MAGNETO special anodes. The platinum electrode was a titanium sheet with a thermal platinum coating, the iridium oxide electrode was a titanium sheet with a IrO_2 coating. The tin-based gas diffusion electrode for CO2R was prepared by spray coating carbon paper (Freudenberg H23C6) with a suspension of 200 mg tin particles (<100 nm, IoLiTec) in 2 mL isopropanol with 0.08 mL PFSA dispersion (FLN-905, Fumatech). The Sn-loading of the GDE was $3.5 \pm 0.5\,\mathrm{mg\,cm^{-2}}$.

3.2.2. Anode pretreatment and characterization

A titanium sheet coated with platinum was used as anode in the metallic (Pt) and oxidized (Pt_{Ox}) state. Before each experiment, the anode was pretreated by a cyclic voltammetry in $0.1\,\mathrm{mol\,L^{-1}}$ $HClO_4$. Scans were performed from -0.1 V to 1 V at a scan rate of $100\,\mathrm{mV\,s^{-1}}$, stopping after the 10th cycle at 0.4 V to obtain the metallic Pt electrode. The oxidized platinum anode was prepared by subsequently oxidizing the metallic platinum anode in the same electrolyte that was used for methanol oxidation ($8\,\mathrm{mol\,L^{-1}}$ CH_3OH in $0.5\,\mathrm{mol\,L^{-1}}$ H_2SO_4). The pre-oxidation was conducted at a constant potential of 2 V for 3 min. For all experiments on methanol oxidation conducted in the electrochemical flow cell, the pretreatment was performed directly within the flow cell. For pretreatment of the samples used for electrode characterization, a beaker was used instead of the flow cell to allow quick removal of the electrodes from the electrolyte. It should be noted that

platinum oxide is reduced in the presence of methanol (see Figure 3.10). Therefore, the electrode samples for characterization were quickly removed from the electrolyte and rinsed thoroughly with deionized water within 10 seconds after oxidation. Samples of the Pt and Pt_{Ox} electrodes were characterized by scanning electron microscopy (SEM), energy dispersive X-ray spectroscopy (EDX), X-ray photoelectron spectroscopy (XPS), and X-ray diffraction analysis (XRD). SEM was performed using a Hitachi SU5000 equipped with a Bruker XFlash 6160 detector for EDX. XPS was carried out on a Kratos Analytical Ultra AxisTM spectrometer. XRD was performed using a Bruker D2 Phaser.

3.2.3. Flow cell setup and reaction conditions

All experiments were conducted in an electrochemical flow cell with an active geometric surface area of 40 cm^2 at room temperature (21 °C - 23 °C). The anolyte and catholyte compartments had a thickness of 2 mm and were separated by a cation exchange membrane (Fumatech, F-14100). For MOR, pretreated platinum electrodes were used in metallic (Pt) and oxidized state (Pt_{Ox})(see chapter 3.2.2). Methanol oxidation was conducted at constant current in 0.5 mol L^{-1} H_2SO_4 with 8 mol L^{-1} CH_3OH. For OER, an iridium oxide (IrO_2) electrode in 0.5 mol L^{-1} H_2SO_4 was used. Cathodic CO2R was performed at a tin-based gas diffusion electrode (Sn-GDE) in 1 mol L^{-1} $KHCO_3$.

The flow cell was operated with two separate cycles of electrolyte and a CO_2 line as shown in Figure 5.2. The reservoir bottle for each electrolyte cycle was filled with a volume of 100 mL. The electrolytes were circulated with a volumetric flow rate of 100 mL min^{-1} (mean linear flow velocity of about 20 mm s^{-1} at the electrodes) from bottom to top of the flow cell using a multichannel peristaltic pump (Cole-Parmer, Masterflex L/S Standard Digital Drive with an 8-Channel pump head).

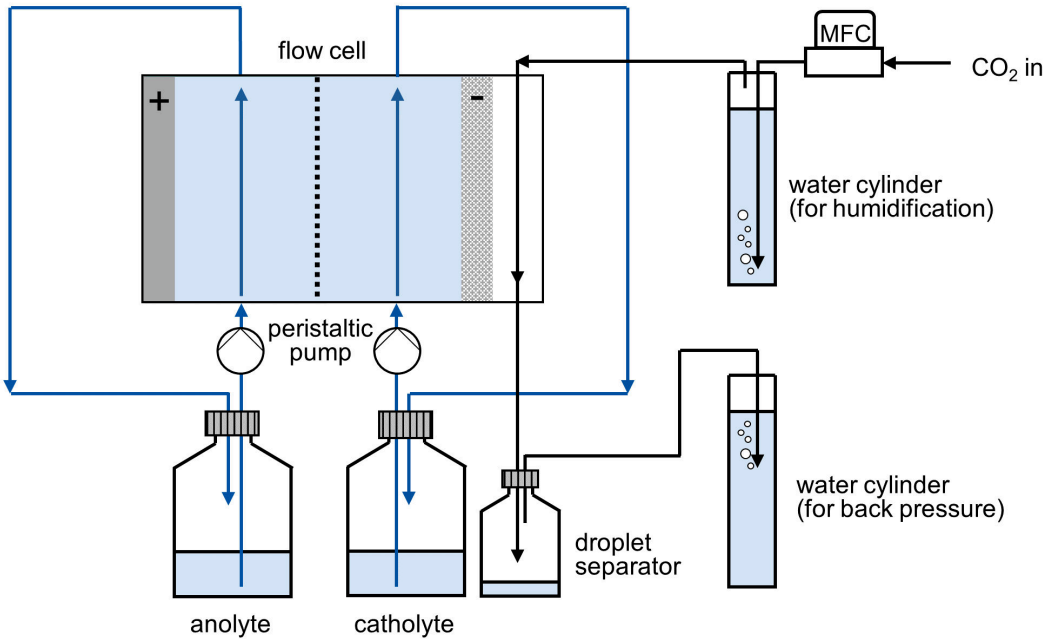

Figure 3.1.: Sketch of the experimental setup with two separated cycles of electrolyte (blue arrows) and the CO_2 flow (black arrows).

The reservoir bottle in each electrolyte cycle was open to the atmosphere to avoid pressure buildup by gas formation. The flow of CO_2 was set to 300 mL min^{-1} with a mass flow controller (Alicat Scientific, MC-5SLPM-D-DB9M/CM). The CO_2 flow was humidified by dispersing the gas flow with a porous ceramic frit in a water-filled cylinder. The CO_2 flow was led from top to bottom of the flow cell. A small bottle was placed in the CO_2 flow behind the flow cell. The small bottle catched droplets in case the electrolyte breaks through the gas diffusion electrode and allowed to observe the amount of liquid breakthrough. The back pressure was set by submerging the gas outlet in a water cylinder (typically 10 - 20 cm) so that neither gas nor electrolyte was breaking through the gas diffusion electrode.

3.2.4. Electrochemical measurements

All electrochemical measurements were performed using a BioLogic VSP potentiostat with a 10 A booster. The potentials were measured using a silver chloride reference electrode (eDAQ, Leakless Miniature Ag/AgCl), which was placed in the anolyte compartment of the flow cell. The measured potentials were subsequently converted in reference to the reversible hydrogen electrode (RHE). Electrode potentials were iR-drop corrected. Ohmic resistances were determined by impedance spectroscopy scanning from 1 Hz to 100 kHz with an amplitude of 20 mV around open circuit potential. Linear sweep voltammetry was performed in the flow cell at a scan rate of $5\,\mathrm{mV\,s^{-1}}$ starting from open circuit potential. Methanol oxidation was conducted at a constant current, recording the potential of both anode and cathode against the reference electrode every 1 s. To investigate potential oscillations during methanol oxidation the potential was measured every 0.01 s. The open circuit potential of the Pt_{Ox} electrode in $0.5\,\mathrm{mol\,L^{-1}}$ H_2SO_4 with $4\,\mathrm{mol\,L^{-1}}$ CH_3OH was measured every 0.2 s directly after the pre-oxidation procedure.

3.2.5. Analytics

Electrolyte samples were taken with a syringe, diluted 1:9 in DI water, and stored in HPLC vials at 4 °C. The samples were analyzed by HPLC with a refractive index detector (Agilent Technologies, 1260 Series). A RSpak DE-413L column (Shodex) was used with a 10 mmol L^{-1} H_3PO_4 solution as eluent. Temperature was set to 45 °C. The injection volume was 10 µL, the eluent flow was 1 mL min^{-1}. An example of a chromatogram is shown in figure 3.2. All Faraday efficiencies were calculated based on the cumulative charge and concentration (see chapter 2.2).

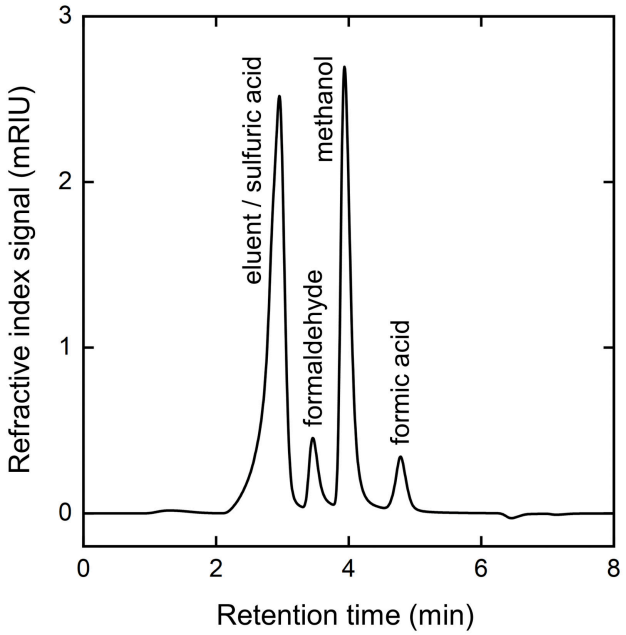

Figure 3.2.: Chromatogram of a prepared solution containing 0.35 mol L^{-1} formaldehyde, 7.82 mol L^{-1} methanol and 0.23 mol L^{-1} formic acid in 0.5 mol L^{-1} sulfuric acid.

3.3. Results and discussion

3.3.1. Characterization of platinum anodes

The SEM images of the Pt and Pt_{Ox} electrode in Figure 3.3 show an identical rough and porous surface structure for both electrodes. No significant change of the surface morphology by the oxidation was observed. The EDX spectra shown in Figure 3.4 exhibited a strong platinum signal for both the Pt and Pt_{Ox} electrode and a pronounced oxygen peak for the Pt_{Ox} electrode. At an accelerating voltage of 15 keV a signal of the titanium sheet below the platinum coating was detected. At 5 keV no titanium signal was observed due to the lower penetration depth of the electrons at a lower accelerating voltage. Other elements or significant impurities in the commercial platinum coating can be excluded, as as no other EDX signals were observed.

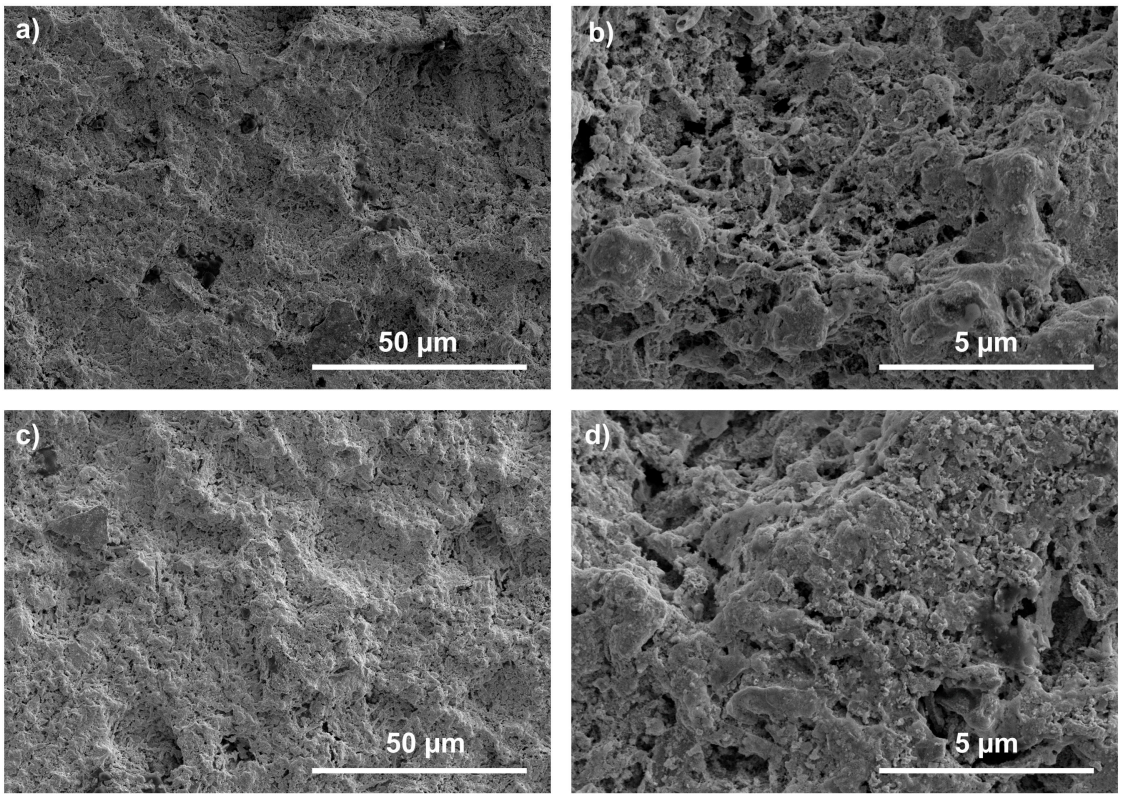

Figure 3.3.: SEM images of (a,b) the Pt electrode and of (c,d) the Pt_{Ox} electrode.

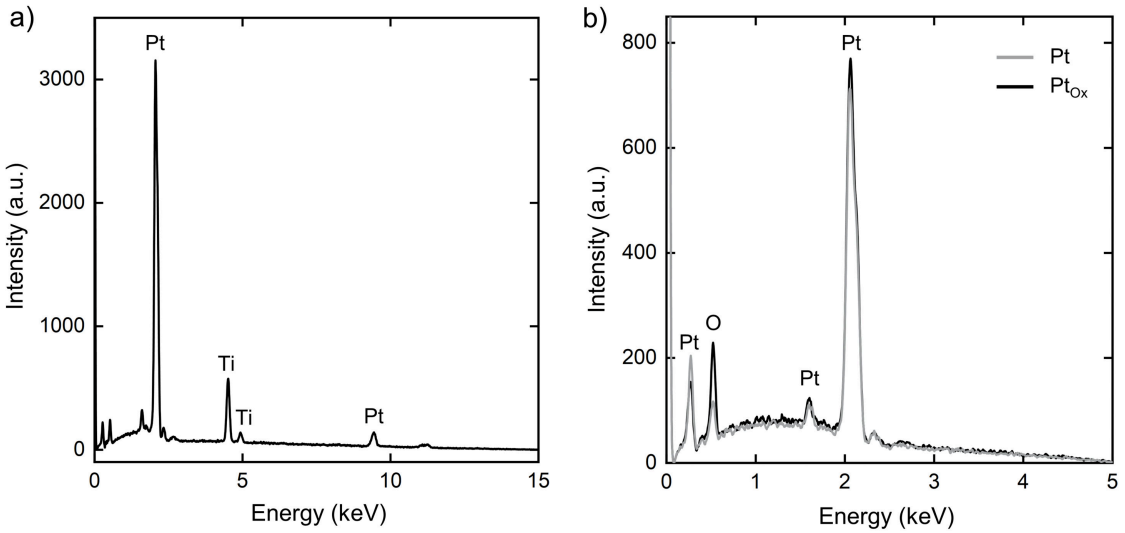

Figure 3.4.: EDX spectra of (a) Pt at an accelerating voltage of 15 keV and of (b) Pt and Pt_{Ox} at an accelerating voltage of 5 keV.

The XPS in Figure 3.5 and XRD spectra in Figure 3.6 of Pt and Pt_{Ox} were similar. Most likely a large fraction of the oxide was reduced directly after the oxidation pretreatment despite the quick removal of the electrode from the methanol containing electrolyte. Although the spectra of Pt and Pt_{Ox} did not show large differences, both XPS and XRD indicated the presence of Pt^{4+}/PtO_2 in the Pt_{Ox} electrode. The presence of PtO_2 in the Pt_{Ox} electrode is in good agreement with the electrochemical measurements, as the anode potential during methanol oxidation on Pt_{Ox} was high enough for platinum oxidation to PtO_2.

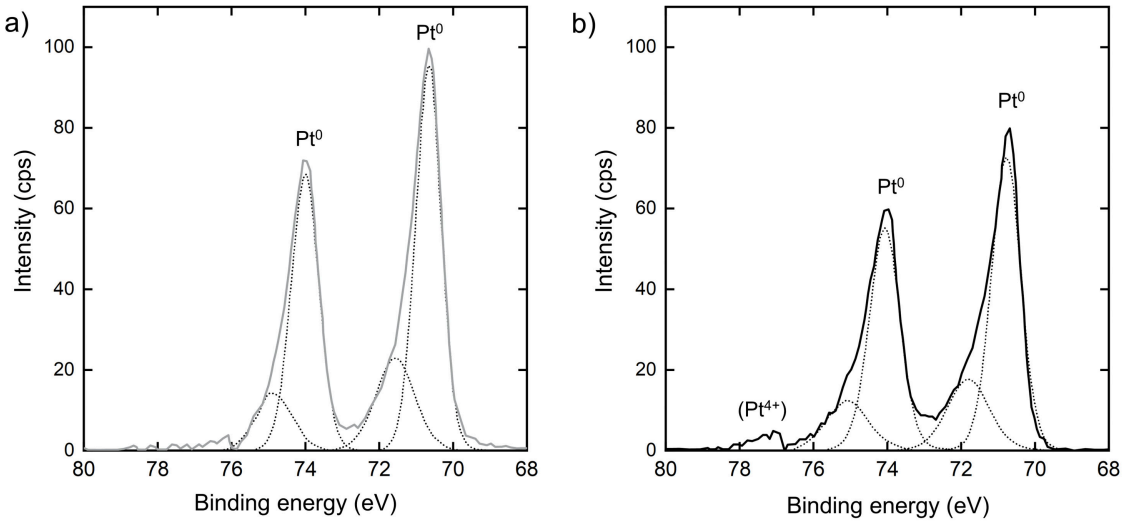

Figure 3.5.: XPS spectra (Pt 4f) of (a) Pt and (b) Pt_{Ox}. Next to the Pt^0 peaks, both spectra exhibited smaller peaks (unlabeled), which could originate from an adsorbate contribution or Pt^{2+}. [Mom2019]

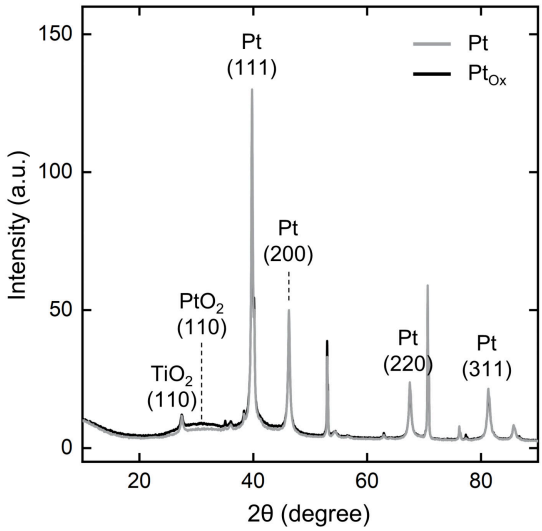

Figure 3.6.: XRD spectra of Pt and Pt_{Ox}.

3.3.2. Methanol oxidation on platinum and platinum oxide

For comparison of the electrode potential required for MOR in comparison to OER, linear sweep voltammetry was performed in the flow cell. Figure 3.7 shows the linear sweep voltammetry of MOR at a platinum electrode compared to OER at both an IrO_2 and a Pt_{Ox} electrode. The platinum electrode exhibited an onset potential of 0.5 V for MOR, which was significantly lower than the potential required for OER with the IrO_2 or Pt_{Ox} electrode. Compared to OER on the IrO_2 electrode, MOR on platinum starts at a 0.9 V lower potential. Thus, the LSV confirmed experimentally that MOR can be operated at a lower potential compared to OER.

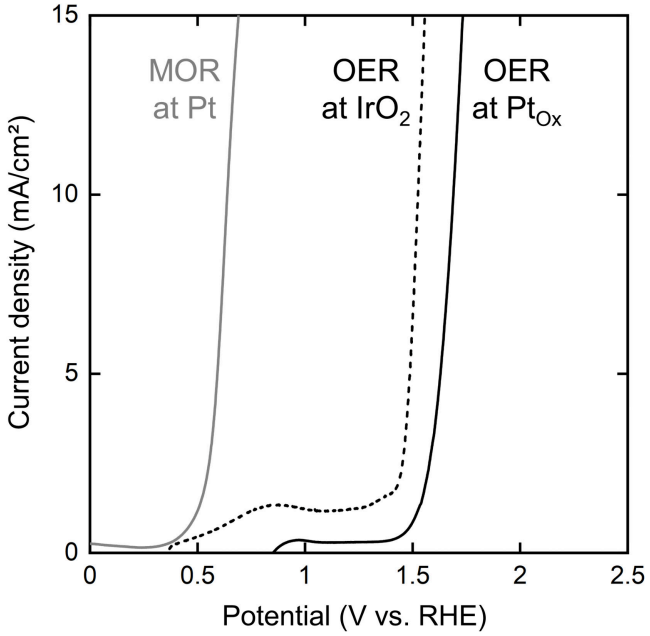

Figure 3.7.: Linear sweep voltammetry at a scan rate of 5 mV s^{-1} for MOR on platinum in 0.5 mol L^{-1} H_2SO_4 with 4 mol L^{-1} CH_3OH compared to OER on platinum oxide and iridium oxide in 0.5 mol L^{-1} H_2SO_4.

The selectivity of methanol oxidation to formaldehyde was studied on platinum and oxidized platinum electrodes at current densities of $25 - 100$ mA cm^{-2}. The Faraday efficiencies for formaldehyde formation are shown in Figure 3.8a with literature results for comparison.

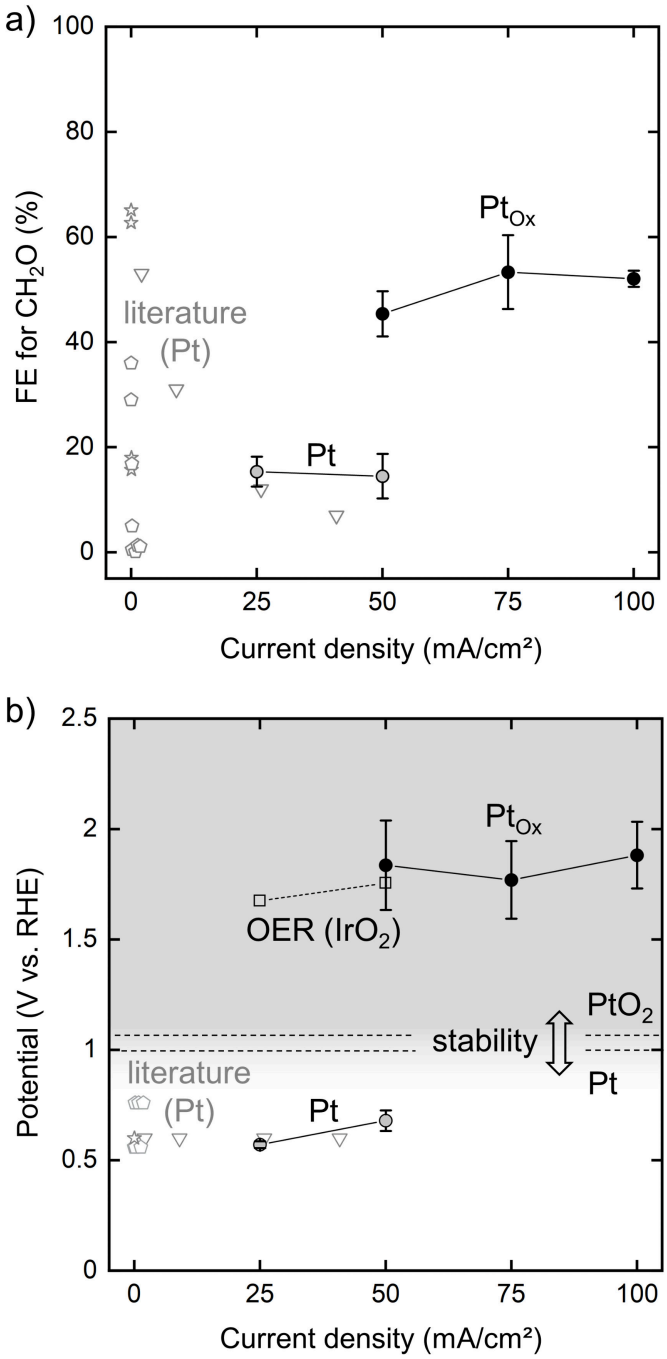

Figure 3.8.: (a) FE for methanol oxidation to formaldehyde on platinum (Pt) and oxidized platinum (Pt_{Ox}) electrodes at different current densities. Methanol oxidation was conducted at constant current for 60 min in 8 mol L^{-1} CH_3OH in 0.5 mol L^{-1} H_2SO_4 and was paired with cathodic hydrogen evolution. The error bars represent mean and standard deviation calculated from triplicates. The open gray symbols represent literature results (triangle: Ota et al. [Ota1984], pentagon: Childers et al. [Chil1999], star: Batista et al. [Bati2003]). (b) Corresponding anode potentials vs. RHE averaged over the experiment duration with the potential of OER on a IrO_2 electrode for comparison (open squares). The horizontal dotted lines indicate the potential regions at pH 0 in which metallic platinum and platinum dioxide are stable. [Lyon2010]

The cathodic reaction was the hydrogen evolution reaction (HER) in both the present results and in literature. The mean FE for formaldehyde on platinum was 15% at 25 mA cm^{-2} and 14% at 50 mA cm^{-2}. Thus, the current density had no significant effect on the FE towards formaldehyde at the tested conditions. Charge not contributing to formaldehyde formation likely formed additional oxidized products, namely formic acid and carbon dioxide. Formic acid was measured in the product mixture corresponding to about 30% FE on Pt and about 20% FE on Pt_{Ox}. Carbon dioxide was not detected directly, but gas evolution was observed. Carbon dioxide is expected to be the only gaseous product for metallic platinum, as the potential was lower than the standard potential of 1.23 V required for oxygen evolution [Hayn2017]. On platinum oxide higher mean Faraday efficiencies were observed, starting at 45% at 50 mA cm^{-2} and reaching a maximum of 53% at 75 mA cm^{-2}. Increasing the current density further to 100 mA cm^{-2} had no significant effect on the FE towards formaldehyde. Besides the formaldehyde produced, formic acid was the major side product on platinum oxide. While similar Faraday efficiencies were reported in literature on platinum before, the current density achieved in this work on platinum oxide shows a 50-fold increase.

Figure 3.8b shows the average anode potentials corresponding to the experimental results shown in Figure 3.8a. The potential required for methanol oxidation on the platinum electrode was 0.57 V at 25 mA cm^{-2} increasing to 0.68 V at 50 mA cm^{-2}. Methanol oxidation on platinum required a significantly lower potential than OER on IrO_2. Methanol oxidation on the oxidized platinum electrode required a considerably higher potential of 1.84 V at 50 mA cm^{-2} than on platinum at the same current density. The potential at the oxidized platinum electrode did not increase clearly with increasing current density. At a current density of 100 mA cm^{-2} a mean potential of 1.88 V was measured. If increasing the current density increased the electrode potential as expected, the difference was small compared to the standard deviation within the triplicates. The average potential of the oxidized platinum electrode was well within the area in which platinum dioxide PtO_2 is stable [Lyon2010].

It is assumed that the significant difference of the required electrode potential for MOR on platinum compared to MOR on platinum oxide is connected to the different reaction mechanisms. It is well known that methanol oxidation on platinum proceeds via several oxidation steps in parallel reaction paths, with CH_2O, HCOOH, CO or CO_2 as possible products [Iwas2003; Bago1977]. The net reaction equation for the electrochemical oxidation of methanol to formaldehyde on platinum is shown in Equation 3.1.

$$CH_3OH \longrightarrow CH_2O + 2H^+ + 2e^- \tag{3.1}$$

Beyond the net reaction and the average potential shown in 3.8b it should be noted that periodic oscillations of the potential were observed for MOR on platinum. The oscillations were not observed for methanol oxidation on platinum oxide and were more uniform than potential fluctuations caused by gas evolution. Oscillations in the electrochemical oxidation of methanol on platinum are a complex, but known phenomenon [Lee2002; Li2008; Mart2008; Viel2014; Mell2018]. The oscillation cycle at constant current can be simplified as illustrated in Figure 3.9: At low potential stable adsorbed carbon monoxide is formed in a side reaction, which causes the potential to increase at constant current density to compensate the blocked platinum sites. The potential increases until hydroxide can adsorb on the platinum surface, which enables the oxidation of the adsorbed carbon monoxide to carbon dioxide. As the blocked sites are cleared, the potential decreases again and the cycle repeats [Li2008].

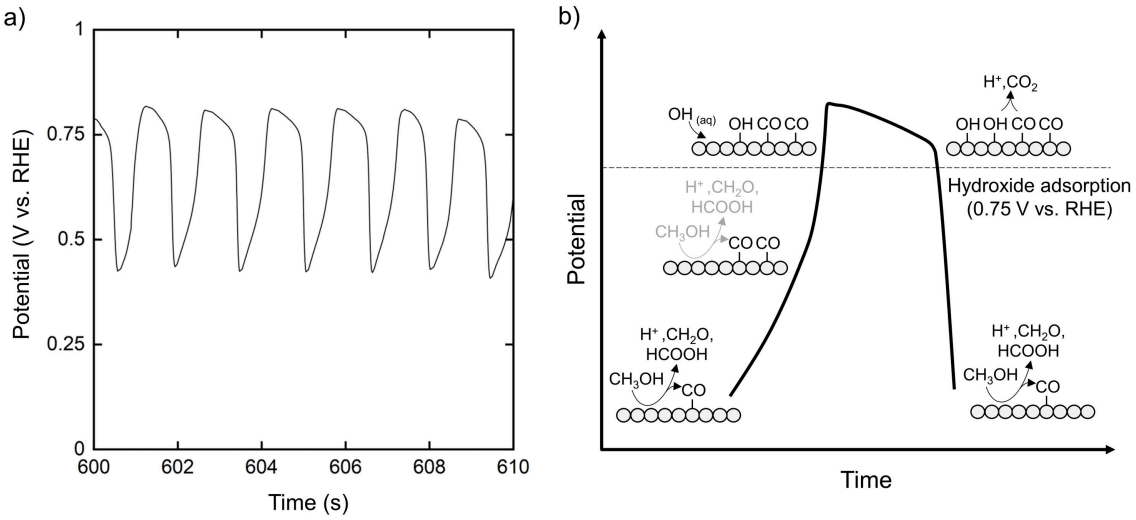

Figure 3.9.: (a) Potential oscillations of MOR on a platinum anode with 8 M CH_3OH in 0.5 M H_2SO_4 at a current density of 25 mA cm^{-2}. (b) Illustration of the oscillation cycle mechanism, the gray cycles represent the platinum surface.

The oxidation of methanol via platinum oxide is thought to involve a multi-step mechanism , as shown in a simplified version in Equations 3.2 and 3.3 [Sitt2008].

$$Pt + H_2O \longrightarrow Pt\text{-}O + 2H^+ + 2e^- \tag{3.2}$$

$$Pt\text{-}O + CH_3OH \longrightarrow CH_2O + H_2O + Pt \tag{3.3}$$

As platinum oxidation is involved in the reaction mechanism, the minimum required potential is higher with a standard potential of at least 1.0 V for platinum oxidation compared to 0.33 V for methanol oxidation to formaldehyde [Hayn2017]. To investigate the second oxidation step (Equation 3.3), the open circuit potential was recorded after pre-oxidation of the Pt_{Ox} electrode for 2 min at 2 V in 8 mol L^{-1} CH_3OH with 0.5 mol L^{-1} H_2SO_4. As shown in Figure 3.10, the open circuit potential was decreasing as reported in literature [Oxle1964; Bati2008; Sitt2008], indicating that the Pt_{Ox} electrode was reduced in the presence of methanol in a chemical redox reaction in the absence of an external electrical current.

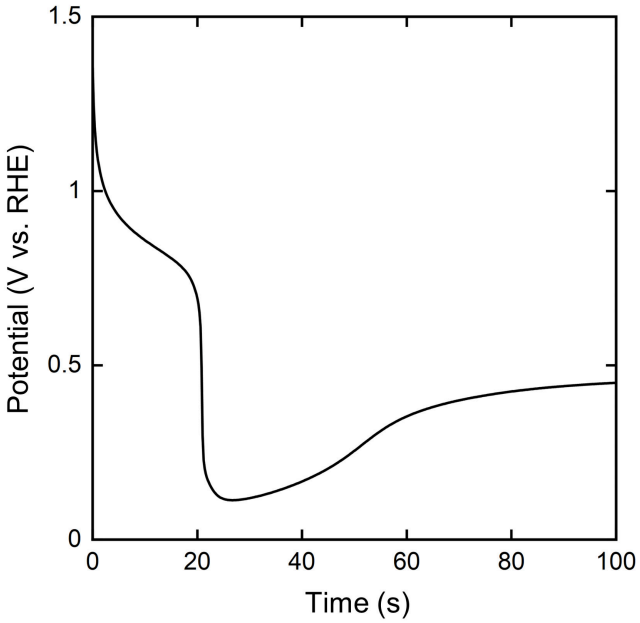

Figure 3.10.: Potential of the Pt_{Ox} electrode measured at open circuit directly after pre-oxidation for 2 min at 2 V in 8 mol L^{-1} CH_3OH with 0.5 mol L^{-1} H_2SO_4.

Neither platinum nor platinum oxide were stable at every current density. The platinum electrode was oxidized when 75 mA cm^{-2} were applied, indicated by a steep increase of the potential to the same level as required for methanol oxidation on platinum oxide. The platinum oxide electrode was reduced when 25 mA cm^{-2} were applied, indicated by a steep decrease of the potential to the platinum level. At 50 mA cm^{-2}, both platinum and platinum oxide were stable over 60 min of methanol oxidation.

The main advantage of methanol oxidation on platinum is the significantly lower anode potential compared to OER. In addition, formaldehyde and formic acid are formed as value-added products. However, a large share of the current contributes to the full oxidation of methanol to CO_2. The selectivity of methanol oxidation to formaldehyde is significantly higher on Pt_{Ox} than on Pt. In this study, formaldehyde was produced for the first time as the main product of the anode at relevant current density. While the FE of methanol oxidation to formaldehyde is promising for a new process, a further increase in selectivity is needed to make the electrochemical production of formaldehyde feasible. The following approaches might increase the selectivity further: In both methanol oxidation on Pt and Pt_{Ox}, it has

been observed that the anions present in the electrolyte can influence the reaction [Bati2003; Sitt2008]. The presence or adsorption of certain anions could favor the partial oxidation of methanol to formaldehyde. The partial oxidation of methanol to formaldehyde competes with the over-oxidation of already formed formaldehyde to formic acid and to CO_2. Higher mass transfer or pulsed electrolysis [Yuan2018] could favor the removal of formaldehyde from the electrode surface, thereby increasing selectivity. Full oxidation of methanol to CO_2 on Pt requires oxygen [Sako2017], which is provided by the oxidation of water in aqueous electrolytes. Methanol oxidation in anhydrous electrolyte [Béla1976] or from the gas phase in a gas diffusion electrode could favor the partial oxidation to formaldehyde.

3.3.3. Paired methanol oxidation and CO_2 reduction

Methanol oxidation at the anode was paired with cathodic CO_2 reduction in a flow cell as depicted in Figure 3.11.

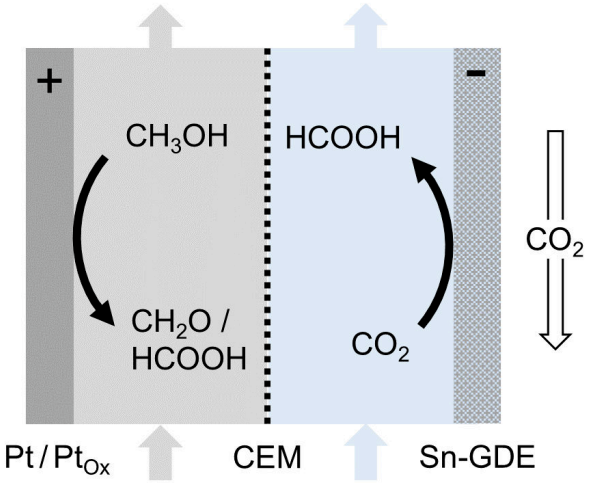

Figure 3.11.: Flow cell setup used for the paired electrolysis with platinum (Pt) or oxidized platinum (Pt_{Ox}) as anode for methanol oxidation and a tin gas diffusion electrode (Sn-GDE) as cathode for CO_2 reduction.

Figure 3.12a shows the cell potential of the three processes, as well as the potential of the anode, cathode and the ohmic drop (electrolytes & membrane) over the cell.

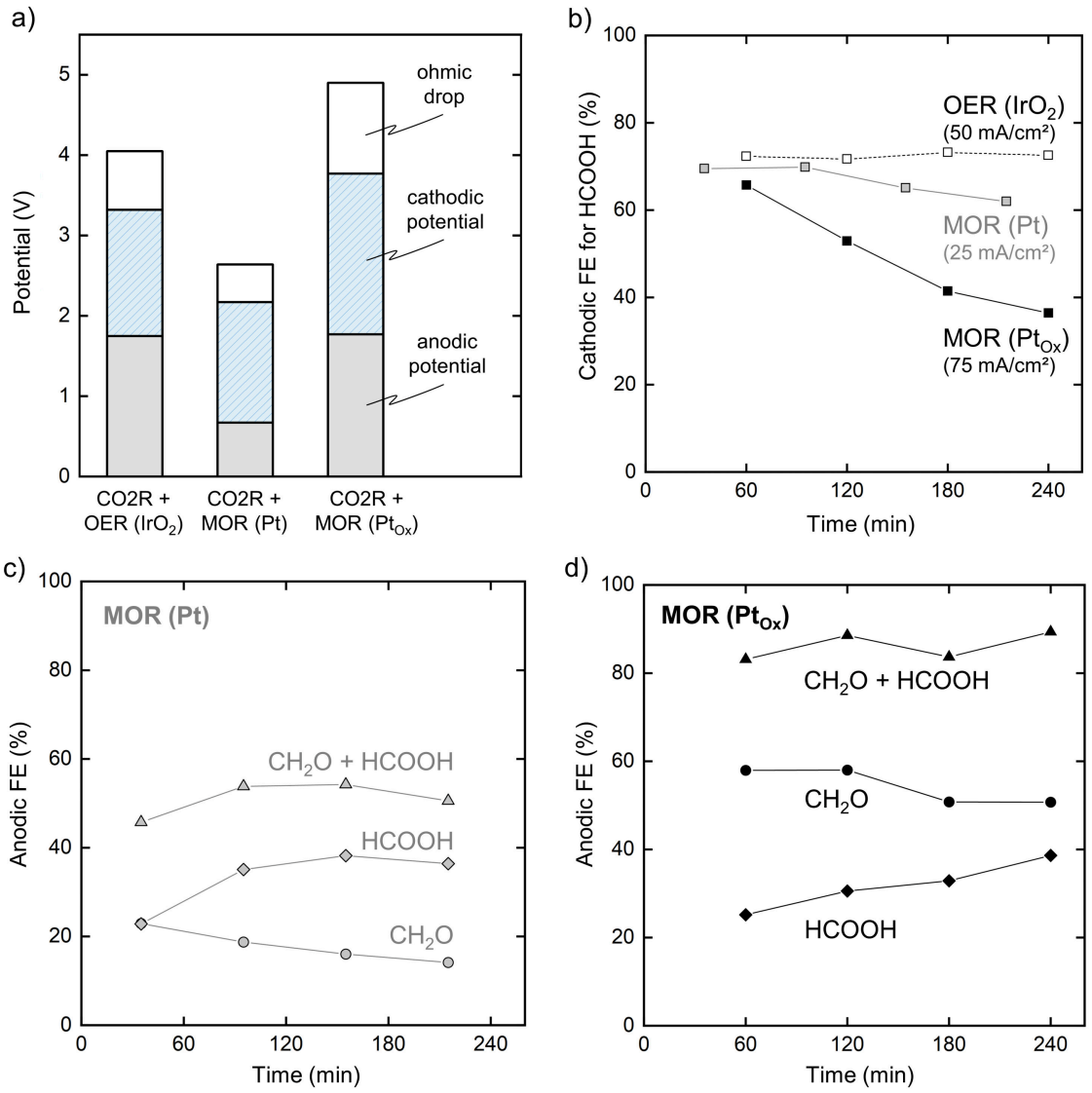

Figure 3.12.: (a) Cell potential for CO2R paired with different anodic reactions averaged over the experiments duration. The cell potential is divided into the potentials of the anode, cathode and the ohmic drop over the cell (electrolytes & membrane). The graphs (b-d) show the FE over time for both sides of the paired processes: (b) Cathodic FE for CO_2 reduction to formic acid in 1 mol L^{-1} $KHCO_3$ paired with different anode reactions. (c) Anodic FE for methanol oxidation on Pt at a current density of 25 mA cm^{-2} and (d) on Pt_{Ox} at 75 mA cm^{-2}. Shown are the anodic Faraday efficiencies for formaldehyde (circle), formic acid (diamond), and the sum of both value-added products (triangle). Methanol oxidation was conducted with 8 M CH_3OH in 0.5 M H_2SO_4.

The cell potential of CO2R paired with OER was 4.05 V divided into 1.75 V at the anode, 1.57 V at the cathode and 0.73 V of the ohmic drop. The anodic potential of CO2R paired with MOR on Pt of 0.67 V was 60% lower than for CO2R with OER, reducing the overall cell potential accordingly. CO2R paired with MOR on Pt_{Ox} had a slightly higher cell potential compared to CO2R with OER, with the benefit of a second value-added product. The higher cell potential was caused by the higher cathodic potential and ohmic drop, while the anodic potential was as high as for OER despite the higher current density. Please see Appendix A.1 for a comparison of the cell potentials at the same current density of 50 mA cm^{-2}. As Pt and Pt_{Ox} were not stable at 50 mA cm^{-2} for 4h in the paired process with cathodic CO2R, the cell potentials were measured over a shorter time span. The current density mainly affected the ohmic drop, while the anodic potentials of the paired processes with MOR on Pt or Pt_{Ox} at 50 mA cm^{-2} (Figure A.1) were similar to the anodic potentials shown in Figure 3.12a.

Figure 3.12b shows the FE at the cathode side for the reduction of CO_2 to formic acid over time for three different anode reactions. OER at IrO_2 was the reference reaction with a constant FE for formic acid of 72% over 4 h. With MOR on Pt as anode reaction, FE at the cathode was 69% for the first 90 min, which was comparable to the FE obtained with OER on IrO_2 at the anode side. After 90 min, the current density gradually declined to 62%. With MOR on Pt_{Ox} as the anode reaction, the FE started nearly as high as with MOR on Pt, but decreased continuously at a faster rate over time, reaching 36% after 4 h. It is hypothesized, that the decreasing cathodic FE was caused by methanol crossover from the anode to the cathode side where the methanol affected the wetting and selectivity of the Sn-GDE. Methanol in the catholyte was reported to increase wetting of GDEs used for CO_2 reduction and cause flooding [Leon2020]. Methanol crossover through polymer electrolyte membranes was investigated extensively in context of direct methanol fuel cells [Hein1999; Nebu2007; Ahme2011; Zhao2007]. Methanol crossover in the paired cell can be driven by two reported transport mechanisms: By diffusion due to the concentration gradient or by electro-osmotic drag along with hydrated protons passing the

membrane [Ahme2011; Zhao2007]. Electro-osmotic drag was reported to be the dominating transport mode during cell operation [Ahme2011], which would result in higher methanol crossover in the paired cell at higher current density. It is assumed, that the faster decline of the cathodic current density observed in combination with MOR at Pt_{Ox} was caused by the increased methanol crossover at higher current density. To test the effect of methanol on the cathode, 1 mol L^{-1} methanol was added to the catholyte without applying current. The addition of methanol dramatically changed the wetting behavior of the Sn-GDE and led to extensive electrolyte breakthrough into the gas compartment. The optimization of the cathode gas diffusion electrode towards a stable three phase boundary was beyond the scope of this work. In general, multiple approaches are feasible to prevent detrimental effects of methanol crossover. Methanol crossover could be mitigated by employing different ion exchange membranes. Special CEM membranes with low methanol crossover have been developed for direct methanol fuel cells [Ahme2011]. Other types of membranes such as anion exchange membranes (AEM) or bipolar membranes (BPM) could disable the main transport mechanism of methanol crossover, as the electro-osmotic drag of methanol is stopped if ions do not migrate from the anode to the cathode side [Li2018]. Methanol tolerance of CO2R could be increased by an omniphobic coating on the cathode or by using a zero-gap assembly, in which a membrane is pressed onto the cathode. Both could prevent breakthrough of the electrolyte through the electrode and thus mitigate the effect of methanol on CO2R.

Figure 3.12c shows the FE for formaldehyde, formic acid, and both products combined over time for MOR on a platinum anode. For MOR on Pt, the FE was initially 23% and decreased gradually over the duration of the experiment. The FE for formic acid was higher than for formaldehyde, rising at the beginning and then remaining relatively stable at around 35%. It is assumed that the change in the FE of formaldehyde and formic acid over time is caused by the increasing concentration of formaldehyde, which can be further oxidized to formic acid in a competing reaction. The FE for formaldehyde and formic acid together reached a maximum value of 54%. The final

concentrations reached after oxidation at constant current for 215 min were 0.11 mol L^{-1} for formaldehyde and 0.14 mol L^{-1} for formic acid, respectively.

Figure 3.12d shows the FE for formaldehyde, formic acid, and both products combined over time for MOR on an oxidized platinum anode. For MOR on Pt_{Ox}, the FE for formaldehyde reached 58% at the beginning and declined slightly over the duration of the experiment to 51% after 240 min. The FE for formic acid increased steadily from initially 25% to 38% at the end of the experiment. The FE for formaldehyde and formic acid combined increased slightly over time, since the decrease of formaldehyde was balanced by the slightly stronger increase of formic acid. The combined FE reached a maximum of 89%. The final concentrations reached after oxidation at constant current for 240 min were 1.14 mol L^{-1} formaldehyde and 0.43 mol L^{-1} formic acid, respectively. The formaldehyde concentration reached is several orders of magnitude higher than previously reported concentrations for electrochemical methanol oxidation [Chil1999; Bati2003; Ota1984]. No significant effect of the cathodic reaction on anodic MOR on Pt or Pt_{Ox} was observed. The Faraday efficiencies were comparable whether MOR was paired with CO2R or with HER.

The effect of different cell potential and FE of the paired processes in Figure 3.12 is merged into a single value in Figure 3.13, which shows the amount of products formed per electrical energy input. CO2R paired with OER yielded up to 3.5 mol of products per kWh. CO2R paired with MOR on Pt formed up to 7.3 mol of products per kWh. Both the lower cell potential and the value-added products of anodic MOR contributed to the higher amount of products. CO2R paired with MOR on Pt_{Ox} formed up to 5.2 mol/kWh with formaldehyde from the anode side contributing a larger share than for MOR on Pt. The total amount of products formed per energy input is lower for Pt_{Ox} than for Pt. However, the process with Pt_{Ox} was operated at a three times higher current density of 75 mA cm^{-2}, which could not be achieved with Pt. Although the contribution of cathodic CO2R to HCOOH decreased over time, both processes with MOR increased the amount of products formed per energy input compared to CO2R with OER.

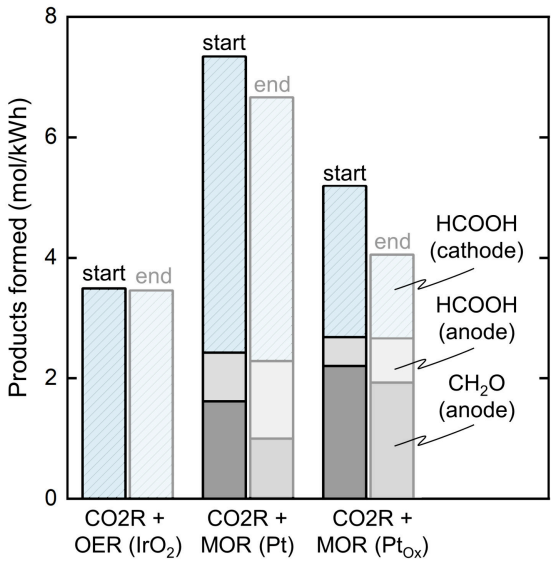

Figure 3.13.: Comparison of the products formed per electrical energy input for the three paired processes described in Figure 3. For each process two bars are shown, indicating the energy efficiency at the start (up to the first sample taken) and at the end of the experiment (up to the last sample taken). The total amount of products formed is divided into HCOOH produced at the cathode (light blue, hatched), as well as HCOOH and CH_2O produced at the anode (light gray and dark gray, respectively).

3.4. Conclusion

Anodic reactions to value-added products such as methanol oxidation can increase the efficiency of reactors for electrochemical CO_2 reduction. This work reports the electrochemical synthesis of formaldehyde by partial methanol oxidation in a flow cell. Methanol oxidation was investigated on platinum electrodes in metallic and oxidized state. Comparing methanol oxidation on both electrodes, the FE for formaldehyde was higher on oxidized platinum, while the potential was lower on metallic platinum. The high FE and potential are attributed to a reaction mechanism, in which platinum is oxidized electrochemically at a high potential, with the oxidized platinum subsequently acting as an oxidant favoring partial methanol oxidation if methanol is in sufficient excess. The results show that a trade-off exists between energy efficiency and FE.

For the first time, the present work demonstrated paired production of formaldehyde and formic acid by methanol oxidation at the anode and pro-

duction of formic acid by CO_2 reduction at the cathode. With oxidized platinum, a combined FE for formaldehyde and formic acid of up to 89% was achieved, reaching a final concentration of 1.14 mol L^{-1} formaldehyde in the paired process. With metallic platinum, the FE for partial methanol oxidation was lower with up to 54% for formaldehyde and formic acid combined. However, less anodic potential was required for methanol oxidation on metallic platinum than on oxidized platinum or for OER. Methanol oxidation was not affected by pairing with CO_2 reduction, while the FE of CO_2 reduction decreased over time when methanol oxidation was the anodic reaction instead of OER. The decreasing FE was attributed to methanol crossover to the catholyte causing flooding of the gas diffusion electrode. Several approaches were proposed to prevent the detrimental effects of methanol crossover in future studies. This work presents the first successful combination of CO_2 reduction with a paired anodic oxidation to formaldehyde as major product at relevant current density, FE, and product concentration. In terms of products formed per electrical energy input, both paired processes using methanol oxidation on metallic or oxidized platinum were more efficient than CO_2 reduction paired with OER. Further research on partial methanol oxidation, the elucidation of the reaction mechanism as well as measures mitigating methanol crossover are necessary to fully exploit the potential of the presented process.

4. Methanol oxidation to formate

Parts of this chapter have been published as:
Jonas Baessler, Niklas Vollmert, Jan Vehrenberg, Miriam Mineur, Sophia Schenke, Lukas Griesberg, Paulina Montero Pineda, and Robert Keller
Reaction engineering for high yield electrosynthesis: Unraveling the impact of reaction conditions and conversion on methanol oxidation to formate
Chemical Engineering Journal, 2024
DOI: 10.1016/j.cej.2024.153000

4.1. Introduction

Anodic methanol oxidation to formic acid presents a promising alternative to OER, as it possesses several favorable characteristics: Formic acid (0.64 - 1.30 $/kg, 29.4 - 59.8 $/kmol) holds higher value compared to methanol (0.34 - 0.58 $/kg, 10.9 - 18.6 $/kmol) [Joun2018; Intr2018a; Intr2018b; Na2019; Wei2021]. Moreover, the methanol oxidation reaction (MOR) to formate exhibits a standard potential of 0.1 V vs. SHE, which is significantly lower than the standard potential of OER, indicating its potential to reduce the electrical energy demand [Wei2021]. Formic acid and formate salts have a broad range of applications in agriculture, plastics, textile, and pharmaceutical industries [Hiet2010].

A broad range of catalysts have been developed and investigated for the electrochemical oxidation of methanol to formate with promising results: High Faraday efficiencies (FE) close to 100% and potentials lower than for typical OER have been reported [Wei2021; Wu2021; Li2020a; Li2020b; Xian2020; Xian2021; Du2023]. MOR has been paired successfully with HER to achieve a more efficient water electrolysis [Li2020a; Li2020b; Xian2020; Xian2021; Du2023] and was paired with CO2R to formate in a concurrent synthesis, which generates formate at both the cathode and anode [Wei2021; Wu2021]. These findings indicate great potential of MOR as an alternative anode reaction to replace OER. However, the achieved formate concentrations were either low or not reported in previous works. Neither the influence of an increasing product concentration has been yet investigated, nor the impact of reaction conditions, ion balance, or water transport. Low formate concentrations are associated with significant costs of downstream processing [Ramd2019] as the aqueous alkaline formate solution typically employed in MOR requires further purification to formate salts or formic acid. To proceed from the promising lab-scale results to an industrial application, it is crucial that MOR performance is investigated at high methanol conversion, considering the effects that arise with process intensification and increasing formate concentration.

In this work, the sensitivity of the FE towards methanol conversion was investigated in a flow cell at high current densities of up to 200 mA/cm^2. Further, the effect of different reaction conditions was analyzed by closely monitoring the reaction via Fourier-transform infrared spectroscopy (FTIR) at a high sampling rate. Copper(II) oxide (CuO) on copper foam was used as a catalyst in the form of a flow-through electrode, which had a very high surface area due to its hierarchical structure over multiple length scales. The impact of the current density, temperature, volume flow, and electrolyte composition on FE and obtainable conversion is investigated and discussed. Furthermore, the influence of different types of ion exchange membranes was assessed. It was investigated how the ionic balances affect the pairing of MOR with cathodic reactions, especially CO2R and HER. Finally, the insights on the reaction conditions were applied to tune the selectivity of MOR, reaching a maximum formate yield of 70 % at 100 mA/cm^2 with an anode potential of 1.33 V vs. RHE. In addition, the change in electrolyte volume is quantified and the implications of the water balance are discussed for paired processes at high conversion. The present results reveal the impact of conversion and reaction conditions on the FE and provide insights for operating MOR at high current density and high conversion in paired processes.

4.2. Material and methods

4.2.1. Materials

Table 4.1 and 4.2 provide an overview of the chemicals and materials used in the present work. All chemicals were used without further purification and were diluted to the desired concentrations with deionized water.

Table 4.1.: Overview of the chemicals used in the present work.

Substance	Formula	Supplier	Grade/Purity
Copper(II) sulfate	$CuSO_4$	VWR	AnalaR NORMAPUR, $\geq$99%
Formic acid	HCOOH	VWR	AnalaR NORMAPUR, $\geq$99%
Methanol	CH_3OH	Merck	EMSURE, Supelco, $\geq$99.9%
Potassium bicarbonate	$KHCO_3$	VWR	AnalaR NORMAPUR, $\geq$99.5%
Potassium hydroxide	KOH	VWR	GPR RECTAPUR, $\geq$85%
Sulfuric acid	H_2SO_4	VWR	AVS TITRINORM, 5 mol/L

Table 4.2.: Overview of the materials used in the present work.

Material	Supplier	Details
Bipolar membrane	Fumatech	Fumasep FBM-PK
Cation exchange membrane	Chemours	Nafion 212
Anion exchange membrane	Fumatech	Fumasep FAA-3-50
Copper foam	AlCarbon	POROFEN-Cu90, 2 mm, 90 ppi
Mixed metal oxide anode	Magneto	MMO coating on titanium sheet
Platinum cathode	Magneto	Pt coating on titatinum sheet
Nickel mesh cathode	Haver&Boecker	Aperture 0.5 mm, wire 0.14 mm

4.2.2. Anode preparation and characterization

The preparation of the anode was adapted with modifications from Huan et al. [Huan2017a; Huan2017b], using copper foam instead of a copper plate as substrate. Copper foam of 2 mm thickness with 90 pores per

inch was ultrasonically cleaned in acetone for 20 min. For electrodeposition of copper dendrites, an area of 50×50 mm of the cleaned copper foam was immersed into a solution of 0.2 mol/L $CuSO_4$ and 3 mol/L H_2SO_4 at 60 °C. A mixed metal oxide coated titanium sheet was used as the counter electrode. Copper dendrites were deposited onto the copper foam at a high current density of 1500 mA/cm^2 provided by a power supply (HMP4040, Rohde & Schwarz) for 60 s, corresponding to a charge of 90 C/cm^2. The solution was not stirred during deposition, as the copper coating was more homogeneous if the solution was only agitated by the gas evolution at both electrodes. After deposition, the foam was thoroughly cleaned with DI water and dried at room temperature. Subsequently, the foam was heated in an oven to oxidize the copper surface to copper(II) oxide (CuO). Starting from 25 °C, the temperature in the oven was increased at a rate of 10 °C/min up to the final temperature of 300 °C, which was maintained for additional 30 min. Figure 4.1 displays photographs of the untreated copper foam (a), the foam after the electrodeposition step (b), and after heat treatment (c). The part of the foam that was immersed during electrodeposition had a dark red color after deposition and drying, indicating the formation of copper(I) oxide (Cu_2O). The part of the foam that was not immersed retained the characteristic brighter copper color and was cut off before the subsequent heat treatment. After heat treatment, the foam exhibited a homogeneous black color, indicating complete oxidation of the surface to copper(II) oxide (CuO).

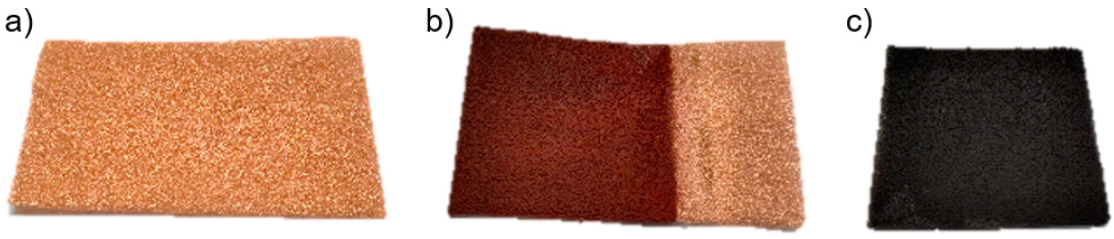

Figure 4.1.: Photographs of a) the untreated copper foam, b) the foam after electrodeposition, and c) after cutting to the final dimensions of 50×50 mm and heat treatment.

The electrode was analyzed after each preparation step by SEM, EDX, and XRD. SEM was performed using a Hitachi SU5000 equipped with a Bruker XFlash 6160 detector for EDX. The XRD measurements were performed on a Malvern Panalytical Empyrean X-ray diffractometer.

4.2.3. Flow cell setup and reaction conditions

The cell setup used for all experiments regarding the impact of conversion and the reaction conditions is depicted in the schematic of Figure 4.2a. All experiments were carried out in a flow cell with an active area of 5×5 cm (flex-E-cell, FXC Engineering). An exploded view of the flow cell is shown in Figure 4.2c. The flow direction of the anolyte and catholyte was from bottom to top. Two layers of copper foam coated with CuO dendrites as described in 'Anode preparation' (Chapter 4.2.2) were used as anode and a platinum (Pt) coated titanium sheet as cathode (Magneto Special Anodes). The electrodes were contacted via electrical contacts that were integrated into the gasket material. The anode was contacted via an integrated copper mesh placed between the two pieces of the CuO foam. The catholyte compartment had a thickness of 3 mm in which a compressible spacer was inserted. The anolyte compartment of the cell had a thickness of 3.5 mm, which was thinner than the two pieces of copper foam, each with a thickness of 2 mm. In the assembled cell, the foam electrodes were compressed to the thickness of the anolyte compartment ensuring that the foam completely filled the anolyte compartment.

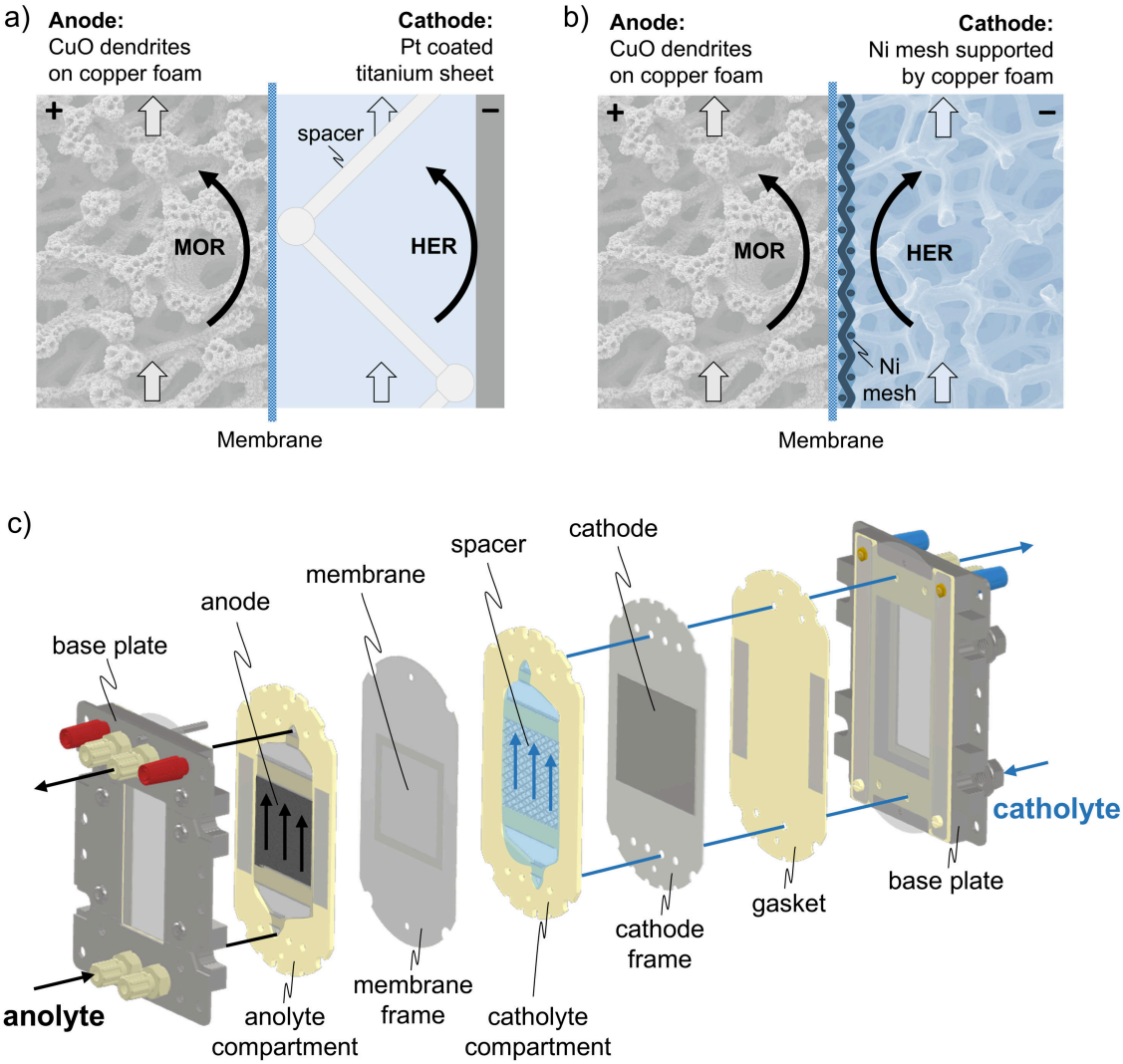

Figure 4.2.: (a) Schematic of the cell setup used for all experiments regarding the impact of the reaction conditions and (b) cell setup without electrolyte gap for demonstration of paired electrolysis. (c) Exploded view of the cell illustrating the electrolyte flow through the cell and the shape of the electrolyte compartments.

The electrolytes were recirculated with a peristaltic pump (Masterflex L/S Digital, Cole-Parmer) through the electrochemical flow cell and heat exchanger (flex-H-cell, FXC Engineering) for temperature control. Transparent fluorinated ethylene propylene (FEP) tubing was connected to the anolyte outlet of the cell for visual detection of gas evolution. The total anolyte volume was 54.5 mL. For the demonstration of paired electrolysis, the cell setup was changed to reduce the cell potential and a second reference electrode was placed in the catholyte. A nickel mesh (aperture width 0.5 mm, wire diameter 0.14 mm) supported by copper foam was used as cathode as shown in Figure 4.2b with 1 mol/L KOH as catholyte. Unless stated otherwise, the anode was reused within each series of experiments regarding one reaction condition parameter. Degradation of the anode was investigated by conducting electrolysis at each parameter setting in duplicate, first in ascending, then in descending order (e.g. 25 °C, 40 °C, 55 °C, 55 °C, 40 °C, 25 °C). If not specified otherwise, electrolysis was performed at a constant current density of 200 mA/cm^2, a temperature of 25 °C, a flow rate of 50 mL/min of both electrolytes, with 2 mol/L potassium hydroxide (KOH) and 1 mol/L methanol as anolyte, 2 mol/L potassium hydrogen carbonate as catholyte and a bipolar membrane (BPM) (Fumasep FBM-PK, Fumatech). The BPM was operated in reverse bias. As alternative membranes a cation exchange membrane (CEM)(Nafion 212, Chemours) and an anion exchange membrane (AEM)(Fumasep FAA-3-50, Fumatech) were used. Fig. 4.3 displays a sketch of the experimental setup with two separate electrolyte cycles. Starting from the flow cell the anolyte was led through a 3D-printed phase separator. The phase separator was used to remove gas from the electrolyte cycle and to exchange the electrolyte between experiments. From the phase separator, the anolyte was pumped with a peristaltic pump (large pump symbol: Masterflex L/S Digital, Cole-Parmer) at a flow rate of 25-100 mL/min through the heat exchanger and the electrochemical flow cell back to the phase separator. The mean linear flow velocity through the anode was approximately 3, 6, and 12 mm/s at volumetric flow rates of 25, 50, and 100 mL/min, respectively. A second cycle for the anolyte analytics was connected to the phase separator, in

which a peristaltic pump (small pump symbol: Reglo ICC, Ismatech) cycled a sample stream of the anolyte at 10 mL/min through the FTIR flow cell probe. The anolyte cycle was filled with anolyte from a reservoir bottle via an additional peristaltic pump (Reglo ICC, Ismatech). During methanol oxidation, this pump was turned off and the connection to the reservoir bottle was blocked. The catholyte side of the setup was identical to the anolyte side but without the analytics. The catholyte was continuously exchanged with fresh electrolyte from the reservoir bottle at a rate of 5 mL/min. The excess catholyte and the hydrogen formed at the cathode could escape the setup via the phase separator.

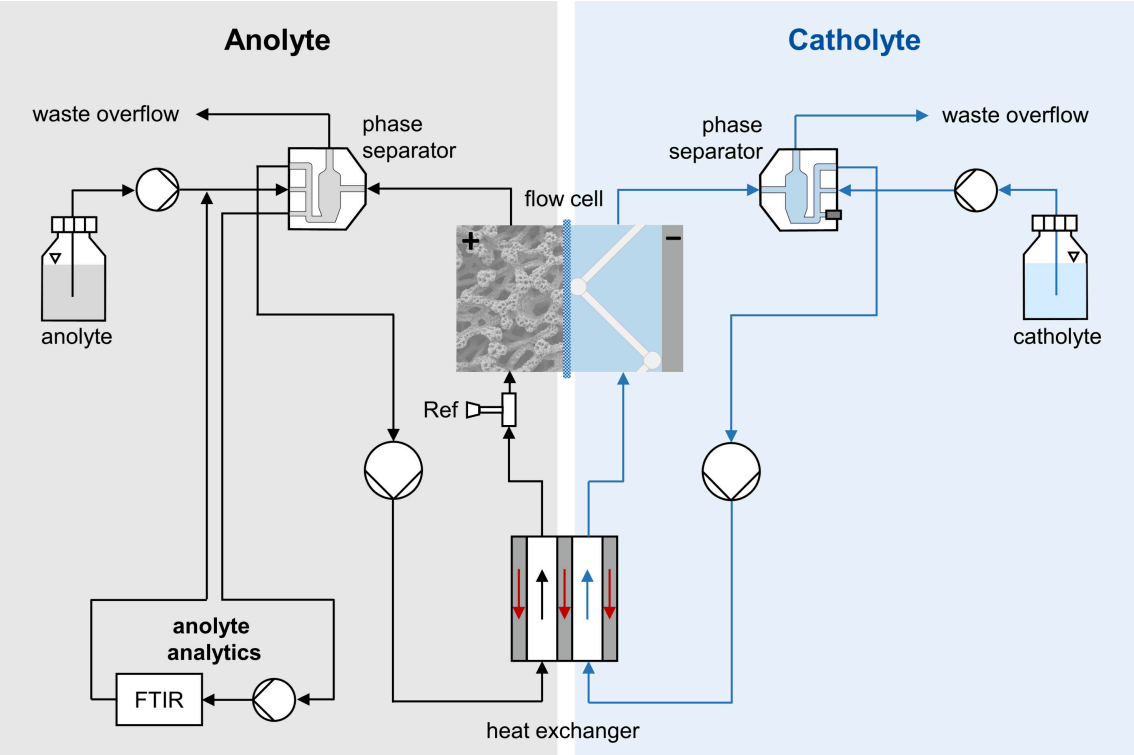

Figure 4.3.: Sketch of the experimental setup with two separate electrolyte cycles (gray: anolyte, blue: catholyte).

4.2.4. Electrochemical measurements

All electrochemical measurements were performed using a BioLogic VSP potentiostat with a 10 A booster. Potentials were measured using a reversible hydrogen electrode (Hydroflex RHE, Gaskatel), which was placed in the anolyte flow. Electrode potentials were not iR-drop corrected, if not stated otherwise. Ohmic resistances were determined by impedance spectroscopy scanning from 100 kHz to 10 Hz with an amplitude of 20 mV around open circuit potential. During impedance spectroscopy all pumps were stopped. Methanol oxidation was conducted at a constant current, recording the potential of both anode and cathode against the reference electrode every 0.5 s. To determine the potential across the membrane, a second reference electrode (Hydroflex RHE, Gaskatel) was placed in the catholyte flow. Using a second channel of the BioLogic VSP potentiostat, the potential of anode and cathode was additionally recorded against the second reference electrode. The membrane potential was calculated from the potential difference between the reference electrodes. Linear sweep voltammetry was performed in the flow cell at a scan rate of 5 mV/s starting from open circuit potential. The electrochemical active surface area (ECSA) was assessed by investigating the double layer capacitance by cyclic voltammetry. The settings for the ECSA measurement were adapted from Li et al. [Li2020c]. The ECSA measurements were conducted in a beaker with an aqueous solution of 1 mol/L KOH and a Platinum counter electrode. The potential was cycled from 1.3 to 1.4 V vs. RHE with 5 cycles per scan rate using the last cycle for evaluation.

4.2.5. Analytics and evaluation

A sample stream from the anolyte was circulated with a peristaltic pump (Reglo ICC, Ismatec) at 10 mL/min through the flow cell probe of a FTIR spectrometer (ReactIR 702L with Micro Flow Cell, Mettler Toledo). The concentrations of methanol, formate, and OH^- during electrolysis were measured by the FTIR spectrometer at a sample rate of 1 sample per 30 s. FTIR spectra were recorded in the wavenumber range of 4000 - 650 cm^{-1}

at a resolution of 8 cm^{-1} with a sample rate of 1 sample per 30 s using the spectrometer software (iC IR 7.1.91 SP1, Mettler Toledo). The flow cell probe of the FTIR was equipped with a diamond window which exhibits high transmission in a broad range of wavenumbers, except in the characteristic diamond region between 2250 - 1950 cm^{-1}. Figure 4.4a displays the FTIR spectra of the anolyte recorded during methanol oxidation at different percentages of methanol conversion and the spectrum of water. For analysis, the spectrum of water was subtracted from the spectra of the anolyte resulting in spectra as shown in Figure 4.4b. Distinct peaks for formate were observed at 1580 cm^{-1} and methanol at 1020 cm^{-1}. The intensity of the spectrum was shifting with changing KOH concentration. A peak of carbonate was closely overlapping with a second peak of formate.

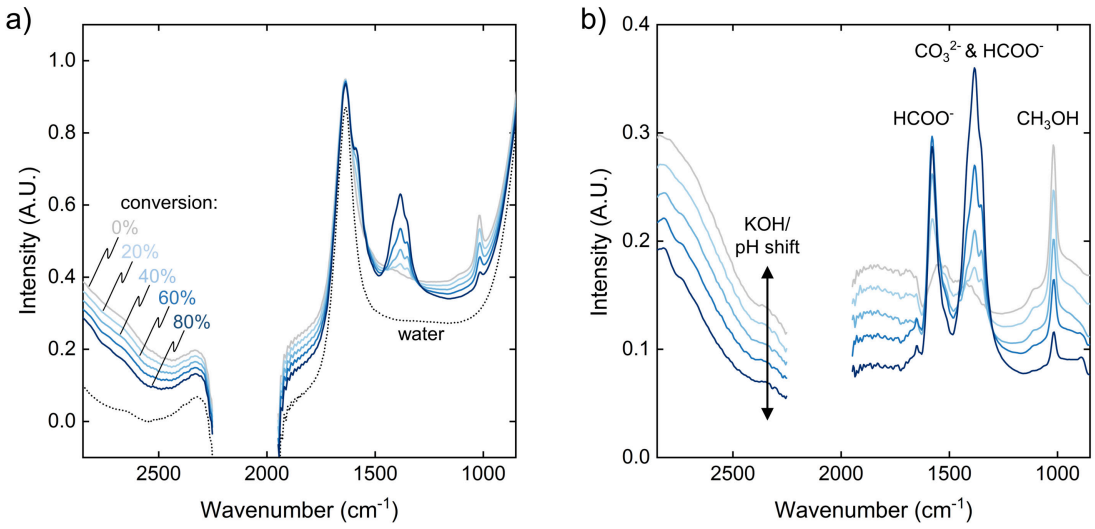

Figure 4.4.: (a) FTIR spectra of the anolyte recorded during methanol oxidation at 0, 20, 40, 60, and 80% conversion and the spectrum of water. (b) Spectra calculated by subtraction of the water spectrum from the spectra recorded during methanol oxidation. The oxidation was conducted at 200 mA/cm^2, 25 °C, 2 mol/L KOH, 1 mol/L methanol, with a BPM.

The peak areas of formate and methanol were evaluated as illustrated in Figure 4.5a. A region with no interfering peaks was evaluated for KOH. As calibration, the correlation between concentration and peak area was determined by measuring samples representing anolyte mixtures of known composition. The calibration samples were prepared in a volumetric flask by weighing each substance added. The measured weight was used to cal-

culate the actual concentration. Figure 4.5b-c shows the linear regression used for the quantification of formate and methanol. The linear regression was determined by the quantification software of the spectrometer (iC Quant 7.1.91, Mettler Toledo). KOH was quantified using a polynomial function fit of second order in OriginPro (Version 2022, OriginLab), as the correlation of the evaluated area to KOH concentration was slightly sublinear (Figure 4.5d).

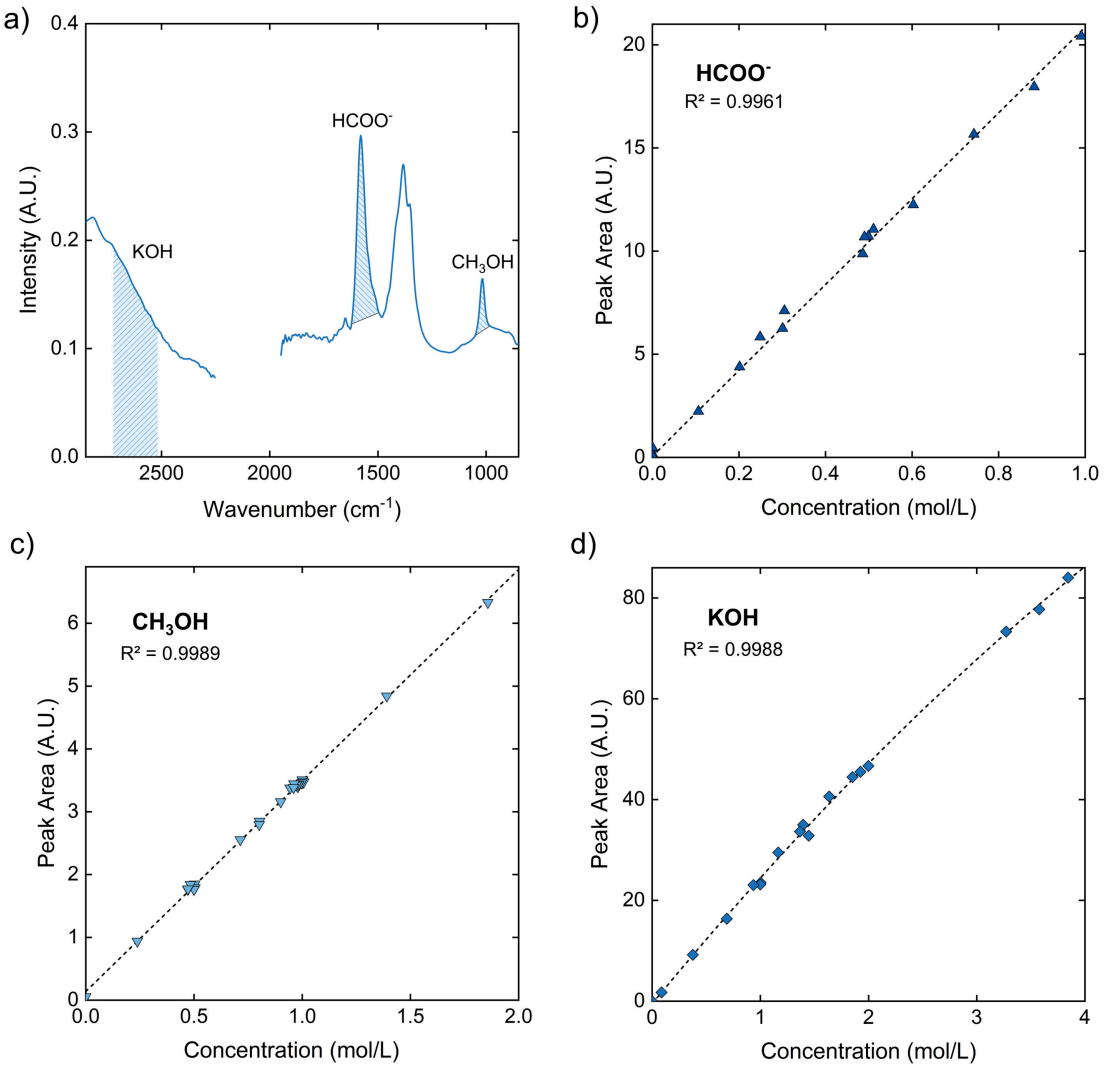

Figure 4.5.: (a) Peak area considered for KOH, $HCOO^-$ and CH_3OH (hatched areas), (b)-(d) calibration data for $HCOO^-$, CH_3OH and KOH (data points), illustrating the correlation of peak area to concentration. The fitted function used for analysis is displayed as a dashed line along with the corresponding R^2.

The concentration data obtained from the FTIR spectra was further processed and analyzed in Origin (OriginLab). Weighted adjacent averaging with a window size of 20 points was applied to the concentration data, which smoothed the data without altering the shape of the curves. Methanol conversion, FE, and formate yield were calculated from the smoothed concentration data according to Equations 4.1 - 4.3.

$$conversion = \frac{c_{0,methanol} - c_{n,methanol}}{c_{0,methanol}} \tag{4.1}$$

$$FE = \frac{zFV}{I} \cdot \frac{c_{n,formate} - c_{n-1,formate}}{t_n - t_{n-1}} \tag{4.2}$$

$$yield = \frac{c_{n,formate}}{c_{0,methanol}} \tag{4.3}$$

where c is the concentration of the regarding substance and the indices denote the start of the experiment (index 0), the current data point (index n) and the previous data point (index $n - 1$). z is the number of electrons transferred per reaction, F the Faraday constant, V the anolyte volume, I the current, and t the time.

To investigate crossover through the membranes, samples of the catholyte were taken after the experiments with different membrane types. The samples were taken with a syringe and analyzed via HPLC (Agilent 1200) with an organic resin column (CS-Chromatographie Service GmbH). The measurements were conducted with a 5 mmol/L H_2SO_4 eluent with a flow rate of 0.5 mL/min at 40 °C using a refractive index detector and a variable wavelength detector.

4.3. Results and discussion

4.3.1. Characterization of copper oxide electrodes

For the present study, copper dendrites were electrodeposited onto an open-cell copper foam at a high current density of 1500 mA/cm^2 and were subsequently oxidized by a heat treatment in air. After oxidation the color of the electrode changed from red to black, indicating an oxidation to CuO [Mile1937].

Figure 4.6 shows SEM images of the copper oxide electrode at four different magnification levels. The open-cell structure of the foam substrate provides large pores, allowing electrolyte flow through the 3D-structured electrode (Figure 4.6a). The pore diameter of the untreated foam is 730 µm $\pm$ 60 µm, which narrows slightly due to the growth of the dendrite layer. The dendrite layer has a cratered surface, caused by hydrogen bubbles during electrodeposition. The craters of the dendrite layer have a diameter of about 50 µm (Figure 4.6b). The deposited dendrite layer features a porous fractal-like structure with interconnected branches of 0.1-10 µm thickness (Figure 4.6c). The surface of the oxidized dendrites exhibits roughness down to the nanometer scale (Figure 4.6d). The electrode features a hierarchical structure with porosity and surface morphology on multiple length scales, thus providing a large surface area for electrochemical reactions.

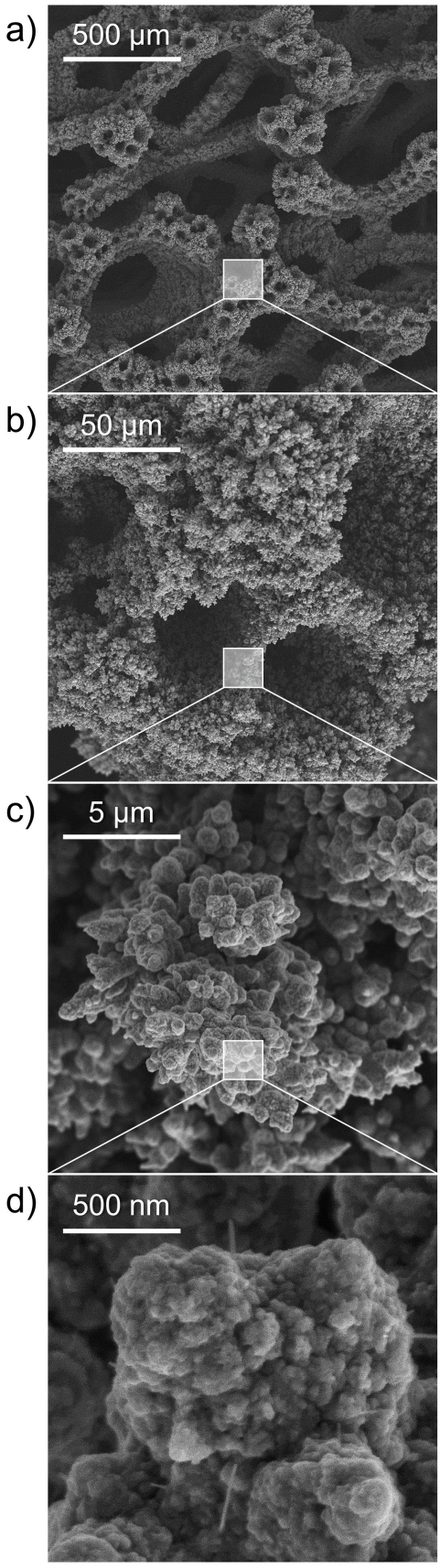

Figure 4.6.: SEM images of the prepared anode at four different magnification levels of ×50, ×500, ×5k and ×50k (a-d).

To understand the effect of each step on the electrode structure, the electrode was analyzed between each preparation step and after use for methanol oxidation. Figure 4.7 provides a comparison of SEM images of the copper foam at various stages of the electrode preparation and after use in a methanol oxidation experiment. Figure 4.7a reveals the open-cell structure of the untreated foam with 90 pores per inch and a pore diameter of about 730 $\pm$ 60 µm. The branches of the foam had a thickness of about 70 - 130 µm and exhibited a smooth surface. The electrodeposition led to the formation of copper dendrites on the branches of the foam (Figure 4.7b). Hydrogen evolution during the electrodeposition step resulted in craters with a diameter of 25-50 µm within the dendrite layer. The dendrites exhibited sharp edges on the micrometer scale, but a smooth surface on the nanometer scale. The microscopic electrode structure changed after the foam was oxidized by heat treatment. The dendrite layer thickness and crater depth increased as illustrated in Figure 4.7c. Furthermore, the surface roughness of the dendrites increased on the nanometer scale. Due to the pore structure, the dendrites formation, and the surface roughness, the electrode had a hierarchical structure and thus offers a high surface area for methanol oxidation. After the electrode was used for methanol oxidation, no significant degradation of the electrode structure was observed as shown in Figure 4.7d. However, the surface roughness on the nanometer scale increased.

The oxidation of the electrode and the presence of CuO were confirmed by the EDX and XRD spectra shown in Figure 4.8. The EDX spectrum of the untreated copper foam showed two small copper peaks at 8.0 and 8.9 keV and a more pronounced double peak of copper at 0.9 keV (Figure 4.8a). After electrodeposition, a small oxygen peak at 0.5 keV became visible. It is assumed that the electrode surface was already oxidized to some extent by contact to ambient air. Subsequent heat treatment resulted in the growth of the oxygen peak, indicating further oxidation of the foam. The oxygen peak increased after the foam was used as anode for methanol oxidation. The growth of the oxygen peak was attributed to an increase of the oxide layer thickness.

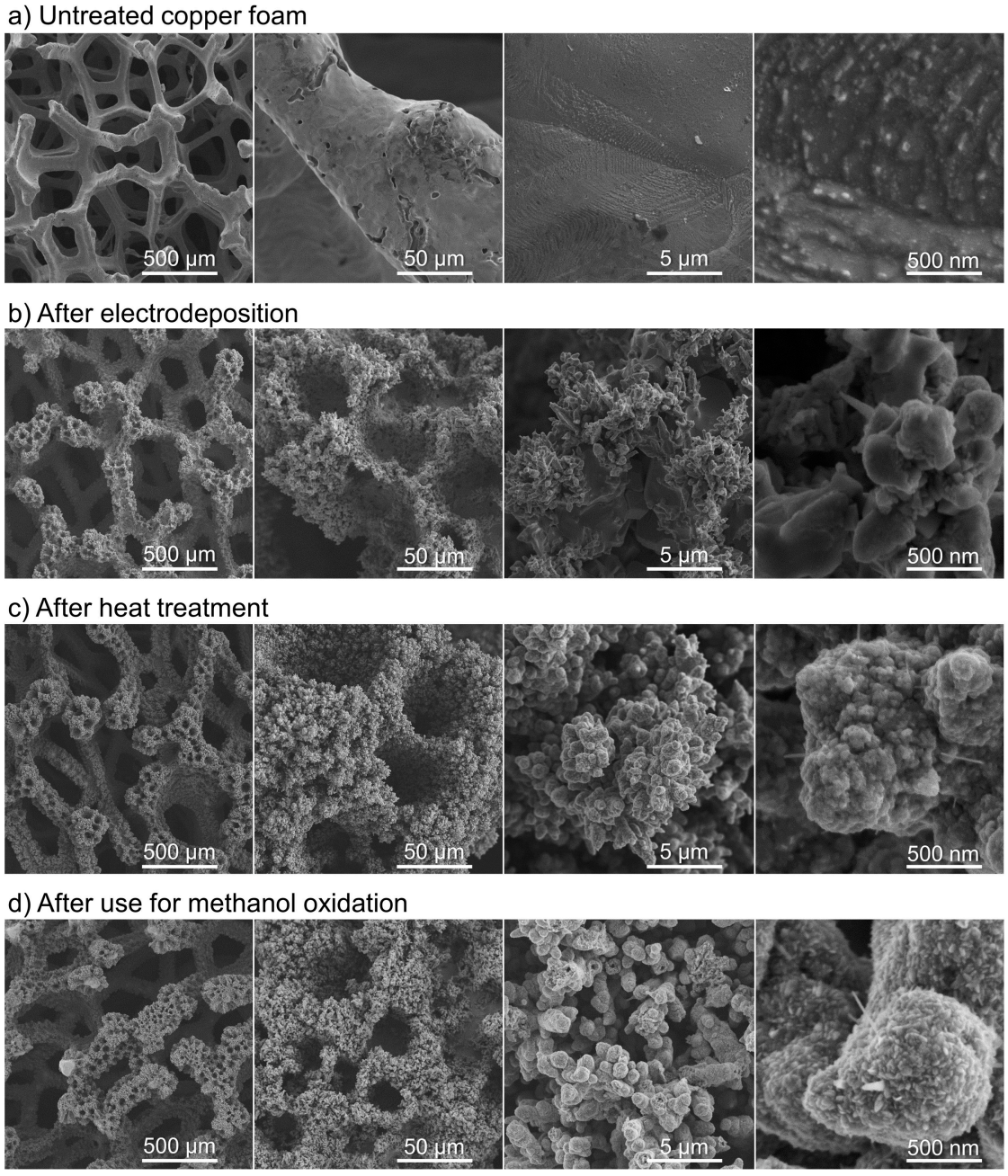

Figure 4.7.: SEM images of a) the untreated copper foam, b) the foam after electrodeposition, c) after heat treatment, and d) after usage in a methanol oxidation experiment.

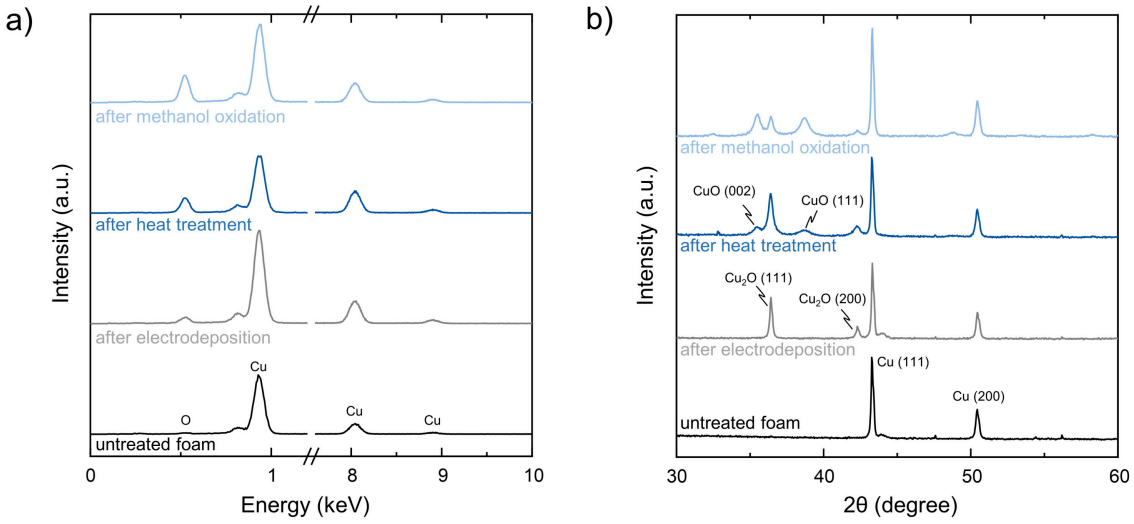

Figure 4.8.: a) EDX and b) XRD spectra of the untreated copper foam (black), the foam after electrodeposition (gray), after heat treatment (dark blue), and after usage in a methanol oxidation experiment (light blue).

The findings from the EDX spectra were supported by the XRD spectra shown in Figure 4.8b. The XRD spectrum of the untreated copper foam exhibited two strong peaks of Cu (111) and (200) at 43.3° and 50.4°, respectively. After the electrodeposition step, two additional peaks emerged at 36.4° and 42.3° corresponding to the crystalline structures (111) and (200) of Cu_2O. Two peaks appeared in the spectrum after heat treatment at 35.5° and 38.6° for CuO (002) and (111), respectively. The detected peaks in the XRD spectra of the heat-treated foam were also reported in the work of Huan et al. [Huan2017a], indicating a successful adaption of the catalyst synthesis process. The black color of the electrode and the presence of both Cu_2O and CuO were consistent with previous studies that found a multilayer oxide structure of dendritic copper oxide electrodes, with copper at the core, covered by a layer of Cu_2O, followed by an outer layer of CuO [Huan2017a; Zhan2018]. Comparing the XRD spectrum of the anode as prepared after heat treatment and after use for methanol oxidation, the CuO peaks became more pronounced and the Cu_2O peaks decreased after use. The change in peak height indicates increased oxidation and growth of the Cu_2O layer during methanol oxidation.

To assess the electrochemical active surface area (ECSA) the double layer capacitance was investigated by cyclic voltammetry in a beaker with a three-electrode setup as described in 4.2.4. The prepared CuO foam electrode with electrodeposited dendrites was investigated before and after use for methanol oxidation. For reference, a flat CuO sheet was used that was oxidized with the same thermal procedure as the foam electrode. The relationship of current density and scan rate is depicted in Figure 4.9 considering the positive and negative current for evaluation. The current densities measured for the foam electrodes were significantly higher than for the flat CuO sheet. Based on the slope of the curves, the following mean values were determined for the double layer capacitance: 0.76 mF/cm^2 for the flat CuO sheet, 302 mF/cm^2 for the foam electrode before methanol oxidation, and 575 mF/cm^2 for the foam electrode after methanol oxidation. These results show that the prepared foam electrode with electrodeposited dendrites exhibited a nearly 400 times larger ECSA than a flat CuO sheet. The ECSA increased by a factor of 1.9 after use for methanol oxidation. The increase in surface area is consistent with the surface structure observed in the SEM images, showing an increased roughness at the nanometer scale after use for methanol oxidation (see Figure 4.7).

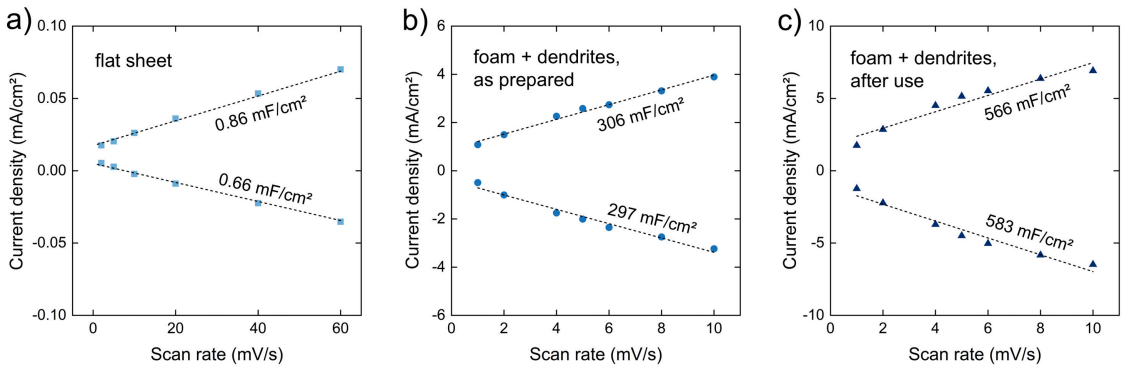

Figure 4.9.: Relationship of current density and scan rate for (a) the flat CuO sheet, (b) the foam electrode with electrodeposited dendrites as prepared, and (c) the foam electrode with electrodeposited dendrites after use for methanol oxidation. The slope indicating the double layer capacitance was determined from a linear fit of the data points.

The prepared hierarchical CuO anode was active for OER and MOR as illustrated in the LSV curves in Figure 4.10. At a potential of 1.59 V vs.

RHE, a current density of 100 mA/cm^2 was reached for OER in 2 mol/L KOH. The OER activity of the prepared anode was comparable to state-of-the-art non-noble metal OER catalysts [Jame2018; Wang2020]. The potential of MOR in 2 mol/L KOH + 1 mol/L methanol reached 100 mA/cm^2 at 1.37 V vs RHE, which is significantly lower than the potential required for typical alkaline OER [Jame2018; Wang2020]. However, compared to the standard potential of MOR, the overpotential was still high. A similiar or higher overpotential for MOR was observed in previous works with non-noble metal electrodes as well [Du2023; Li2020a; Li2020b; Wei2021; Wu2021; Xian2020], indicating the need for further improvements to reduce the energy demand of MOR.

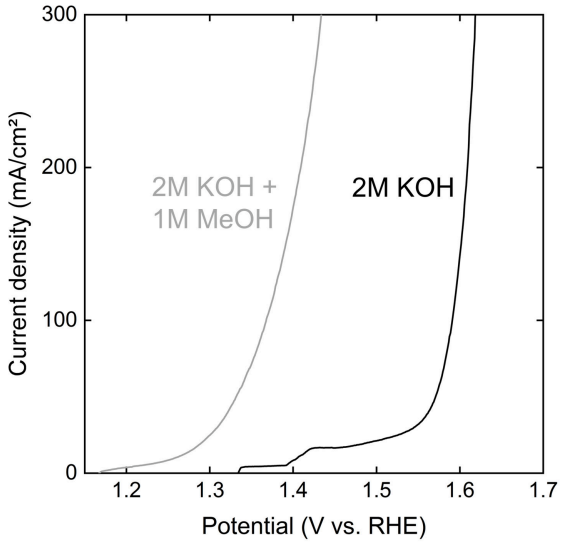

Figure 4.10.: LSV curves (iR-drop compensated) of the prepared CuO anode measured at a sweep rate of 5 mV/s in 2 mol/L KOH (OER) and 2 mol/L KOH with 1 mol/L methanol (MOR).

4.3.2. Impact of conversion

The time-dependent concentrations of methanol and formate during methanol oxidation with the prepared CuO anode in the flow cell setup are illustrated in Figure 4.11a. The decrease of the methanol concentration was nearly linear over time, resulting in a linearly increasing conversion, which was calculated from the methanol concentration by equation 4.1. In con-

trast to the linear course of methanol, the formate concentration increased with a decreasing slope to a maximum concentration of 0.42 mol/L. Based on the absence of unidentified substances in the FTIR and additional HPLC analysis of the anolyte, it was concluded that all methanol that was not converted to formate was further oxidized to carbonate.

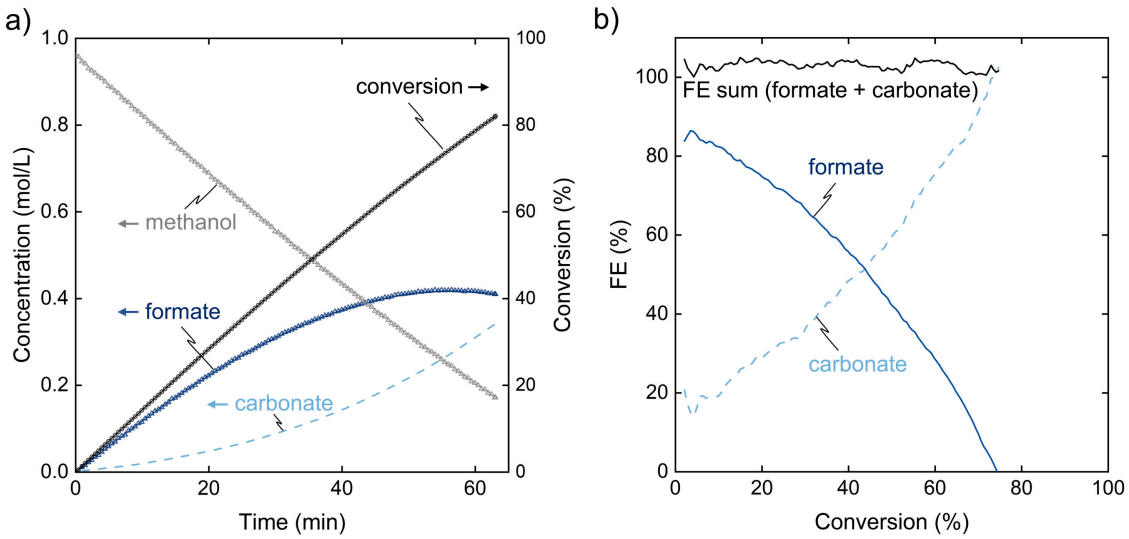

Figure 4.11.: (a) Concentration of methanol (gray) and formate (blue) measured by the FTIR online analytics during an oxidation experiment at 200 mA/cm^2. The conversion (black) was calculated from the methanol concentration. The carbonate concentration (light blue, dashed) was calculated from the difference of methanol and formate concentration based on the assumption of carbonate being the only side product. (b) The sum of formate and carbonate FE (black), the formate FE (blue) and the carbonate FE (light blue, dashed) were calculated from the concentration data.

Consistent with this conclusion, it was observed that the carbonate peak increases with increasing conversion in the FTIR spectrum (Figure 4.4). Unfortunately, the carbonate peak could not be reliably quantified, as it strongly overlapped with a second formate peak. However, the conclusion was tested in regard of the carbon and charge balance of the anolyte. If carbonate is the only side product of MOR, the carbonate concentration can be determined by calculating the difference between the consumed methanol and the produced formate. Figure 4.11a depicts the carbonate concentration calculated from this difference as a dashed line. The FEs of formate and carbonate calculated from the concentration curves by Equation 4.2 add up to nearly 100% over the entire experiment as shown in

Figure 4.11b. Please note that the FE is plotted over the methanol conversion instead of the reaction time. The representation of FE as a function of the conversion allows a more straightforward comparison of experiments with different initial reactant concentrations, current densities, and electrolyte volumes. The FE sum of approximately 100% (103% on average) shows that the balances of carbon and charge are closed providing a strong indication of no further side reactions. Other possible side reactions would have resulted in detectable products and do not match the balances of charge and carbon which indicate a transfer of about six electrons per methanol consumed that was not converted to formate. Furthermore, no gas evolution was observed, excluding a significant contribution of oxygen evolution or other gas forming side reactions. Validating the visual detection limit of gas evolution showed that oxygen evolution would have been clearly visible at a partial current density of 4 mA/cm^2 (corresponds to 2% of the 200 mA/cm^2 typically used). Therefore, the absence of other products and the closed balances justify the assumption of carbonate formation as the only notable side reaction which is consistent with previous studies on alkaline methanol oxidation to formate on copper-based electrodes [Wei2021; Heli2004]. The formate FE initially reached 85% but decreased significantly with increasing conversion - reaching zero at 74% conversion, while the carbonate FE increased from less than 20% up to 100%. The course of the FE indicates that methanol oxidation to formate (Equation 4.4) competed with carbonate formation. Heli et al. proposed a mechanism for methanol oxidation on copper in alkaline solution, which involves the formation of a Cu^{III} species, which catalyzes the oxidation of methanol and its intermediates to formate or carbonate [Heli2004]. For the nature of the Cu^{III} entity, copper oxy-hydroxide (CuOOH) and a Cu^{III} radical ($CuOO^{\bullet}H$) were proposed [Heli2004; Flei1972; Meye1972; Wels1990]. Based on the course of the FE, it is hypothesized that carbonate was formed in two different pathways as was found for MOR on NiOOH [Phan2024]: further oxidation of formate to carbonate (Equation 4.6) and methanol oxidation to carbonate (Equation 4.5). Methanol was initially present in high excess, whereas, at the end of the experiment, the concentration of formate was

more than two times higher than the concentration of methanol. The increasing ratio of formate to methanol favors formate oxidation over formate formation, which is a plausible explanation for the decrease in formate FE with increasing conversion. The low initial carbonate formation at near-zero formate concentrations indicates that formate is the preferred product of methanol oxidation.

$$CH_3OH + 5OH^- \longrightarrow HCOO^- + 4H_2O + 4e^- \tag{4.4}$$

$$CH_3OH + 8OH^- \longrightarrow CO_3^{2-} + 6H_2O + 6e^- \tag{4.5}$$

$$HCOO^- + 3OH^- \longrightarrow CO_3^{2-} + 2H_2O + 2e^- \tag{4.6}$$

It should be noted that the pathway of carbonate formation does not change the overall result from an application perspective, as it does not affect the overall carbon and charge balance. The overall reaction scheme for the superposition of methanol oxidation to formate and simultaneous formate oxidation to carbonate is identical to the full oxidation of methanol to carbonate (Equation 4.4+4.6 = 4.5).

4.3.3. Impact of the reaction conditions

To investigate the impact of the reaction conditions on MOR and to optimize the reaction for high formate yield at high conversion, current density, temperature, flow rate, electrolyte composition and the type of ion exchange membrane were systematically varied. Figure 4.12a presents the FE plotted over conversion for three distinct current densities: 50, 100, and 200 mA/cm^2. With decreasing current density, the FE for formate increased and higher conversions were achieved before the FE declined to zero. At a current density of 50 mA/cm^2, a maximum FE of 92% and a conversion of 88% were achieved, in contrast to 85% FE and 78% conversion at 200 mA/cm^2. The relationship between FE and current density was nonlinear, as the increase in FE from 200 to 100 mA/cm^2 was approximately equal to the increase in FE from 100 to 50 mA/cm^2. The decreasing FE with

increasing current density hints toward mass transfer limitation. The local concentration of formate within the porous dendrite layer is expected to rise as the current density increases, while the local concentration of methanol decreases correspondingly. The higher ratio of educt to product facilitates the selectivity of methanol oxidation to formate at a lower current density.

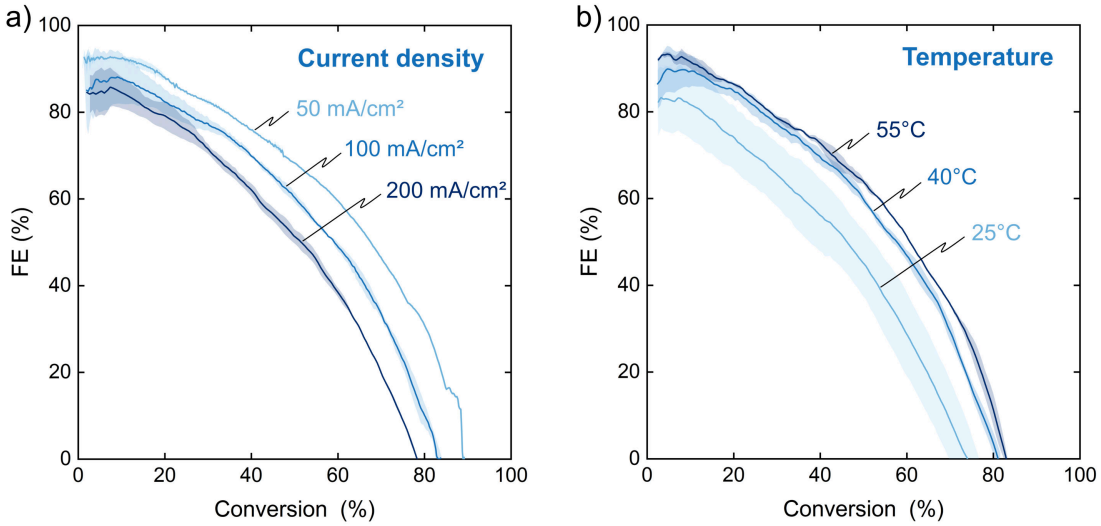

Figure 4.12.: (a) FE for formate plotted over the conversion of methanol for three different current densities. (b) Influence of the anolyte temperature on the FE to formate over increasing methanol conversion. The mean FE (continuous line) and the range of the replicates (boundaries of the filled area) are shown. If not stated otherwise in the plot, the oxidation was conducted at 200 mA/cm^2, 25 °C, 50 mL/min, 2 mol/L KOH, 1 mol/L methanol and with a BPM.

Figure 4.12b illustrates the impact of temperature on the FE over conversion. With increasing temperature, the FE for formate increased, and higher conversions were achieved before the FE declined to zero. Specifically, at a temperature of 55 °C, a maximum FE of 93% and a conversion of 83% were attained, whereas at 25 °C, the FE and conversion were slightly lower, at 83% and 74%, respectively. Despite an increased fluctuation of the results at 25 °C, the positive effect of higher temperatures on FE is evident. With increasing temperature, more formate and less carbonate were formed. Higher temperatures could directly affect selectivity by either altering the reaction kinetics or by improved mass transport. A significant contribution of the improved mass transfer is assumed, as diffusion coefficients are expected to increase approximately two-fold over the investi-

gated temperature range of 25-55 °C [Bhat1968; Pare2013]. The improved mass transfer increases both the rate at which methanol is transported from the bulk electrolyte to the electrode surface and the rate at which formate is transported in the opposite direction. Hence, an improved mass transfer increases the concentration ratio of methanol to formate at the electrode surface, which increases selectivity towards formate.

Interestingly, the flow rate of the electrolyte through the foam anode had no significant effect on the FE as shown in Figure 4.13a for flow rates of 100, 50 and 25 mL/min. A higher flow rate increases the convective mass transport to the electrode surface [Wals2018], which typically improves the selectivity at higher current density, as concentration gradients from the bulk electrolyte to the electrode surface are mitigated [Pére2020].

It is hypothesized that the flow rate had no significant influence on the FE due to a combination of multiple effects: Convective flow is assumed through the macroscopic pores of the open-cell copper foam (pore size of about 500 µm), but mainly diffusive transport in the porous dendrite layer due to the small pore size between the dendrites of about 1-10 µm. The assumed mass transport is illustrated in the qualitative schematic of concentration gradients in Figure 4.13b. The flow rate can affect the convective transport from the bulk electrolyte to the surface of the dendrite layer, reducing the thickness of the concentration boundary layer. However, the diffusive transport resistance of the porous dendrite layer would remain unaffected, thus reducing the overall effect of the flow rate. Furthermore, the rear areas of the electrode were likely less affected by mass transfer as the local current density is expected to decrease with increasing distance from the membrane due to the increasing electrolyte resistance. Finally, the mass transfer in flow-through foam electrodes increases sublinear with increasing flow rates. Cognet et al. [Cogn1995] found that the relationship between the mass transfer coefficient k and the flow velocity u is $k \sim u^{0.42}$ for a similar foam electrode with 100 pores per inch. Assuming that the same relationship can be applied to the electrode used in this work, increasing the flow rate by 100% would increase the mass transfer coefficient only by 34%. As the relationship between the mass transfer coefficient and

FE is presumably sublinear as well, it is hypothesized that the FE is even less influenced by the flow rate. Thus, a combination of the described effects seems to reduce the impact of the flow rate on the FE to an extent below significance.

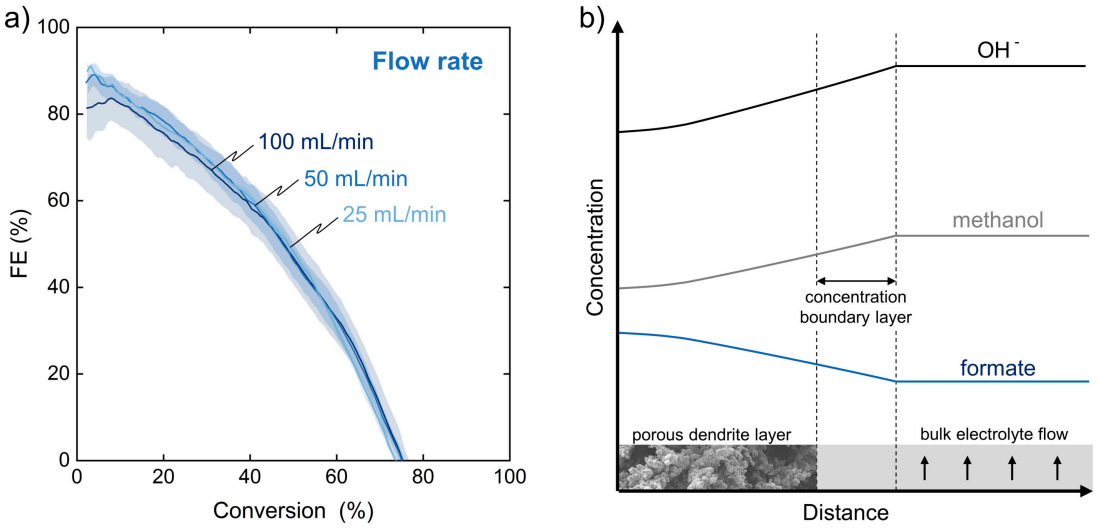

Figure 4.13.: (a) Influence of the flow rate on the FE to formate over increasing methanol conversion. The mean FE (continuous line) and the range of the replicates (boundaries of the filled area) are shown. The oxidation was conducted at 200 mA/cm^2, 25 °C, 2 mol/L KOH, 1 mol/L methanol, with a BPM. (b) Qualitative schematic of the concentration gradients at the electrode surface.

Figure 4.15a depicts the relationship between FE and conversion for three distinct concentrations of KOH (1, 2, and 4 mol/L). At low conversion, a higher KOH concentration led to a decrease in FE. It is assumed that the higher OH^- concentration facilitates the undesired side reactions resulting in full oxidation to carbonate, as the side reactions (Equation 4.5 & 4.6) require more OH^- per electron than the partial oxidation of methanol to formate (Equation 4.4). Specifically, an initial FE of 91% was attained at 1 mol/L KOH, compared to 65% when a KOH concentration of 4 mol/L was used. However, as the conversion increased, the FE declined steeper with 1 mol/L KOH, reaching 0% FE at a lower conversion compared to the higher KOH concentrations. It is hypothesized that the FE declined more pronounced with 1 mol/L KOH because a minimum concentration of OH^- ions is required for selective oxidation of methanol to formate at CuO.

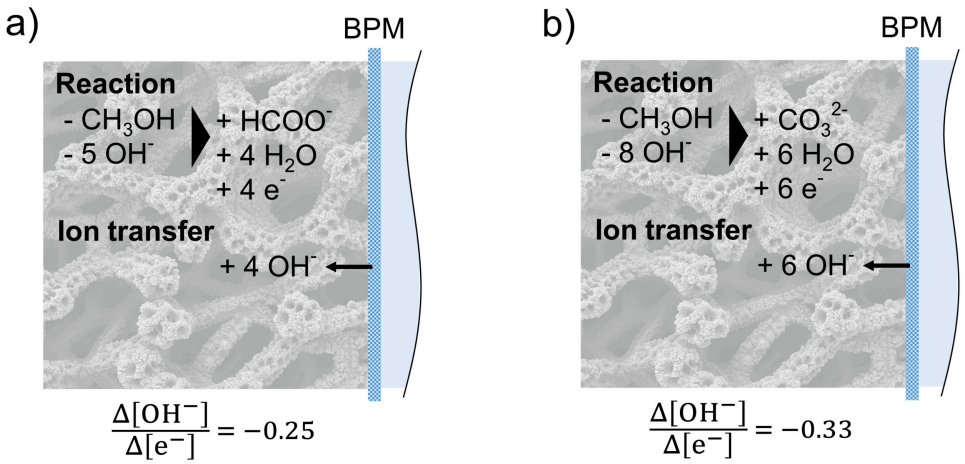

Figure 4.14.: Balances of the anode side with a BPM for (a) methanol oxidation to formate and (b) methanol oxidation to carbonate.

At least 5 OH^- ions are consumed per oxidized methanol (Equation 4.4), while up to 4 OH^- ions can be compensated by ion transfer to the anolyte (see Figure 4.14). In total, at least one OH^- ion is depleted per oxidized methanol. Thus, an initial concentration of 1 mol/L KOH is not sufficient to completely convert 1 mol/L methanol without a significant drop in pH. Figure 4.15c depicts the decreasing KOH concentration in the anolyte during methanol oxidation to formate. While the rate of KOH consumption was similar, the rate was not identical for the different initial KOH concentrations. The slope of the KOH concentration was slightly steeper at high initial KOH concentration and low formate FE, which is in good agreement with the theoretical rates of KOH consumption determined from the ion balances. The ion balances shown in Figure 4.14 result in slightly different rates of KOH consumption of 0.33 vs. 0.25 KOH consumed per electron transferred for methanol oxidation to formate vs. methanol oxidation to carbonate. In the experiments with 1 mol/L KOH the concentration of KOH decreased to 0.29 mol/L at the point of zero FE. The local OH^- concentration at the electrode surface was likely lower than the measured bulk concentration, as pronounced concentration gradients as shown in Figure 4.13 are expected at high current density. To avoid a steep decline of the FE, the amount of KOH should be chosen such that a sufficient excess of OH^- remains at high conversion. In future studies, adding KOH continuously or stepwise

could counter the neutralization of OH^- caused by the formate formation and maintain an optimal pH.

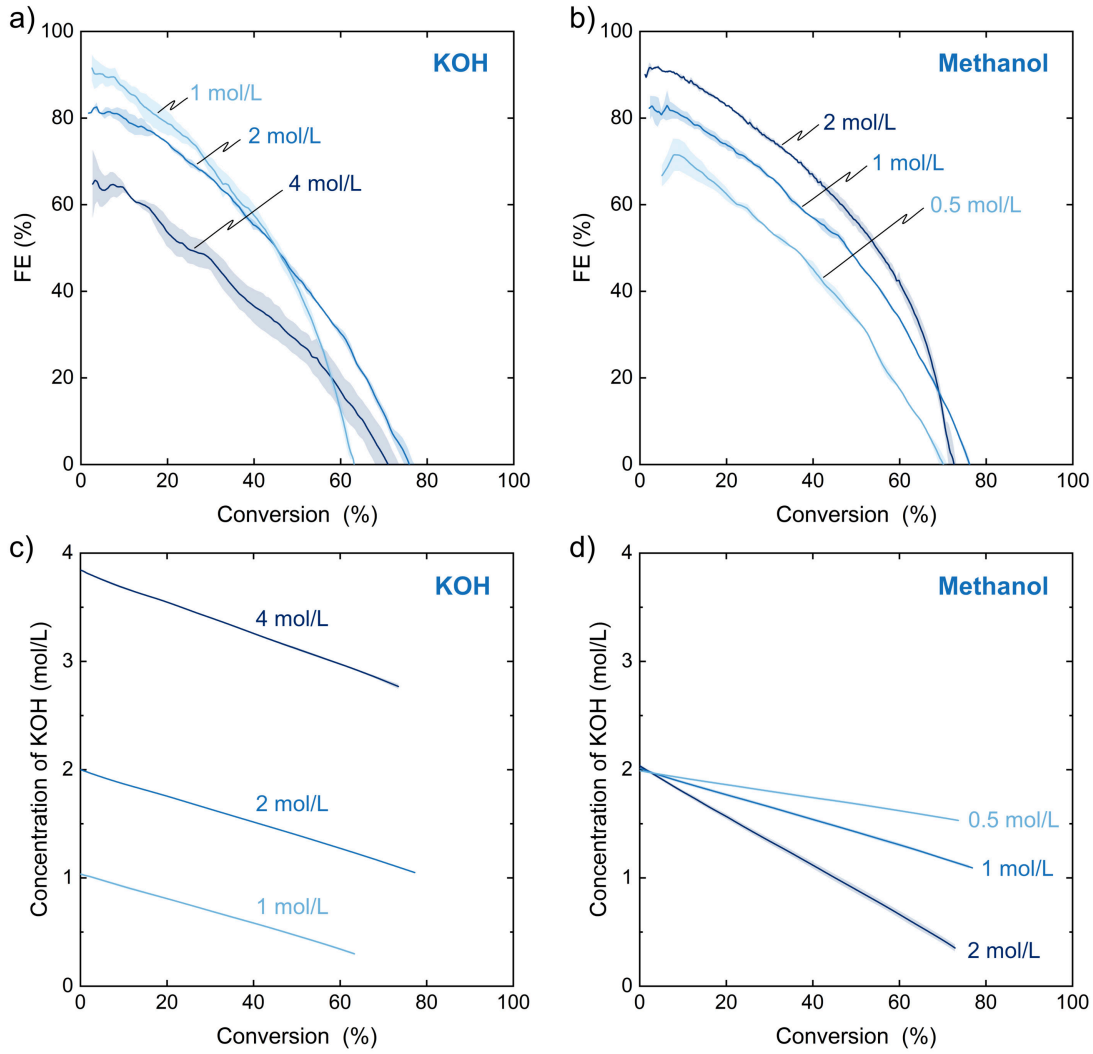

Figure 4.15.: FE for formate plotted over methanol conversion showing the influence of (a) the initial KOH concentration and of (b) the initial methanol concentration. (c-d) KOH concentration in the same experiments plotted over methanol conversion. The mean FE and the mean KOH concentration (continuous lines) are shown along with the range of the replicates (boundaries of the filled area). If not stated otherwise in the plot, the oxidation was conducted at 200 mA/cm^2, 25 °C, 50 mL/min, 2 mol/L KOH, 1 mol/L methanol, with a BPM.

Figure 4.15b illustrates the effect of methanol concentration on the FE over progressing conversion with three different initial methanol concentrations (2, 1, and 0.5 mol/L). Initially, a maximum FE of 92% was observed with 2 mol/L methanol, in contrast to the 71% achieved with 0.5 mol/L. In general, higher methanol concentrations resulted in higher FE for formate.

The ratio of methanol to formate at a given percentage of conversion was similar, independent of the initial methanol concentration. The increased FE is attributed to the higher absolute methanol concentration and to the associated higher mass transport of methanol to the electrode, which likely facilitates methanol oxidation to formate. However, at high conversion, the FE decreased more pronounced with 2 mol/L methanol, than at lower initial methanol concentrations.

The sharp drop of the FE with 2 mol/L methanol and 2 mol/L KOH is similar to the experiment with 1 mol/L methanol and 1 mol/L KOH (see Figure 4.15a). As discussed in the previous paragraph, it is assumed that the FE decreases strongly when the OH^- concentration in the electrolyte becomes too low and the local reaction environment at the electrode surface becomes too acidic. Figure 4.15d shows the KOH concentration plotted versus conversion for the experiments with different methanol concentrations. In the experiment with 2 mol/L methanol and 2 mol/L KOH, the sharp drop of the FE occurred when the KOH concentration was low. The KOH concentration declined down to 0.35 mol/L at the end of the experiment. The initial ratio of methanol to KOH of 1:1 was too low to maintain a sufficient OH^- concentration at high methanol conversion.

Figure 4.16a illustrates the impact of the membrane type on the FE. The BPM exhibited the highest initial FE of 76%, followed by the CEM with 57%, and the AEM with 36%. With progressing conversion, the FE decreased for all tested ion exchange membranes. In contrast to all other reaction conditions tested, clear indications of corrosion of the CuO electrode were observed at the end of the MOR experiments with the AEM and the CEM. A blue hue was visible in the anolyte indicating dissolved copper ions and the electrode color changed partially from black (CuO) to copper (metallic Cu). Therefore, a new anode was used for each membrane experiment. The corrosion of the CuO electrode is attributed to the less favorable ion balance of the AEM and CEM causing a reduced local pH at the membrane electrode interface, which is discussed in more detail in the subsequent paragraphs.

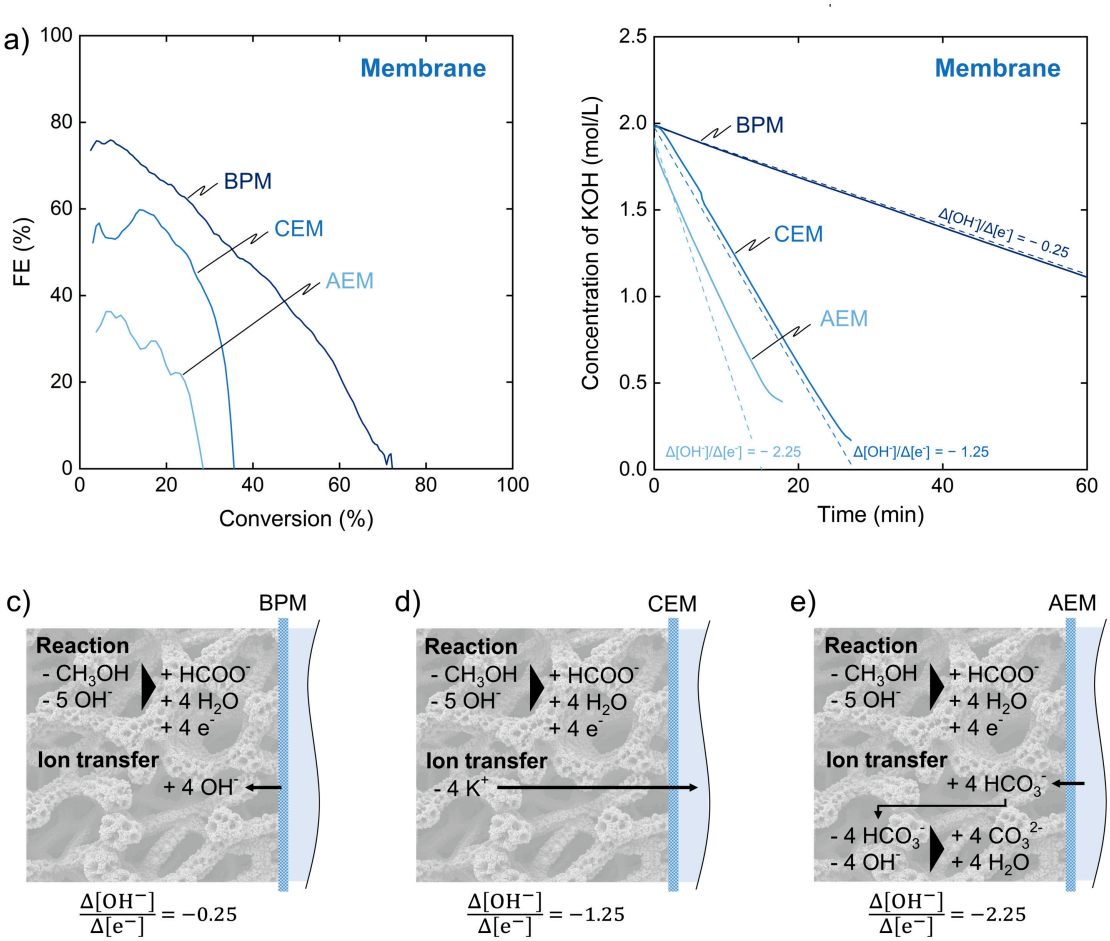

Figure 4.16.: (a) Influence of the membrane type on the FE to formate over increasing methanol conversion. The oxidation was conducted at 200 mA/cm^2, 25 °C, 50 mL/min, 2 mol/L KOH and 1 mol/L methanol. (b) Decreasing KOH concentration during the experiments (continuous line). Calculated concentration curves (dashed line) for the theoretical ratios of OH^- consumption per electron transferred are shown for comparison. (c)-(e) Balances of the anode side considering methanol oxidation to formate and ion transfer through the different membrane types. Based on the balances, theoretical ratios of OH^- consumption per electron transfer are given.

The choice of ion exchange membrane significantly influences the ion transport through the membranes and thus, the overall ion balance. Figure 4.16b shows the KOH concentration decreasing over time.

The decline in KOH concentration occurred at a substantially slower rate with a BPM compared to a CEM or AEM. The distinct slopes observed for the KOH concentration over time can be attributed to the different ion balances of the three membrane types (Figure 4.16c-e). In the case of the BPM, the reaction of methanol to formate consumes 5 OH^- ions, while 4 OH^- ions are supplied to the anolyte through ion transfer resulting from water dissociation in the BPM.

When employing a CEM, the charge transport across the membrane relies on the transfer of K^+ ions from the anolyte to the catholyte. Consequently, the consumption of OH^- ions is not compensated by ion transfer through the membrane as it is with a BPM. As a result, the ratio of OH^- ions consumed per electron transferred is considerably higher in a CEM compared to a BPM. The observed decline in KOH and OH^- concentration is in good agreement with the OH^-/e^- ratio of -1.25, resulting from the ion balance of the CEM. The lower conversion achieved with a CEM is likely caused by the rapid decline in OH^- concentration. Although a concentration of 0.23 mol/L OH^- remained in the bulk electrolyte at the end of the experiment, the OH^- concentration in the porous dendrite layer of the anode is expected to be significantly lower. Corresponding to the experiments with lower KOH concentration the quickly declining FE at low OH^- concentration indicates that a low pH impedes methanol oxidation to formate. Interestingly, the initial FE was lower with a CEM or AEM compared to a BPM even before the different KOH concentration of the bulk electrolyte is expected to have a significant impact. This observation can be attributed to the local reaction conditions in the region of the electrode, which is adjacent to the membrane and therefore directly impacted by the membrane transport. As stated above, the part of the anode directly adjacent to the membrane will be the most active. Due to the iR drop, electrode segments at a greater distance to the membrane will be less active.

When using an AEM, the anions in the catholyte determine the ion trans-

fer across the membrane. $KHCO_3$ was used in the catholyte to mimic the conditions of electrochemical CO2R. It is assumed that most of the charge transport across the membrane occurs via the transfer of HCO_3^- ions and that each HCO_3^- transported neutralizes another OH^- for conversion to CO_3^{2-} in the highly alkaline anolyte, as shown in the ion balance (Figure 4.16e). The measured decline in the KOH and OH^- concentration is more pronounced with an AEM compared to a CEM. However, the slope of the measured decline is less negative than the OH^-/e^- ratio of -2.25 derived from the ion balance for the AEM. This suggests that additional ions may be transported across the membrane, potentially mitigating the decrease in OH^-. It is plausible that CO_3^{2-} and OH^- were involved to some extent in the charge transfer across the AEM, despite their low concentration in the catholyte. As will be shown, a different catholyte composition changes the ion balance for the AEM (see Chapter 4.3.4). With regard to a stable pH in the anolyte, the transport of OH^- as the only anion across the membrane is ideal. For common catholytes of alkaline water electrolysis, such as KOH or NaOH, no difference in the ion balance between AEM and BPM is expected.

In addition to the ion transfer required for charge transport, other transport phenomena across the membrane should be considered as well. The crossover of methanol and formate through the membrane to the cathode side can cause the loss of reactant and product or negatively affect the catholyte reaction. The catholyte was analyzed via HPLC after the oxidation experiments with the three different membrane types (see Table A.1). There was no significant crossover of methanol or formate through the BPM. The CEM retained the negatively charged formate but was permeable to uncharged methanol. Methanol can pass through the CEM by diffusion driven by the concentration difference, but also by electroosmotic drag along with the transported cations [Ahme2011]. The AEM was permeable to formate and methanol, which can both diffuse through the membrane driven by the concentration difference.

Besides the influence on FE and conversion, the reaction conditions also affect the potential of the anode. Figure 4.17 compares the mean anodic

potential during methanol oxidation at different reaction conditions. Typical chronopotentiometry curves are provided in the Appendix (Figure A.2). The anodic potential increased significantly with increasing current density (Figure 4.17a), which was primarily attributed to the increasing voltage drop across the resistance of the electrolyte. The electrolyte gap to the membrane was minimized as the foam electrode was placed in direct contact with the membrane. However, it should be noted that the electrolyte conductivity can still have a significant effect on the local potential distribution within the foam electrode. The potential decreased slightly with increasing temperature (Figure 4.17b), which is due to improved kinetics and electrolyte conductivity. The flow rate had no clear effect on the potential (Figure 4.17c). The potential decreased with increasing KOH concentration and the corresponding higher electrolyte conductivity (Figure 4.17d). The influence of the methanol concentration on the potential was small in the investigated concentration range. The results suggest a slightly higher potential at higher methanol concentration (Figure 4.17e), which agrees with a lower conductivity expected at higher methanol concentration [Boru2021]. The membrane had no significant effect on the anodic potential (Figure 4.17f). It should be noted that the experiments with the CEM and AEM were not performed in duplicate due to the corrosion of the CuO electrode (see discussion of Figure 4.16).

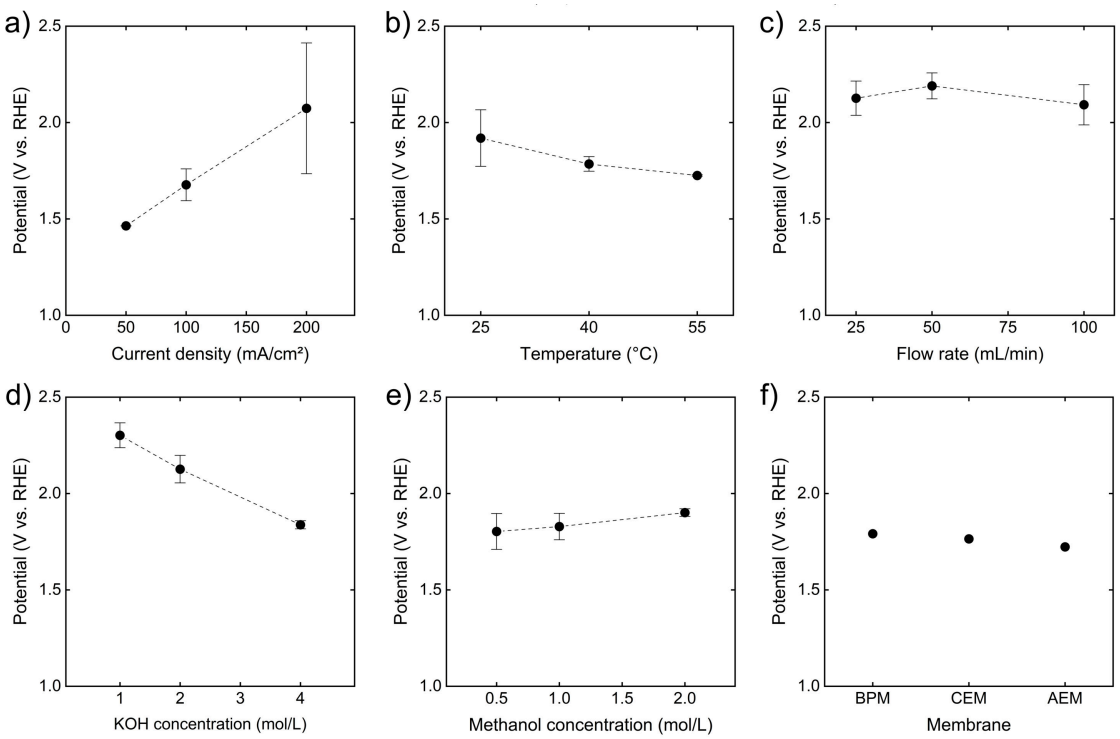

Figure 4.17.: Mean anodic potential during methanol oxidation at different reaction conditions: (a) current density, (b) temperature, (c) electrolyte flow rate, (d) initial KOH concentration, (e) initial methanol concentration, and (f) membrane. The error bar represents the range of the replicates. If not indicated otherwise by the values of the x-axis, the oxidation was conducted at 200 mA/cm^2, 25 °C, 50 mL/min, 2 mol/L KOH, 1 mol/L methanol and with BPM.

While the duration of use showed no clear effect on the FE, an increase in the anodic potential was observed from experiment to experiment at high current density and low temperature. The potential did not increase between the experiments when the anode was operated at low current density or high temperature. Considering both anodic potential and FE for formate, three parameters (current density, KOH concentration, and methanol concentration) presented a trade-off between electrical energy demand and product selectivity. However, an increased temperature improved both anodic potential and FE.

4.3.4. High yield synthesis and considerations for paired processes

To demonstrate a paired electrolysis with high-yield MOR, MOR was paired in two different setups with alkaline HER utilizing the insights gained from the investigation of the reaction conditions. The two setups depicted in Figure 4.18a-b employ different membranes and electrolyte management creating opposite characteristics that will be discussed in the following paragraphs.

The BPM setup with separated electrolytes and a BPM allows the operation of anodic MOR and a cathodic reaction practically independent of each other. The BPM retains both anions and cations, effectively preventing the exchange of anions or cations between anolyte and catholyte. The OH^- migration to the anolyte mitigates the decreasing pH with progressing conversion as shown in Figure 4.16. With these characteristics, the BPM setup is suitable to pair MOR at high yield with most cathodic reactions, including electrochemical CO2R. Successful operation of CO2R with BPMs was documented with electrolyte gap [Li2018; Wrob2023] and in zero-gap configuration [Siri2022; Xie2022].

The AEM setup utilizes a shared electrolyte, which is cycled through the anode and cathode compartments. In contrast to the BPM setup, anodic MOR, and a paired cathodic reaction are not independent of each other as both sides share the same electrolyte. For successful pairing, the cathodic reaction must be compatible with the electrolyte of MOR, while MOR must be compatible with the reactants and products of the cathodic reaction. Compatibility implies that the substances in the electrolyte (KOH, methanol, formate, educt, and product of the cathodic reaction) do not undergo undesired reactions or interact negatively with the desired reactions. While the options for compatible cathodic reactions are limited, alkaline HER was successfully paired with MOR in shared electrolyte setups with no negative interactions reported [Li2020a; Li2020b; Xian2020; Xian2021; Du2023].

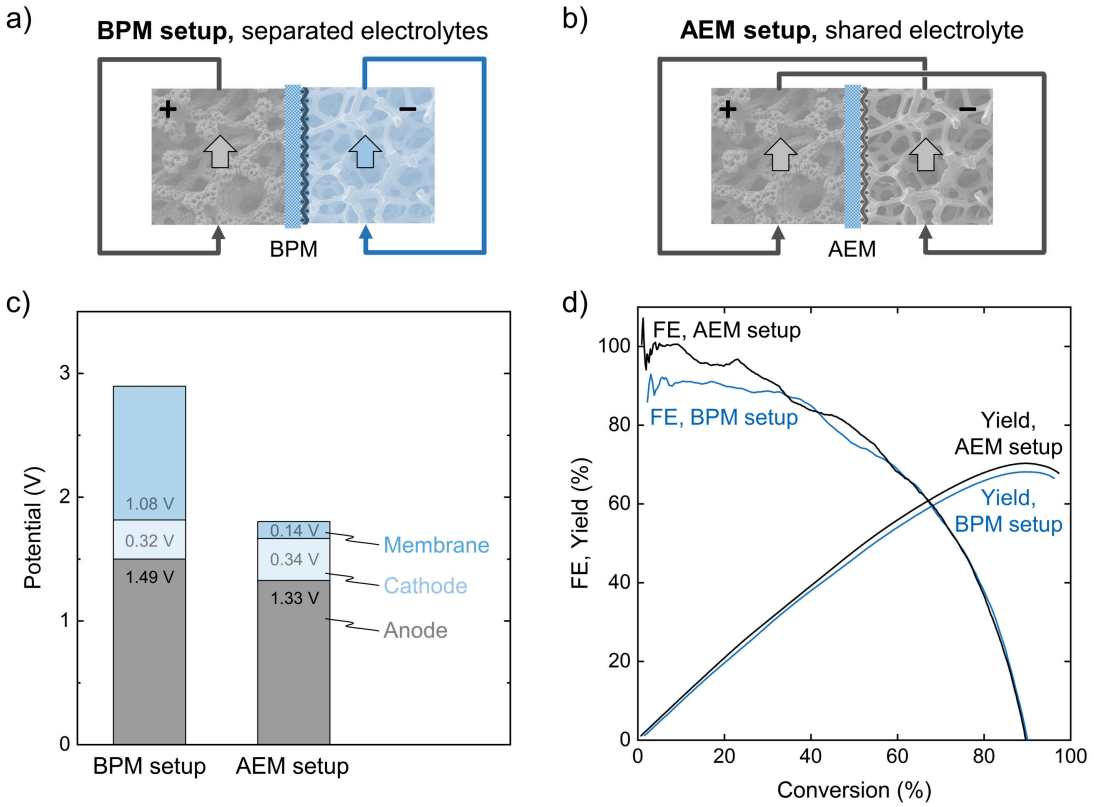

Figure 4.18.: (a-b) Setups used for paired synthesis of anodic MOR to formate and cathodic HER. (c) Cell potential of both setups divided into the contributions of membrane, cathode, and anode potential. (d) FE and yield of formate plotted over the conversion of methanol for both setups. The oxidation was conducted at 100 mA/cm^2, 55 °C, 50 mL/min, 2 mol/L KOH and 1 mol/L methanol.

Both setups were operated at a current density of 100 mA/cm^2 with the same reaction conditions, pairing high-yield MOR with alkaline HER. Figure 4.18c shows the mean cell potential for the paired electrolysis divided into the potentials of membrane, cathode, and anode. The cell potential of the BPM setup was 2.9 V and 1.8 V for the AEM setup. The higher cell potential of the BPM setup was mainly caused by the higher membrane potential of the BPM compared to the AEM setup. BPMs require an additional potential for water dissociation within the membrane [Pärn2021], the measured membrane potential of 1.08 V was within the manufacturers specifications of $<$ 1.2 V at 100 mA/cm^2. The effective separation of the electrolytes by the BPM came at the cost of a higher cell potential. However, the trade-off between higher potential and improved ionic balance of the separate

electrolytes is not a challenge unique to paired electrolysis with MOR. For example, BPMs are considered for CO2R despite their higher membrane potential as BPMs can prevent salt formation and increase CO_2 utilization [Sass2023]. The cathodic potentials for HER were acceptable for a demonstration of a paired electrolysis focused on anodic MOR, but are higher than for state-of-the-art alkaline HER catalysts [Wang2020] as the plain nickel mesh used as cathode is not an optimized catalyst. The mean anodic potential was remarkably low with 1.49 V for the BPM setup and 1.33 V for the AEM setup, which is significantly below typical alkaline OER potentials [Jame2018; Wang2020].

The weight change of the electrolyte was measured to test the hypothesis that the electrolyte volume changes at high conversion. The weight change corresponds to a change in the electrolyte volume as the change in density was neglectable. For the BPM setup the weight of the anolyte increased by 10.7%, while the weight change of the shared electrolyte in the AEM setup was -0.7%. Leakage can be excluded, as the weight did not change as the setup was operated with running pumps but without current. The slight reduction in electrolyte weight in the AEM setup is most probably due to hydrogen evolution and evaporation since the volatile components of the electrolyte can escape along with the hydrogen gas formed at the cathode. The observed increase of anolyte weight was larger than expected for a symmetrical water balance of the BPM setup, in which the water split in the BPM originates at equal parts from anolyte and catholyte as shown in Figure 4.19.

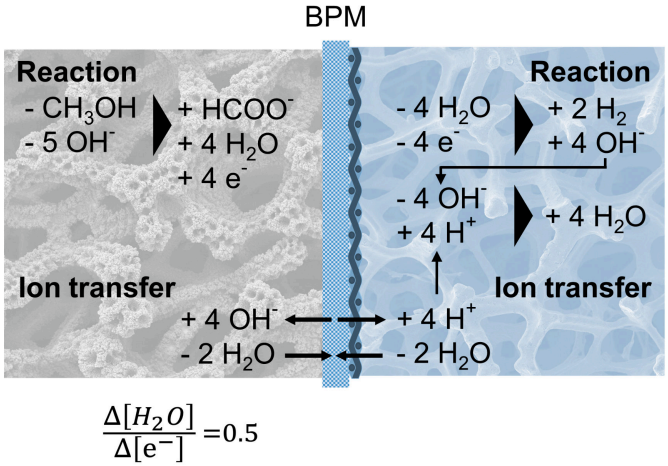

Figure 4.19.: Water balance of the BPM setup assuming symmetrical water transport from anolyte and catholyte to the BPM. The net ratio of water added per electron transferred is 0.5 for symmetrical water transport. At the end of the experiment a charge of 19650 C was transferred, the ratio of 0.5 would correspond to a weight increase of about 3.4%.

The additional weight increase was attributed to an asymmetrical water balance, which led to an increased water transport to the anolyte. The asymmetrical properties of BPMs were discussed in previous studies [Bals2007; Oene2021; Pärn2021]. A net water transport to the anode side could occur if the water drag of the OH^- ions transferred to the anolyte exceeds the diffusion of water from the anolyte into the membrane. It should be noted that water transport through CEMs or AEMs is typically more pronounced with reported water transfer numbers (moles of water transferred per faraday of electricity) of 2-15 depending on the ionomer, the transferred ion and the humidification of the membrane [Xie1995; Zlot2017; Solb2023]. These findings highlight that the volume change of the electrolyte and the water balance of the cell should be considered for electrosynthesis at high product concentrations. While the volume change of the electrolyte in the AEM setup was negligible, the volume change of the anolyte in the BPM setup was taken into account for the evaluation. In the following, the impact of the water balance is discussed - on the practical operation of anodic MOR and its implications on the reaction efficiency. In the BPM setup, the water transport across the membrane dilutes the reactant and prod-

uct concentration in the anolyte. This dilution of the reactant concentration (methanol) can decrease the selectivity for formate, as the results show that the formate FE decreases with lower methanol concentration (see Figure 4.15). From the perspective of downstream processing, a dilution of the product is undesirable, as this is likely connected to increase separation costs. In the present case, the observed dilution rate of 10% might be acceptable. Nevertheless, dilution is linked to the amount of charge transferred and will, therefore, increase for higher product concentrations. In contrast to the BPM setup, the water balance of the AEM setup with a shared electrolyte is closed. Hence, water transport does not negatively affect the product concentration in the AEM setup.

Figure 4.18d illustrates the FE and the yield for MOR to formate over progressing methanol conversion for both setups. Both setups exhibited a high initial FE of 95-101% for the AEM setup and 86-93% for the BPM setup. With increasing methanol conversion the FE of both setups converged, reaching a high conversion of 90% before the FE decreased to zero. Operating MOR at an elevated temperature of 55 °C and a reduced current density of 100 mA/cm^2 showed a higher selectivity compared to applying the settings not in combination as shown in Figures 4.12a and 4.12b. Both setups achieved high maximum yields of up to 70% for the BPM setup and 68% for the AEM setup. In summary, both setups reached a high FE and formate yield at low anodic potential. The BPM setup is less energy efficient due to the higher membrane potential, but more versatile in pairing with other reactions as the setup can be operated with separated electrolytes. In contrast, the AEM setup is more energy efficient with a low membrane potential, but less versatile. Compatible cathodic reactions are limited to reactions such as HER that can be operated in the shared alkaline electrolyte containing methanol and formate. The presented results show that MOR can be operated in both setups at reduced anodic potential compared to OER, while providing formate at high yield as additional value-added product.

4.4. Conclusion

In summary, the present work investigated the impact of reaction conditions and conversion on methanol oxidation to formate on a hierarchically structured electrode and demonstrated paired electrolysis at a high formate yield. The hierarchically structured CuO anode exhibited a high surface area with porosity on different length scales from 500 µm to 500 nm and was highly active for methanol oxidation. The reaction progress was monitored with fast sampling analytics, which allowed us to reveal the relationship between FE and conversion. A high initial FE of 85% at 200 mA/cm^2 was observed which declined with increasing slope over the progressing conversion of methanol, reaching 75% conversion before the FE declined to zero. The conversion had a significant impact on the selectivity by changing the ratio of methanol to formate, as methanol oxidation to formate was competing with the subsequent oxidation of formate to carbonate.

Decreasing the current density or increasing the temperature increased both the initial FE and the obtainable conversion before the FE declined to zero. An increased electrolyte flow rate had no significant effect on MOR suggesting that concentration gradients formed mainly inside the porous dendrite layer. The results on different electrolyte compositions and membrane types highlight the importance of the ionic balance for a stable electrosynthesis at high conversion.

Applying the insights into the reaction conditions, a paired synthesis of cathodic HER and anodic MOR to formate was demonstrated at 100 mA/cm^2 with an initial FE close to 100% reaching a formate yield of up to 70% at 90% conversion. To the best of the author's knowledge, the achieved conversion and yield are the highest values reported so far. The anode potential of 1.33 V vs. RHE for MOR at the hierarchical non-noble metal CuO electrode was lower than for alkaline OER. However, there is still room for further improvement as the anodic potential was significantly higher than the standard potential of MOR to formate. Furthermore, two setups with different characteristics were compared and the implications for paired electrolysis were discussed. This work presents the first paired elec-

trolysis with methanol oxidation to formate reaching a high formate yield and explicitly investigating the impact of reaction conditions and increasing conversion. The findings on the effect of conversion, ion balance, and pairing provide valuable insights for further research on methanol oxidation to formate and paired electrolysis. In a broader context, the reported methodology holds potential for investigating electrosynthesis at industrially significant yield and conversion.

5. Feed and bleed operating mode for electrochemical flow cells

Parts of this chapter have been published as:
Jonas Baessler, Malte Wehner, Mojtaba Mohseni, Julian Neumann, Matthias Wessling, and Robert Keller
Feed and bleed operating mode for electrochemical flow cells: Challenges, solutions and practical insights
ChemElectroChem, 2025
DOI: 10.1002/celc.202500034

5.1. Introduction

Electrochemical studies often remain confined to fundamental research at low current density and low product concentration, focusing more on initial selectivity than long-term stability. Fundamental studies are important; however, investigating electrochemical synthesis at industrially relevant conditions is imperative to proceed from laboratory towards application [Burd2019; This2024; Huan2024a; Perr2019]. For industrial electrolysis, predominantly flow cells are used because they enable continuous production processes and controlled flow regimes, e.g., for chlor-alkali or water electrolysis [Berg1982; Lang2024]. Flow cells are preferable to beakers or H-cells at lab-scale as well since they represent industrial conditions, ease scale-up, and provide well-defined and reproducible conditions [Rive2015; Plet2018; Wals2019].

Although the influence of reaction conditions and the cell setup are often discussed [Endr2017; Venn2019; Perr2020; Quen2023; Perr2019; Möhl2018; Shin2023; Regn2024], the operating mode of the flow cells received less consideration. Electrochemical flow cells at lab-scale are typically operated in two modes: batch or single-pass [Plet2018; Aren2020; Corn2024]. In batch mode (also known as semi-batch or batch recirculation [Tanb2020; Wals2019]), the electrolytes are circulated through the cell in a closed loop [Malj2020]. High product concentrations can be obtained over time [Wals2019]; however, batch mode is unsuitable for continuous synthesis in steady-state. In single-pass mode (see also continuous flow or flow electrochemistry [Noël2019; Tanb2020; Nich2020]), the electrolyte is passed through the cell only once, which readily enables steady-state operation [Malj2020]. Nonetheless, achieving a high product concentration in the single-pass mode sets constraints on the flow channel geometry and the flow rate [Gree2015]. Due to their specific characteristics, neither batch nor single-pass are suitable to investigate continuous production in flow cells that resemble industrially relevant conditions regarding product concentration, cell geometry and flow velocity.

Beyond batch and single-pass, a third operating mode is commonly employed for continuous production in industrial electrosynthesis [Plet1993; Good1995; Lund2001; Danl1984], electrodialysis and filtration [Bake2012; Cher1998; Mint1963], which was coined 'feed and bleed' in the field of membrane technology [Bake2012; Cher1998; Mint1963] (see also 'continuous reactor with recycle' [Good1995]). In feed and bleed mode, the electrolyte is circulated in a loop at a high flow rate through the flow cell. Concurrently, a small volume flow enters the loop (Feed), while an equivalent volume flow leaves the loop (Bleed) [Bake2012]. In industrial organic electrosynthesis the recirculation often involves one or more separation steps to obtain a purified product stream while the remaining electrolyte is recycled [Lund2001; Danl1984]. In contrast to batch and single-pass mode (see schematic illustrations in Figure 5.1), feed and bleed allows continuous production in steady state at high product concentration without setting constraints to the flow conditions within the cell. While 'feed and bleed' is commonly employed in industrial electrosynthesis, it is only scarcely used to study electrochemical reactions at lab-scale [Raki1999; Domi2013; Drög2024].

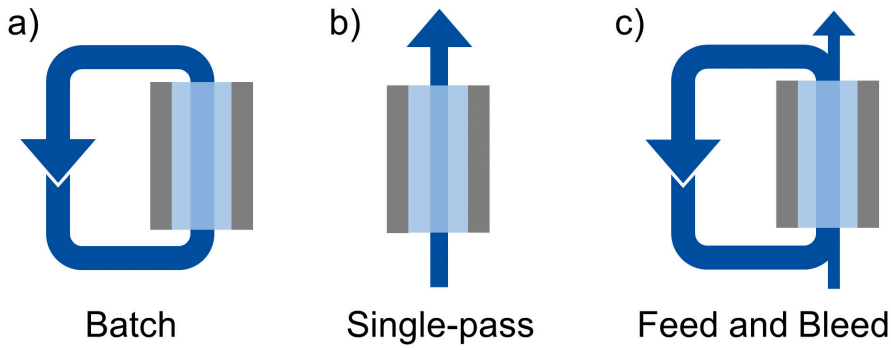

Figure 5.1.: Schematic representation of the three operation modes for electrochemical flow cells.

This work provides valuable tools and insights for the feed and bleed operation mode in lab-scale electrosynthesis, and discusses its unique characteristics in direct comparison with batch and single-pass mode. Equa-

tions for modeling and evaluation of feed and bleed systems are developed, and influencing factors such as the feed flow rate and the electrolyte volume are discussed. Furthermore, this work presents an experimental setup for feed and bleed mode that can also be operated in batch and single-pass mode. Online FTIR analysis monitoring the product concentration provides quantitative insights into the specific characteristics of the flow cell operating modes. Feed and bleed operation is demonstrated at lab-scale and directly compared with batch and single-pass at the example of methanol oxidation to formate in a flow cell with an active electrode area of 25 cm^2 at a current density of 200 $mA\,cm^{-2}$. This work facilitates the adoption of 'feed and bleed' for lab-scale research, provides valuable tools for investigating electrosynthesis under industrially relevant conditions and assesses stability during steady-state operation.

5.2. Material and methods

5.2.1. Theoretical analysis

All feed and bleed equations were derived from a mole balance around the electrolyte in the system, which was assumed to be ideally mixed. Further details on the ideally mixed model and the balance equation are provided in the results section 5.3.1. The assumption of ideal mixing of the electrolyte was evaluated by a comparison to a non-ideally mixed model (see Appendix A.3). The feed and bleed models were implemented with Python using the GEKKO Optimization Suite [Beal2018]. All other calculations were performed in Excel (Microsoft) and Origin (OriginLab).

5.2.2. Phase separator

The phase separator was fabricated by 3D printing (printer: Form 3, material: High Temp Resin V2, Formlabs). After printing, the phase separator was thoroughly rinsed with isopropanol and cured in a 'Form Cure' device (Formlabs) at the manufacturer's recommended settings of 80 °C for 120 min. The phase separator was connected via three threaded ports for G1/4" tubing connectors and two smaller threaded ports for UNF 1/4" 28G tubing connectors. The material of the phase separator was transparent, allowing to observe the separation chamber during operation. The visibility of the separation chamber was improved by applying a clear adhesive film on the dull front surface of the phase separator.

5.2.3. Experimental comparison of operation modes

All experiments were performed in an electrochemical flow cell (flex-E-cell, FXC Engineering) with an active geometric area of 5 cm by 5 cm with two electrolyte compartments separated by a bipolar membrane (Fumasep FBM-PK, Fumatech) in reverse bias. The anolyte was a aqueous solution of 2 mol L^{-1} potassium hydroxide (KOH, 85 %, VWR) and 1 mol L^{-1} methanol (CH_3OH, 99.9 %, Merck), the catholyte was a solution of 1 mol L^{-1}

potassium hydroxide. The anode was copper foam (POROFEN-Cu90, Al-Carbon) coated with copper(II) oxide dendrites. The anode preparation procedure was adapted with modifications from Huan et al. [Huan2017a]. Anodic methanol oxidation was paired with hydrogen evolution at the cathode, which was a nickel mesh (aperture width 0.5 mm, wire diameter 0.14 mm, Haver & Boecker) supported by copper foam. Both the anode and the cathode were in direct contact with the membrane without an electrolyte gap. The flow cell was operated at constant current supplied by a potentiostat (VSP with 10A booster, Biologic) at a current density of 200 mA cm^{-2}. Potentials were measured using a reversible hydrogen electrode (RHE)(Hydroflex, Gaskatel). The cell setup and anode preparation were identical to the methods described for the investigation of methanol oxidation to formate in Chapter 4, please refer to Section 4.2.2-4.2.3 for further details. Figure 5.2 shows a schematic of the cell and the experimental setup consisting of two separate electrolyte cycles.

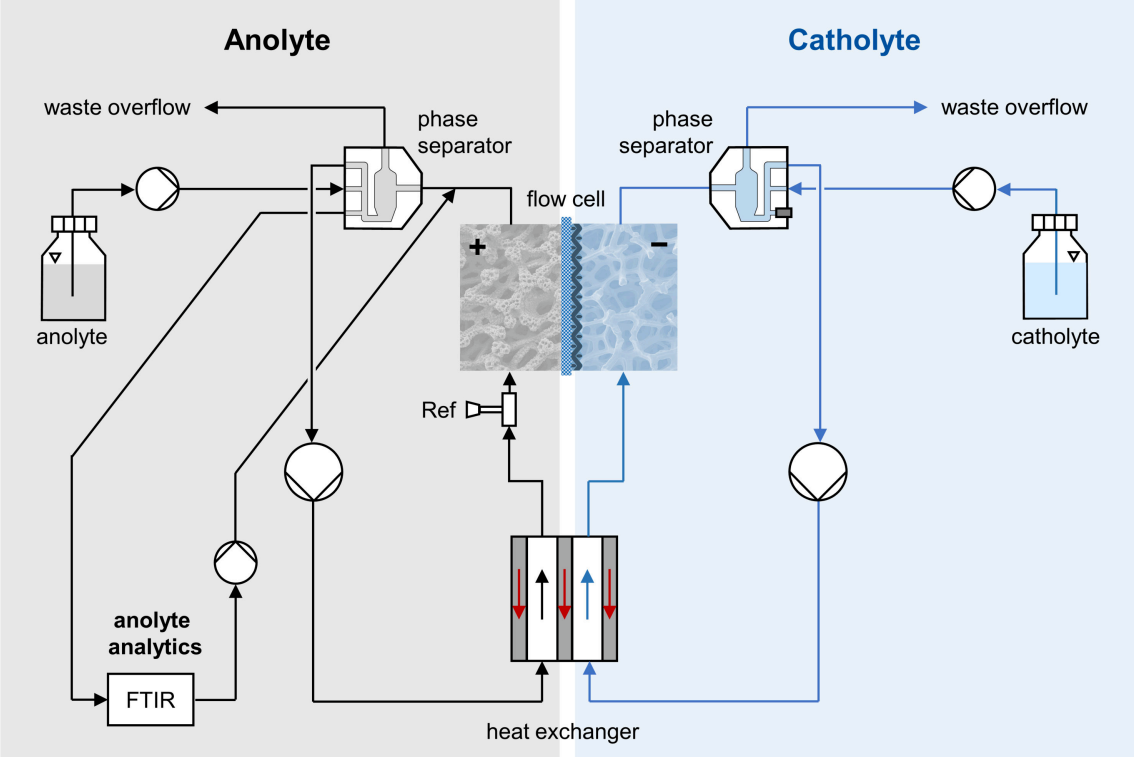

Figure 5.2.: Experimental setup used for batch, single-pass, and feed and bleed mode.

The electrolytes were circulated with a peristaltic pump (Masterflex L/S Digital, Cole-Parmer) through the electrochemical flow cell and a heat exchanger (flex-H-cell, FXC Engineering). The heat exchanger was connected to a thermostat set to 25 °C. Each electrolyte cycle contained a phase separator as discussed in Section 5.3.2 for removal of excess volume and gas bubbles. The total anolyte volume in the setup was 56.5 mL, which was determined by measuring the volume of water that fits into the anolyte cycle. A sample stream from the anolyte was circulated at 10 mL min^{-1} through the flow cell probe of an FTIR spectrometer (ReactIR 702L with Micro Flow Cell, Mettler Toledo). The concentrations of methanol and formate were measured with an FTIR spectrometer at a sample rate of 2 min^{-1}. The concentration data obtained from the spectrometer software (iC-IR, Mettler Toledo) was further processed and analyzed in Origin (OriginLab). Weighted adjacent averaging with a window size of 20 points was applied to the concentration data, which removed noise from the data without altering the shape of the concentration curves. For further information on the FTIR analytics please refer to Section 4.2.5. The sample stream and feed stream were supplied by peristaltic pumps (Reglo ICC, Ismatec). For all experiments, the cathode side was operated in feed and bleed mode at a volume flow of 50 mL min^{-1} in the loop and 5 mL min^{-1} for the feed. Detailed pump settings on the anode side for batch, single-pass, and feed and bleed operation are illustrated in Figure 5.3. In batch mode, the feed pump was set to zero flow rate and the electrolyte was recirculated in a closed system (Figure 5.3a). For single-pass mode, the feed pump and the recirculation pump for the loop were set to equal flow rates, allowing the electrolyte to pass through the cell only once (Figure 5.3b). For feed and bleed mode, the loop flow rate was significantly higher than the flow rate of the feed (Figure 5.3c). For cleaning the setup, the feed was set to a high flow rate and the loop pump to a slightly lower flow rate which enabled quick purging of the electrolyte (Figure 5.3d).

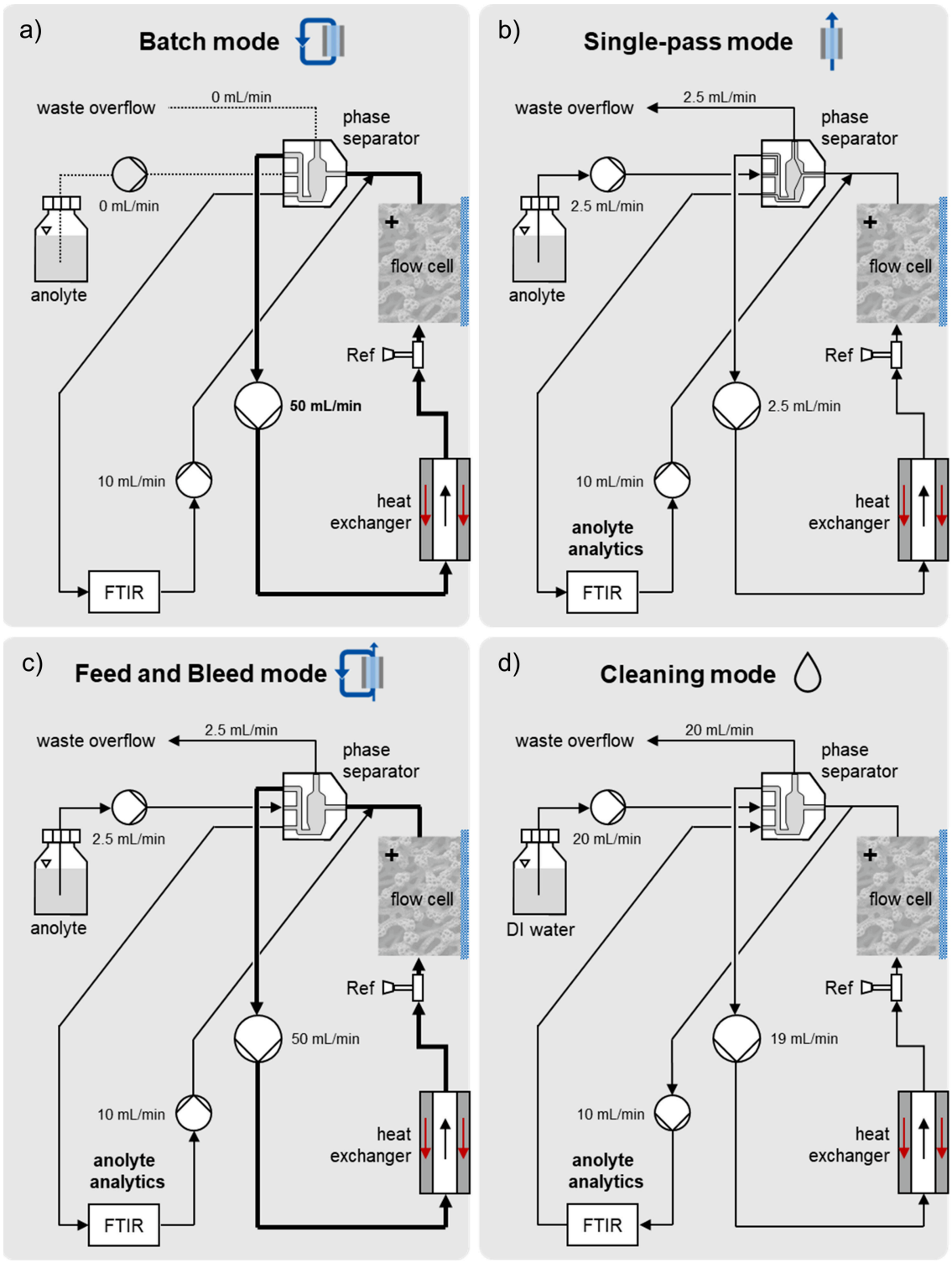

Figure 5.3.: Flow sheet of the anode side of the experimental setup, illustrating the pump settings used for the different operating modes: a) Batch mode, b) Single-pass mode, c) Feed and Bleed mode, d) Cleaning mode.

5.3. Results and discussion

5.3.1. Feed and bleed system behavior

At high recirculation flow rates, the feed and bleed system can be considered as an ideally mixed volume, as shown in Figure 5.4. A comparison of the ideally mixed model with a non-ideally mixed model is provided in the Appendix (Section A.3), indicating that the assumption of ideal mixing is justified for typical feed and bleed operation with a high recirculation rate.

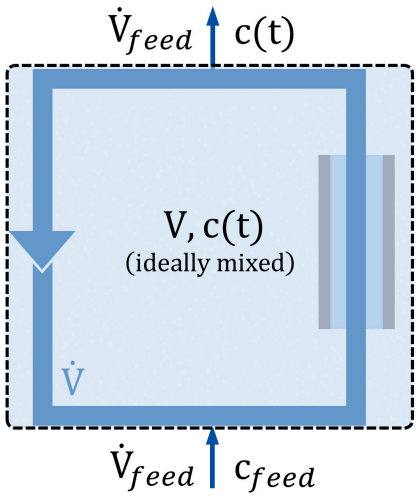

Figure 5.4.: Model of the feed and bleed setup assuming ideal mixing for the total electrolyte volume in the system.

The ideally mixed model can be described by a mole balance around the feed and bleed system as shown in Equation 5.1. The mole balance describes the change in product concentration $c(t)$ in the ideally mixed electrolyte volume V depending on the volume flow rate of the feed $\dot{V}_{feed}$, the product concentration in the feed c_{feed} and the electrochemical reaction with the current density i, the geometric electrode area A, the Faraday efficiency FE, the number of electrons transferred to form the product z, and the Faraday constant F. The following equations and calculations assume that the product concentration in the feed and the initial product concentration in the

electrolyte are both zero ($c_{feed} = c_0 = 0\,\mathrm{mol\,L^{-1}}$), which corresponds to the experiments of this work and most electrosynthesis applications.

$$V\frac{dc(t)}{dt} = \dot{V}_{feed}\,(c_{feed} - c(t)) + \frac{iA \cdot FE}{zF} \tag{5.1}$$

Besides the electrochemical reaction, the system behavior is governed by the electrolyte volume in the system and the feed flow rate. The effect of both parameters on the product concentration is illustrated in Figure 5.5, starting at t=0 when the current is switched on and a product-forming reaction begins. The concentration curves can be described by Equation 5.2, which is the analytical solution of the mole balance (Equation 5.1). The feed flow rate $\dot{V}_{feed}$ determines the rate at which the electrolyte solution in the system is replaced, which allows the adjustment of the obtainable product concentration (and thus conversion) at steady-state as shown in Figure 5.5a.

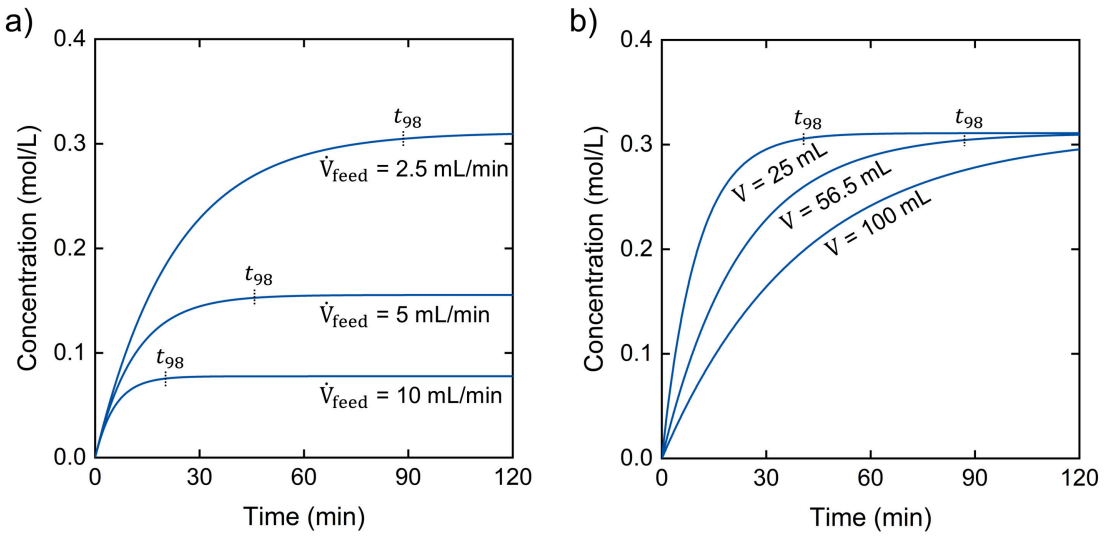

Figure 5.5.: Product concentration curves of feed and bleed systems calculated with the ideally mixed model, starting at t=0 when the current is switched on and a product-forming reaction begins. The plots show the influence of (a) the volume flow of the feed and (b) the total electrolyte volume in the system. The varied parameters are indicated in each plot, and all other parameters remained unchanged at the values of the experimental setup ($\dot{V}_{feed} = 2.5\,\mathrm{mL\,min^{-1}}$, $V = 56.5\,\mathrm{mL}$, $i = 200\,\mathrm{mA\,cm^{-2}}$, $A = 25\,\mathrm{cm^2}$, FE = 100%, and z=4 electrons transferred per reaction).

Reducing the feed flow rate from 5 to 2.5 mL min^{-1} doubles the steady state concentration in agreement with Equation 5.3. However, lowering the feed flow rate increases the time until steady state is reached. In this work, the transient phase refers to the period in which the product concentration is $<$ 98% of the steady-state value. The duration of the transient phase t_{98} can be calculated according to Equation 5.4, which was derived from the ideally mixed model.

$$c(t) = \frac{iA \cdot FE}{zF\dot{V}_{feed}} \cdot (1 - \exp(-\frac{\dot{V}_{feed}}{V} \cdot t)) \tag{5.2}$$

$$c(t \to \infty) = \frac{iA \cdot FE}{zF\dot{V}_{feed}} \tag{5.3}$$

$$t_{98} = -V/\dot{V}_{feed} \cdot \ln(1 - 0.98) \tag{5.4}$$

The transition time increases proportional with the electrolyte volume V of the system, as shown in Figure 5.5b. A low volume is advantageous in enabling the system to respond quickly and reach a steady state faster.

The Faraday efficiency (FE) is one of the most important metrics in electrosynthesis. In comparison to the straightforward FE calculation for batch or single-pass mode (see Equations 5.5 and 5.6), the specific behavior of the feed and bleed system must be considered to evaluate the FE from measured product concentration data correctly. Feed and bleed operation in a steady state resembles the single-pass mode (compare Equation 5.3 and 5.6); however, the use of Equation 5.6 for the feed and bleed mode does not allow for accurate FE calculation in the transient phase. To overcome this limitation, Equation 5.7 was derived from the ideally mixed model to calculate the FE during the entire feed and bleed operation. Please refer to Table 5.1 for an overview of the equations for FE calculation in different flow cell operating modes.

Table 5.1.: Equations for FE calculation from discrete points of product concentration for the different operating modes. The indices n and $n-1$ describe two consecutive discrete points in time.

Mode	Equation	
Batch	$FE_n = \frac{zFV}{iA} \cdot \frac{c_n - c_{n-1}}{t_n - t_{n-1}}$	(5.5)
Single-pass	$FE_n = \frac{zF\dot{V}_{feed}}{iA} \cdot c_n$	(5.6)
Feed&bleed	$FE_n = \frac{zF\dot{V}_{feed}}{iA} \left(c_{n-1} + \frac{c_n - c_{n-1}}{1 - \exp\left(-\frac{\dot{V}_{feed}}{V} \cdot (t_n - t_{n-1})\right)} \right)$	(5.7)

If the internal volume and the feed flow rate are known, the FE of the product-forming reaction can be calculated from discrete points of the product concentration, as demonstrated in Figure 5.6. Figure 5.6a displays discrete concentrations of a curve calculated for a constant FE of 100%. Calculating the FE from the discrete concentration points matches the true FE of the calculated concentration curve exactly, as shown in Figure 5.6b. The proposed equation for FE calculation allows for determining the FE from discrete concentration measurements during both the transient phase and steady state. In addition to model-based validation, the approach of the FE calculation was validated experimentally, as described in Appendix A.3.

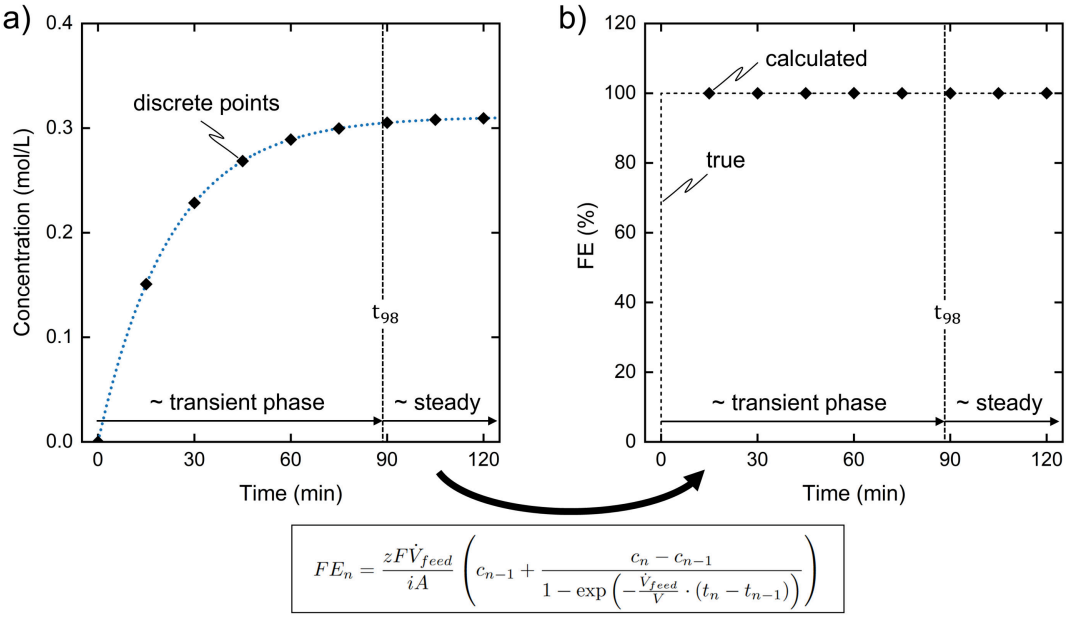

Figure 5.6.: a) Discrete points on a product concentration curve calculated for a constant FE of 100% (blue dotted line). The parameters of the experimental demonstration (see Figure 5.9) were used for the calculation ($\dot{V}_{feed}$ = 2.5 mL min^{-1}, V = 56.5 mL, i = 200 mA cm^{-2}, A = 25 cm^2, and z = 4). The end of the transient phase is indicated by a vertical dashed line. **b)** FE calculated from the discrete concentration points by Equation 5.7 (also shown in the Figure) compared to the true FE.

5

5.3.2. Phase separation in a feed and bleed system

In the experimental demonstration of the feed and bleed operation mode discussed in Section 5.3.3, gas evolution was only observed on the cathode side. However, gas evolution is common in many electrochemical processes, often involving hydrogen or oxygen evolution in aqueous electrolytes. Gas evolution might occur as an undesired side reaction or result from the intended reaction (e.g., water electrolysis). To prevent gas accumulation within the recirculation loop, it is necessary to remove gas bubbles from the liquid electrolyte. For that purpose, a low volume phase separator was designed (Figure 5.7a). The phase separator was 3D-printed with threaded ports for standard tubing connectors. The two-phase stream from the electrochemical cell enters the phase separator on the single inlet on the left side in a tangential fashion, resembling a hydrocyclone. Thus, sec-

ondary flow is introduced in the central chamber and facilitates bubble removal through the bleed stream at the top. The bubble-free electrolyte flows through tangential outlets at the bottom of the separation chamber towards the outlet on the right side, where it mixes with the incoming feed stream. An additional outlet on the bottom right allows for analysis of the composition of the product stream (see Figure 5.2 for the experimental setup). The phase separator was designed for a low internal volume and uses two different separation principles depending on the volume flow. When the separator was operated at low volume flow ($< 20\,\mathrm{mL\,min^{-1}}$), gas bubbles ascended towards the top outlet as illustrated in Figure 5.7b. This observation indicates that the buoyancy of the gas bubbles was the primary driving force of separation at low-volume flows. With increasing volume flow ($> 20\,\mathrm{mL\,min^{-1}}$), gas bubbles were more finely dispersed in the electrolyte, and the centrifugal forces started to contribute to the separation process. This dynamic was facilitated by the tangential inlet design, which imparted a hydrocyclone-like motion to the incoming flow, forcing the gas bubbles to accumulate at the center of the chamber as depicted in Figure 5.7c. The centrifugal force pushes the liquid electrolyte towards the outer walls of the separation chamber, ensuring that the electrolyte exits through the tangential outlets at the bottom without gas bubbles. The effect of centrifugal forces intensified with increased volume flow, efficiently segregating the gas bubbles from the liquid electrolyte. This mechanism highlights the capability of the phase separator to adapt its separation strategy based on the flow conditions, ensuring effective gas removal despite its low internal volume of 4 mL. The design of the 3D-printed phase separator with low internal volume reduces the time required to reach a steady state and the residence time in the loop. Both of which are beneficial for feed and bleed operations.

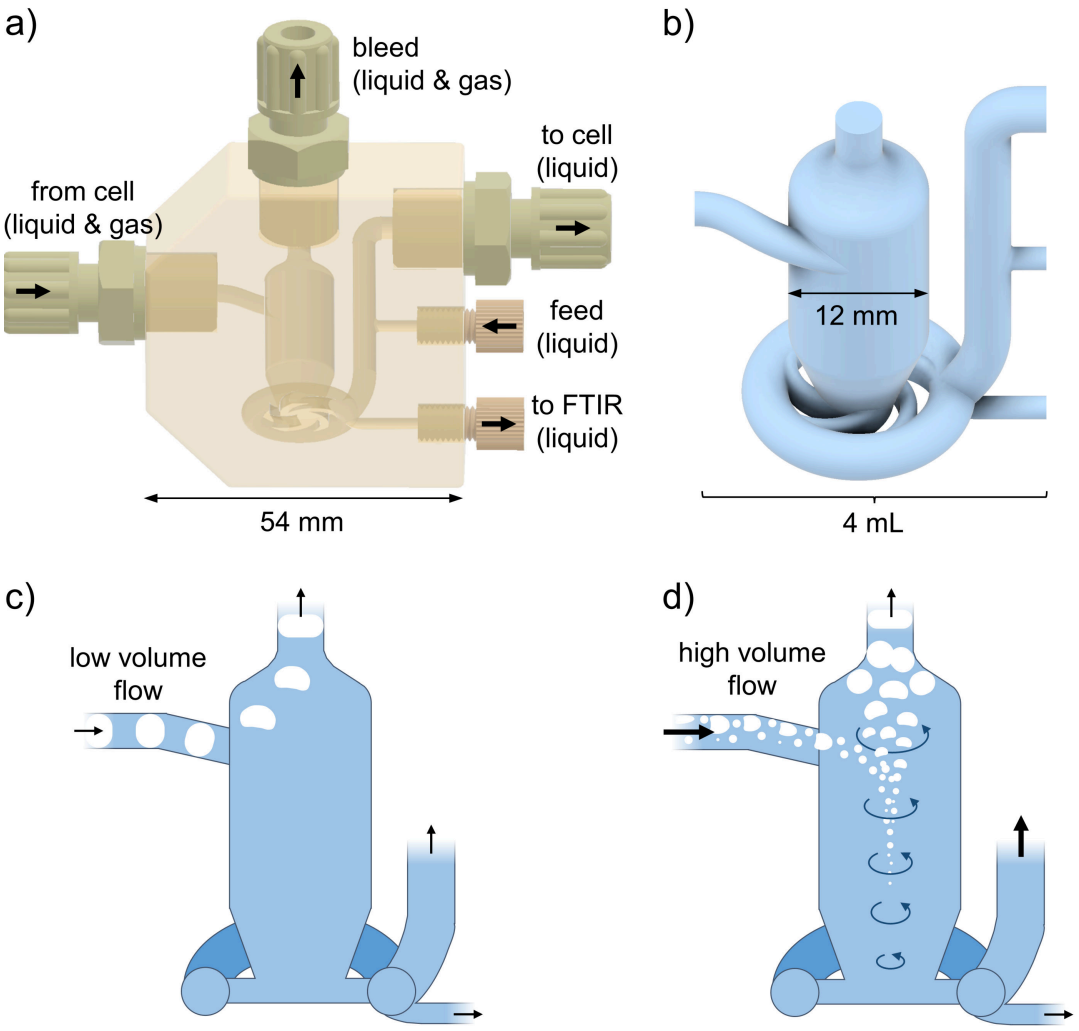

Figure 5.7.: a) CAD image of the phase separator with an inlet on the left side, an overflow outlet at the top, and an analysis outlet, a feed inlet, and a cell stream outlet on the right side. **b)** Internal channels and separation chamber of the phase separator. **c)** At low volume flow rates gas bubbles from the electrochemical cell rise to the bleed outlet, **d)** At high volume flow rates the gas separation is supported by a hydrocyclone-like motion in the central chamber.

5.3.3. Methanol oxidation: Comparison of operation modes

Electrochemical methanol oxidation is a promising anodic reaction, that can provide value-added products while operating at a lower electrode potential than oxygen evolution [Li2020a; Du2023; Xian2021; Baes2023; Schw2024]. Methanol oxidation to formate readily reaches high conversion and product concentration [Baes2024]; hence, it has been selected for investigating the operation modes at an industrially relevant current density of 200 mA cm^{-2}. Formic acid and salts of its conjugate base formate are widely used chemicals with a broad range of applications [Hiet2010]. For comparison of the operating modes (Figure 5.8 and 5.9), the ideal concentration curves for methanol oxidation to formate in batch, single pass, and feed and bleed mode were calculated and then compared to the corresponding curves that were measured experimentally. A constant FE of 100% for formate was assumed as the ideal case for the calculation, while a lower FE was determined in the experiments (Figure 5.8 and 5.9). The same volume, flow rate, and current density were used for the calculation as in the experiments. All experiments were carried out with the same experimental setup, which can be used for all three operating modes depending on the pump settings (see Figure 5.3).

In ideal batch mode at constant FE, the reactant concentration decreases linearly while the product concentration increases linearly, as depicted in the calculated concentration curves in Figure 5.8a. With increasing experiment duration, an increasing amount of methanol is converted to formate. In comparison to ideal reactor models in chemical reaction engineering, the behavior of a flow cell in batch mode with closed recirculation corresponds to an ideal batch reactor (stirred tank), as both represent a closed system. The slope of the changing concentrations depends on the current density i, the electrode area A, the FE, the number of electrons transferred per reaction z, and the electrolyte volume V in the batch setup (refers to the equation in the plot of Figure 5.8a).

During methanol oxidation with the experimental setup operating in batch

mode, a nearly linearly decreasing methanol concentration was observed as shown in Figure 5.8c, in agreement with the model prediction. However, the formate concentration in the experiment increased with decreasing slope, reaching a maximum concentration of 0.44 mol L^{-1}. Comparing experimental (d) and calculation data (a) suggests a decreasing FE over time for formate formation since its concentration does not follow a linear increasing trend throughout the experiment. The FE correlates with the slope of the formate concentration and is calculated with Equation 5.5 from the change in formate concentration between two time points. Figure 5.8e illustrates the decreasing FE and increasing methanol conversion over time determined from the concentration data of the experiment. Although FE for formate formation was above 90% within the first 5 minutes of the experiment, the FE dropped significantly afterward, reaching 0% at 56 min. One credible explanation for the decreasing FE is the further electro-oxidation of formate to carbonate, which is a known side product of methanol oxidation on copper oxide [Heli2004; Wei2021]. Section 4 demonstrated the effect of the ratio of formate to methanol on the FE for anodic oxidation of methanol to formate, elaborating on possible pathways for formate loss.

In batch operation mode, a high conversion of nearly 80% of the initial 1 mol L^{-1} methanol was reached within the experiment duration of less than 60 min. The rapid progress of the oxidation was enabled by the high current density of 200 mA cm^{-2} and the high ratio of geometrical electrode area (25 cm^2) to electrolyte volume (56.5 mL). These results show that the batch operation mode is well suited to achieve high conversion and high product concentrations. However, the concentration of reactant and product are constantly changing. Since no steady state is reached, a single batch experiment cannot distinguish temporal effects such as possible deterioration of the electrode from the influence of the increasing reaction progress.
In ideal single-pass mode at constant FE, product and reactant concentrations are constant after a short transient phase, as shown in the calculated concentration curves in Figure 5.8b. A flow cell in single-pass mode behaves similarly to an ideal plug flow reactor (PFR), where the reaction progress increases with the distance the flow travels through the reactor.

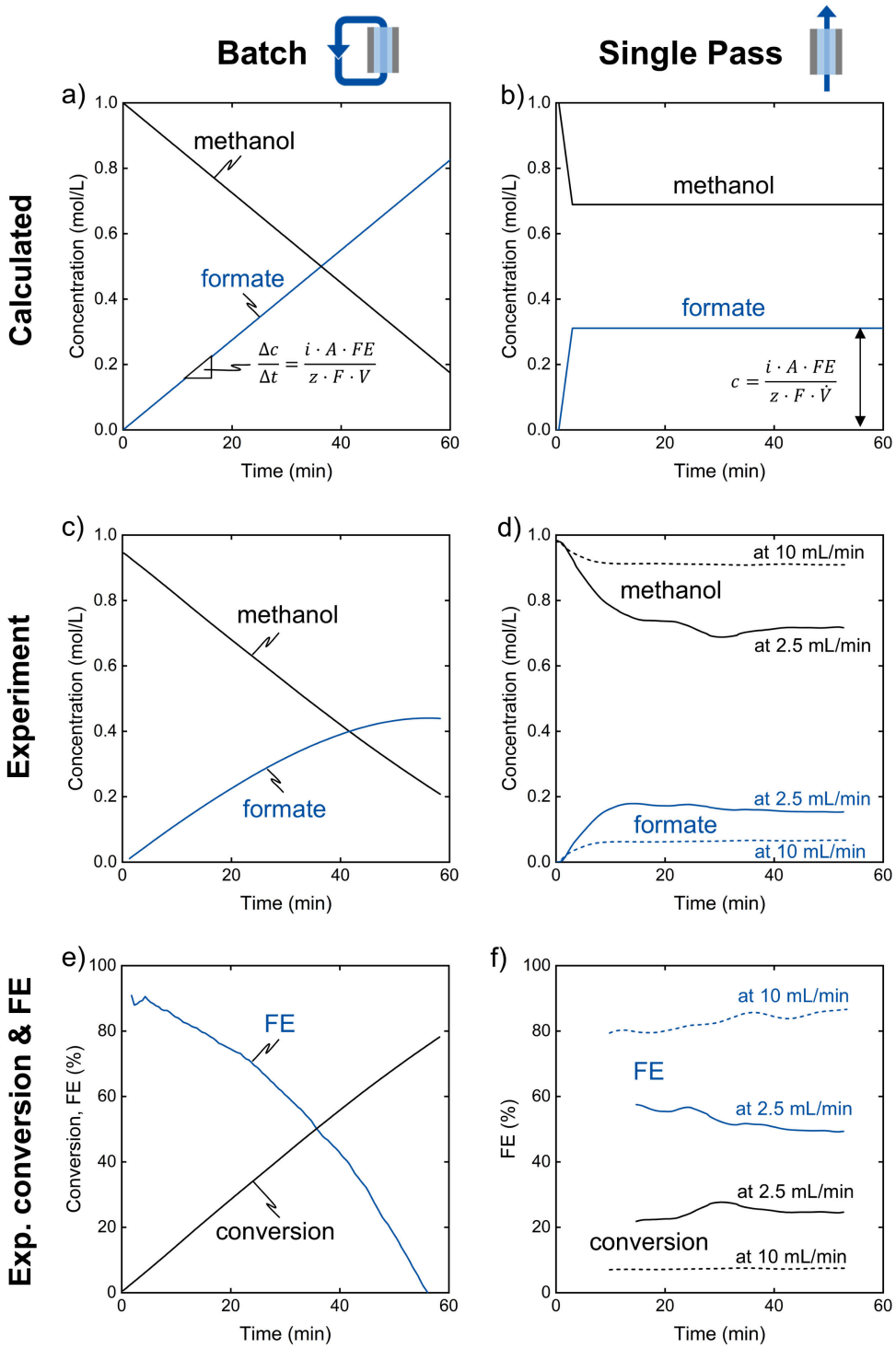

Figure 5.8.: a-b) Ideal concentration curves calculated for methanol oxidation to formate in batch and single pass operation mode with a constant FE of 100%. The calculation was performed with the same volume, flow rate, and current density as the experiments. **c-d)** Measured concentrations during oxidation experiments in batch (V = 56.5 mL, $\dot{V}$ = 50 mL min^{-1}) and single pass (two experiments, at $\dot{V}$ = 2.5 mL min^{-1} and at $\dot{V}$ = 10 mL min^{-1}). **e-f)** Methanol conversion and FE for formate determined from the measured concentration data by applying Equations 5.5-5.7. **Experimental conditions:** 200 mA cm^{-2}, 25 °C, 2 mol L^{-1} KOH, 1 mol L^{-1} methanol.

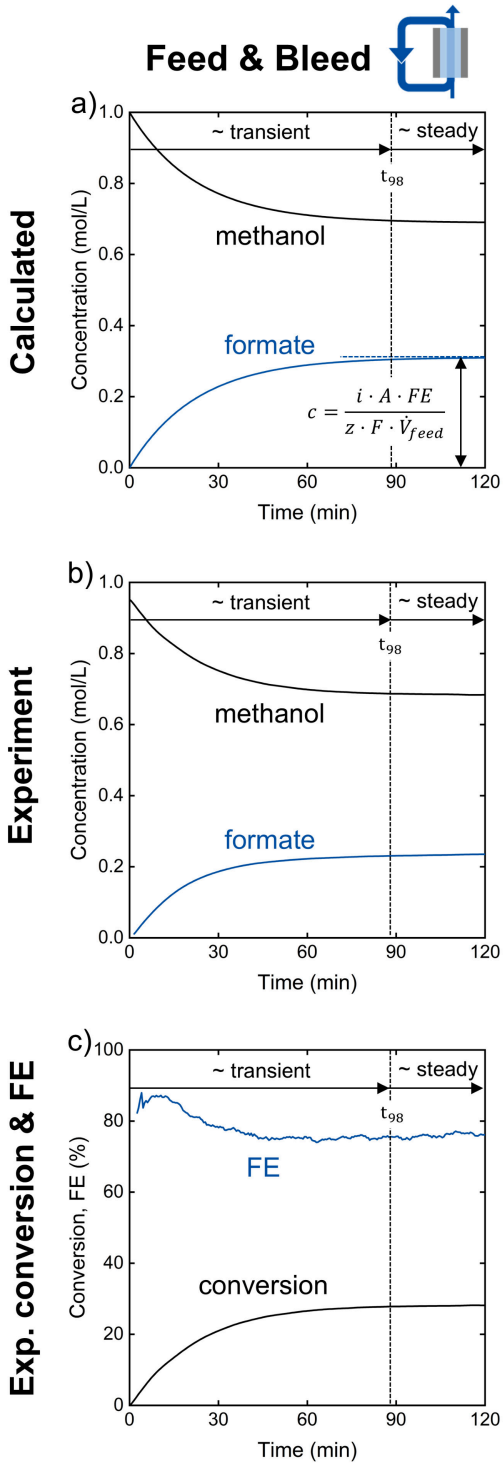

Figure 5.9.: a) Ideal concentration curves calculated for methanol oxidation to formate in feed and bleed operation mode with a constant FE of 100%. The calculation was performed with the same volume, flow rates, and current density as the experiments. **b)** Measured concentrations during oxidation experiments in feed and bleed operation mode (V = 56.5 mL, $\dot{V}_{cycle}$ = 50 mL min^{-1}, $\dot{V}_{feed}$ = 2.5 mL min^{-1}). **c)** Methanol conversion and FE for formate determined from the measured concentration data by applying Equations 5.5-5.7. **Experimental conditions:** 200 mA cm^{-2}, 25 °C, 2 mol L^{-1} KOH, 1 mol L^{-1} methanol.

The short transient phase in the calculation is caused by the residence time of the flow in the cell and the time delay until the flow reaches the point of concentration measurement. Assuming an ideal plug flow without back mixing, the transient phase in the calculation is short. The product concentration in single pass mode is determined by the current density i, the geometric electrode area A, the FE, the number of electrons transferred per reaction z, and the flow rate $\dot{V}$ through the cell (refers to the equation in the plot of Figure 5.8b). Methanol oxidation in single-pass mode was investigated in two separate experiments at a flow rate of 2.5 mL min^{-1} and 10 mL min^{-1}. As expected, more methanol was converted to formate at a flow rate of 2.5 mL min^{-1} than at 10 mL min^{-1}, as shown in the concentration curves in Figure 5.8d. The transient phase was significantly longer than in the ideal calculation, which was attributed to non-ideal flow (back mixing, dead volumes, and recirculated anolyte through the FTIR spectrometer). After the initial transient phase, the concentrations of methanol and formate were fairly constant, with slight fluctuations for the experiment at 2.5 mL min^{-1}. Figure 5.8f shows FE and conversion over time calculated from the single pass concentration data by Equation 5.6 and 4.1. The non-ideal transient phase was not evaluated as the applied FE equation was derived from the ideal system behavior. The experiment at 2.5 mL min^{-1} showed a lower FE at higher methanol conversion (49-57% FE at 22-28% conversion), compared to the experiment at 10 mL min^{-1} (80-86% FE at 7.0-7.5% conversion). As observed in the batch experiment, the FE was lower at higher conversion, since an increasing ratio of formate to methanol facilitates the overoxidation of formate to carbonate. However, the lower FE at 2.5 mL min^{-1} can be only partially explained by the higher conversion. Figure 5.10 directly compares the three different operating modes by plotting the FE against the conversion showing that at the same conversion the FE in single-pass mode at 2.5 mL min^{-1} was significantly lower than for batch mode at a flow rate of at 50 mL min^{-1}. The difference is attributed to an increasing mass transfer limitation with decreasing single-pass flow rate. The flow rate of 2.5 mL min^{-1}, required for about 25% conversion, corresponds to a very low mean linear flow velocity of approximately 0.3 mm s^{-1}

in the cell. In single pass mode, product concentration and mass transfer cannot be investigated separately, as both product concentration and mass transfer are directly dependent on the flow rate. In this context, the shape of the channel inside the cell is crucial (cross-section area of the flow and active electrode area). In small meandering microfluidic channels, a flow velocity with sufficient mass transfer can be achieved even at a low flow rate so that a high product concentration can be achieved in single pass mode [Plet2018]. However, in flow cells with a larger cross-section area of the flow, such as the flow cell used in this work (cross-section: 1.75 cm^2), the single pass mode is unsuitable for high product concentrations due to mass transfer limitations. A major advantage of the single pass mode is the operation in a steady state, which is reached quickly with only a short transient phase. Steady-state operation enables long-term experiments and facilitates the investigation of temporal effects such as electrode degradation.

In ideal feed and bleed mode at constant FE, the reactant concentration decreases, and the product concentration increases until a steady state is reached, as depicted in the calculated concentration curves in Figure 5.9a. In a steady state, the rate of product formation at the electrode equals the rate of product removal through the bleed stream. The concentration curves for an electrochemical flow cell in feed and bleed mode present a behavior similar to an ideal continuous stirred-tank reactor (CSTR). For ideal feed and bleed, the product concentration converges to the concentration ideal single-pass would reach at the same feed flow rate (compare equations in Figure 5.8b and 5.9a). This work considers the system in a steady state when the product concentration reaches 98% of its final value. The end of the transient phase when 98% of the final concentration is reached is marked by a black dashed line in the plot and was calculated by Equation 5.4. The duration of the transient phase depends on the electrolyte volume V in the system and on the feed rate $\dot{V}_{feed}$. During methanol oxidation with the experimental setup operating in feed and bleed mode, the measured concentration curves of methanol and formate closely resembled the ideal calculation (Figure 5.9b). However, the formate concentration converged to

0.24 mol L^{-1} in the experiment compared to 0.31 mol L^{-1} in the calculation that assumed a constant FE of 100%. The lower formate concentration can be attributed to a FE $<$ 100%. The FE in feed and bleed mode can be determined from the formate concentration even before a steady state is reached by applying Equation 5.7. Figure 5.9c shows the FE and methanol conversion calculated from the concentration data. The initial FE for methanol oxidation was high, reaching up to 88%. With increasing methanol conversion, the FE converged to 76% at 28% conversion at steady state.

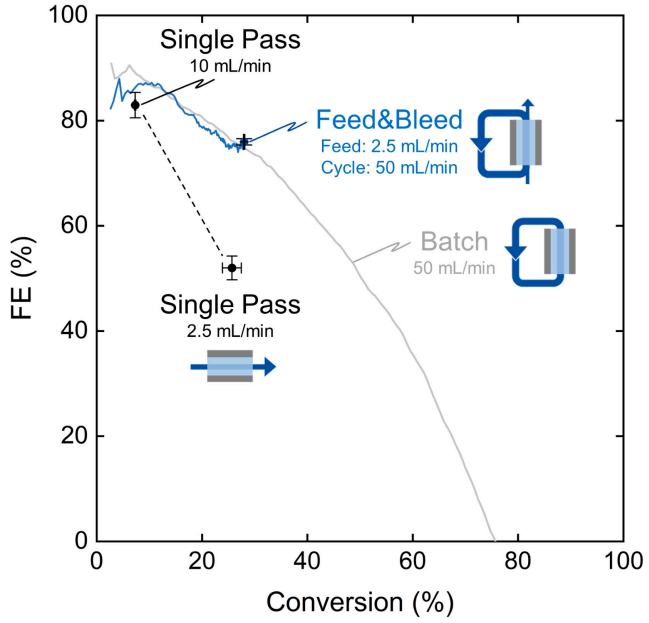

Figure 5.10.: FE for formate plotted over methanol conversion from the data of Figure 5.8 and 5.9, comparing batch, single pass, and feed and bleed operating mode. **Experimental conditions:** 200 mA cm^{-2}, 25 °C, 2 mol L^{-1} KOH, 1 mol L^{-1} methanol.

If the FE is plotted against conversion as shown in Figure 5.10, the resulting FE curve of feed and bleed closely aligns with the curve obtained in batch operation. The FE curves deviated slightly at low conversion, which was likely caused by artifacts of non-ideal mixing and the reduced accuracy of the FTIR analytics at low formate concentration. The difference between the FE at the steady state operating point in feed and bleed mode and in batch mode at the same conversion of 28% was remarkably low (76% vs. 74.7%). The good agreement of batch and feed and bleed FE demon-

strates that the proposed calculation method provided accurate FE data for most of the transient phase and the steady state operating point. Furthermore, the results illustrate that feed and bleed can be operated in a steady state at high conversion without mass transfer limitation. In contrast to the single-pass mode, the achievable conversion in feed and bleed mode was successfully decoupled from the flow rate in the cell, as the steady state conversion can be increased by decreasing only the feed flow rate. The feed and bleed mode follows the same relationship of FE and conversion as observed in batch mode (see Figure 5.10), but in contrast to batch mode, a single point on the conversion-FE curve can be selected for continuous operation. Therefore, feed and bleed can provide a unique opportunity to investigate electrochemical processes at both steady state and industrially relevant reaction conditions with high product concentration and conversion. Figure 5.11 demonstrates feed and bleed operation over an extended experimental duration of six hours showing no significant change in FE and conversion after the transient phase.

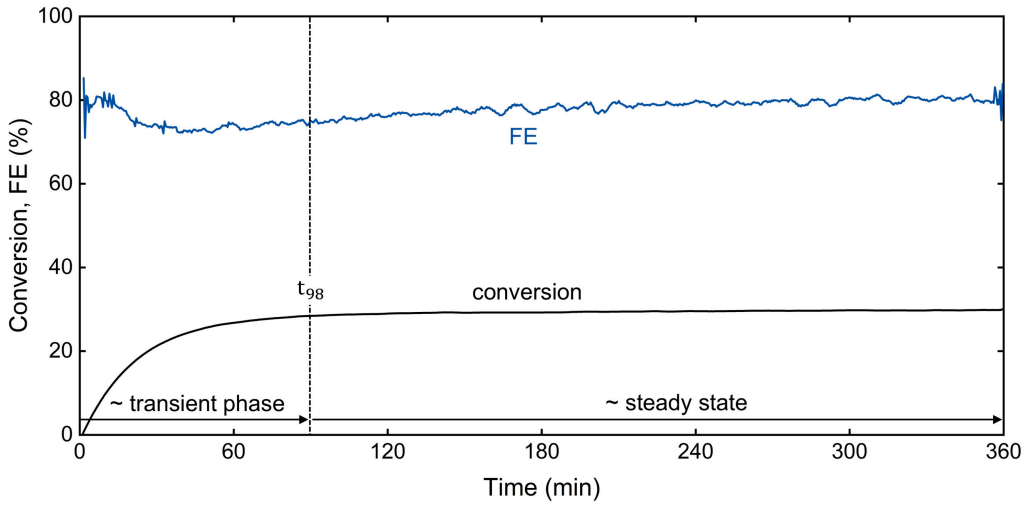

Figure 5.11.: Methanol conversion and the FE for formate plotted over time for an extended experimental duration of six hours. **Experimental conditions:** 200 mA cm^{-2}, 25 °C,$\dot{V}_{cycle}$ = 50 mL min^{-1}, $\dot{V}_{feed}$ = 2.5 mL min^{-1}, 2 mol L^{-1} KOH, 1 mol L^{-1} methanol.

5.4. Conclusion

This work explored the 'feed and bleed' operating mode for electrosynthesis in flow cells, specifically targeting its utility in lab-scale research. A model was presented to facilitate the understanding and analysis of the behavior of the feed and bleed system in both transient and steady state. A novel 3D-printed phase separator was developed to efficiently tackle gas separation from the electrolyte loop, leveraging gravity and centrifugal forces for effective separation while maintaining a low internal volume. This separator can be reproduced through additive manufacturing techniques using readily accessible materials.

Moreover, a versatile experimental setup was introduced with a low internal volume tailored for the feed and bleed operating mode. The setup's capability to operate in batch and single-pass mode as well enabled a direct comparison of all three operating modes at the example of methanol oxidation to formate. Furthermore, the setup can be employed in future studies to select the operating mode depending on the research question without the need for hardware changes. Online FTIR analytics, featuring a high sampling rate, provided comprehensive insights into the characteristics of each operation mode, offering valuable guidance for researchers in selecting the most suitable operating mode for their experiments. Notably, the comparison highlighted that the feed and bleed mode uniquely supported continuous operation at both steady-state and high conversion levels.

The presented study spotlights the advantages of feed and bleed operation in comparison to batch and single-pass modes, solves practical challenges, and provides valuable insights for applying feed and bleed in lab-scale research. The unique characteristics of feed and bleed render it particularly suitable for investigating continuous processes at a steady state over extended periods while maintaining industrially relevant conditions with high product concentration. Beyond the demonstrated setup for liquid product streams, the feed and bleed approach also holds potential for applications involving microfluidic reactors, gaseous product streams, or automated experimentation.

6. Conclusion and Outlook

Electrochemical processes, such as CO_2 reduction and water electrolysis, represent promising alternatives to conventional fossil-based routes for the production of basic chemicals. The present thesis addressed three critical challenges in the transition of electrochemical processes from laboratory-scale research to viable industrial application: i) high energy demand and costs, ii) need for studies at industrially relevant conditions, and iii) process stability over time. Energy demand and costs were tackled by investigating selective methanol oxidation for paired electrolysis, which reduced energy demand and provided additional value-added products. Two reaction systems were investigated in electrochemical flow cells, yielding high concentrations of formaldehyde or formate. Methanol oxidation and the paired process were studied at industrially relevant conditions which provided novel insights into the impact of methanol conversion and the interactions between anode and cathode side. Methanol crossover and the ion balance were identified as crucial phenomena for the stability of the paired process. Furthermore, the present thesis introduced the feed and bleed operation mode for electrochemical flow cells. The feed and bleed mode enabled steady-state operation at high product concentration, allowing to investigate the stability of electrochemical processes at industrially relevant conversion.

Methanol oxidation to formaldehyde was investigated on platinum electrodes in metallic and oxidized state in Chapter 3, presenting the first targeted electrochemical synthesis of formaldehyde. The Faraday efficiency (FE) for formaldehyde was higher on oxidized platinum, while the potential was lower on metallic platinum, hence showing a trade-off between energy efficiency and Faraday efficiency. Besides formaldehyde, formic acid

was observed as additional value-added side product of methanol oxidation on both oxidized and metallic platinum. Anodic methanol oxidation to formaldehyde was paired with cathodic CO_2 reduction to formate. The oxidized platinum anode achieved a combined FE of up to 89% for formaldehyde and formic acid in the paired process, leading to a final formaldehyde concentration of 1.14 mol/L (representing 14% yield). On the other hand, metallic platinum exhibited a lower FE, reaching up to 54% for both products combined. However, the anodic potential for methanol oxidation on metallic platinum was significantly lower than on oxidized platinum or for OER. In terms of products formed per electrical energy input, both paired processes using methanol oxidation on metallic or oxidized platinum were more efficient than CO_2 reduction paired with OER. Methanol crossover was found to decrease the FE at the cathode, highlighting the impact of interactions between anode and cathode side on process stability.

Chapter 4 focused on methanol oxidation to formate on a hierarchically structured CuO electrode while exploring the impact of reaction conditions, conversion and interactions within the paired process. The CuO anode exhibited porosity on different length scales, thereby creating a high electrochemical active surface area 400 times larger than a flat CuO sheet. Employing the CuO anode for methanol oxidation, a high initial formate FE of 85% was reached at a current density of 200 mA/cm^2. As methanol conversion increased, the FE declined, reaching zero at 75% conversion. The increasing conversion affected selectivity by altering the ratio of methanol to formate, as methanol oxidation to formate competed with the subsequent oxidation of formate to carbonate. The significant impact on selectivity highlighted the importance of reporting and investigating the performance of electrochemical reactions at relevant levels of conversion. Regarding the reaction conditions, the influence of current density, temperature, electrolyte flow rate, electrolyte composition and membrane type on methanol oxidation to formate was investigated. Employing optimized conditions, anodic methanol oxidation to formate paired with cathodic hydrogen evolution reached an initial formate FE close to 100% at 100 mA/cm^2 with an anodic potential of 1.33 V vs. RHE. The paired electrolysis successfully

demonstrated the synthesis of formate as value-added product at relevant current density and yield (70%) with a reduced energy demand compared to typical OER. Furthermore, the characteristics of two different setups for paired electrolysis were discussed employing either an AEM or a BPM. The comparison of the two setups and different membrane types emphasized the necessity of considering both ion and water balance for paired electrolysis at high conversion and product concentration.

Chapter 5 introduced the 'feed and bleed' operating mode for electrochemical flow cells using methanol oxidation to formate for experimental characterization. The chapter provided equations for understanding and analyzing feed and bleed systems and discussed influencing factors, such as feed flow rate and internal volume. Moreover, a 3D-printed phase separator was developed for space-efficient gas separation from the electrolyte loop. The feed and bleed mode was compared experimentally to single-pass and batch operation by employing methanol oxidation to formate. The comparison highlighted the characteristics of each operation mode, discussing product/reactant concentration, conversion, and Faraday efficiency. Only the feed and bleed mode allowed steady-state operation at high product concentration which provides the unique opportunity to investigate the stability of electrochemical processes at industrially relevant conditions.

In summary, the main findings of this thesis are:

- Formaldehyde can be synthesized by methanol oxidation on platinum electrodes, with oxidized platinum achieving higher Faraday efficiency (up to 58%), while metallic platinum requires a lower anodic potential (0.6 V vs. RHE).
- Methanol oxidation to formate at hierarchically structured CuO electrodes achieves high Faraday efficiency at high current densities of up to 200 mA/cm^2 at a lower potential than OER. Optimizing the reaction conditions significantly improves both the Faraday efficiency (up to nearly 100%) and the overall formate yield (up to 70%).

- Conversion and product concentration have a critical impact on the selectivity of methanol oxidation to formate with the Faraday efficiency declining to zero at high conversion.
- Interactions between the anode and cathode side, such as ion transfer, water and reactant crossover are crucial for the stability and performance of paired electrolysis at high product concentration.
- The 'feed and bleed' operating mode is a versatile alternative to conventional batch or single-pass operation of electrochemical flow cells, enabling steady-state operation at high product concentration.

Further research is needed to fully leverage the beneficial characteristics of methanol oxidation to formaldehyde as anodic reaction. On the catalysis side, an improved catalyst with high selectivity to formaldehyde at low overpotential would be required, combining the benefits of metallic and oxidized platinum. Employing electrodes with an optimized macro- and microstructure could increase mass transfer and active surface area of the electrode compared to the porous sheet electrodes used in the present work. Optimizing the reaction conditions and investigating the impact of increasing conversion as demonstrated for formate synthesis might further enhance formaldehyde production. Pulsed electrolysis on metallic electrodes could facilitate the reduction of adsorbed CO to formaldehyde reversing overoxidation and maintaining a low potential by clearing catalyst sites blocked by CO [Yuan2018]. Methanol oxidation under water free conditions is another promising approach to increase selectivity to formaldehyde [Schw2024]. The electrolyte gap in the present work is associated with significant energy losses, especially at high current density. Implementation of methanol oxidation to formaldehyde in a zero-gap configuration could minimize ohmic losses and facilitate efficient paired processes without any liquid electrolyte gap using membrane electrode assemblies. In combination with zero-gap compatible electrodes, methanol could also be supplied in a gaseous feed at elevated temperatures to improve mass transfer to the electrode.

The present work demonstrated a high formate yield, however further research is necessary to develop more efficient catalysts for methanol oxi-

dation to formate or formic acid especially focusing on increasing selectivity at high conversion and reducing the overpotential. If suitable catalysts are developed for acidic conditions, the synthesis of formic acid instead of formate could avoid stochiometric neutralization of OH^- and would likely facilitate downstream processing. Further research could explore the impact of the electrode thickness and structure on formate selectivity and investigate a possible trade-off between maximizing surface area and mass transport. The thick dendrite layer deposited in the present work provided a high surface area, however a thinner dendrite layer could improve selectivity to formate by faster diffusive mass transport to the inner regions of the porous layer. Future work could investigate reaction conditions tailored for the changing requirements from initial conversion to high product concentration providing the groundwork for efficient formate production. Initially high current density can be applied but should be reduced with increasing conversion. High methanol concentrations (> 2 mol/L) can be combined with moderate KOH concentration (about 1 mol/L) to further increase formate FE if KOH is added continuously to counter the neutralization of OH^- caused by the formation of formate. A paired synthesis of anodic methanol oxidation to formate and cathodic hydrogen evolution would be feasible with a shared electrolyte even without a membrane or diaphragm. In contrast to conventional water electrolysis, no oxygen is produced during methanol oxidation, so that no gas retaining separator is needed to prevent oxyhydrogen formation. Operation without a traditional separator could further reduce the cell potential and would facilitate cell concepts beyond planar flow such as swiss-roll electrodes with axial flow, porous electrodes with perpendicular flow or intertwined 3D-printed electrodes.

The feed and bleed operating mode can be utilized for future research on electrochemical processes in steady state at high product concentration. In contrast to conventional batch or single-pass operation, the feed and bleed mode allows to investigate stability and performance at different levels of conversion independent of flow velocity or changing concentrations. From a practical side, the electrolyte volume in the setup could be further reduced by a more compact setup with shorter tubing of smaller

diameter leading to a shorter transition time until steady state is reached. Implementation of feed and bleed in a microfluidic setup would allow to investigate relevant product concentrations at small scale with even shorter transition times. The feed and bleed mode offers the possibility to quickly screen the influence of reaction conditions during continuous operation by changing a specific parameter (e.g., temperature, flow velocity, electrolyte composition) and observing the response such as the potential or product concentration. Perspectivically, the feed and bleed operating mode could be used in combination with an automated experimental setup with online analytics. Thus, a software solver controlling the reaction conditions paired with the feedback from the feed and bleed setup as a hardware model could automatically optimize reaction conditions. While the present work demonstrated the feed and bleed mode using methanol oxidation to formate with a liquid product stream, the mode could be applied to reaction systems with a gaseous product stream as well. The investigation of stability and performance at different levels of conversion with high product concentrations would be of particular interest for electrochemical CO_2 reduction.

The present thesis focused on the technical aspects of selective methanol oxidation for paired synthesis addressing key challenges of electrochemical processes. However, future research should take the broader context of selective methanol oxidation into account, considering both costs and carbon emissions of methanol, electricity, and downstream processing. Holistic assessment of the process could address trade-offs between product concentration, production rate and selectivity from an environmental and economic perspective. The experimental data and findings of this work can facilitate a realistic assessment of selective methanol oxidation and contribute to identify research needs. Beyond methanol oxidation, the methodological aspects of this work can be transferred to investigate other electrochemical processes at industrially relevant conditions. The present work thus contributes to the overarching goal of bringing renewable electrochemical processes into industrial application.

A. Appendix

A.1. Methanol oxidation to formaldehyde

Cell potential at equal current density

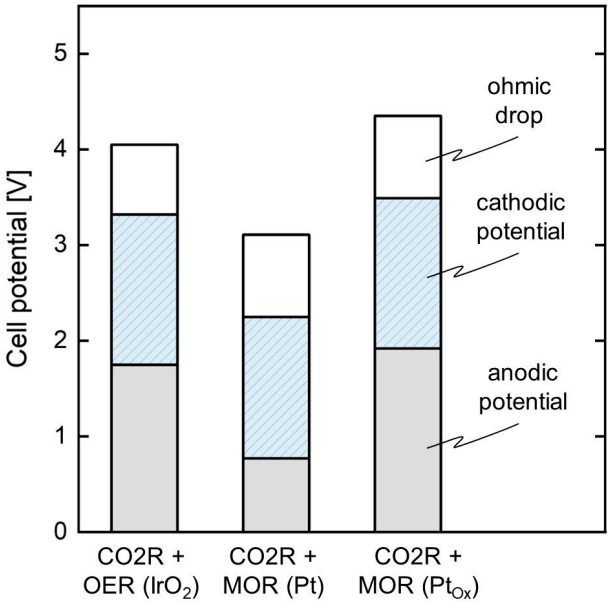

Figure A.1.: Cell potential for CO2R paired with different anodic reactions at the same current density of 50 mA cm^{-2}. The cell potential is divided into the potentials of the anode, cathode and the ohmic drop over the cell (electrolytes and membrane). Pt and Pt_{Ox} were not stable at 50 mA cm^{-2} for 4h, thus the potentials were averaged over a shorter time span of 25 min.

A.2. Methanol oxidation to formate

Chronopotentiometry curves

The chronopotentiometry curves in Figure A.2 show the anodic potential of MOR over time for three different current densities. The anodic potential increased with increasing current density. A minor increase in potential was observed over time for all three current densities. The increase in potential could be caused by a change in the reaction, as the formate FE decreased while more carbonate was produced towards the end of the experiments. In addition, the concentration of hydroxide ions decreased with the increasing formate concentration over time. The lower conductivity of formate compared to hydroxide could also contribute to the slight increase in potential.

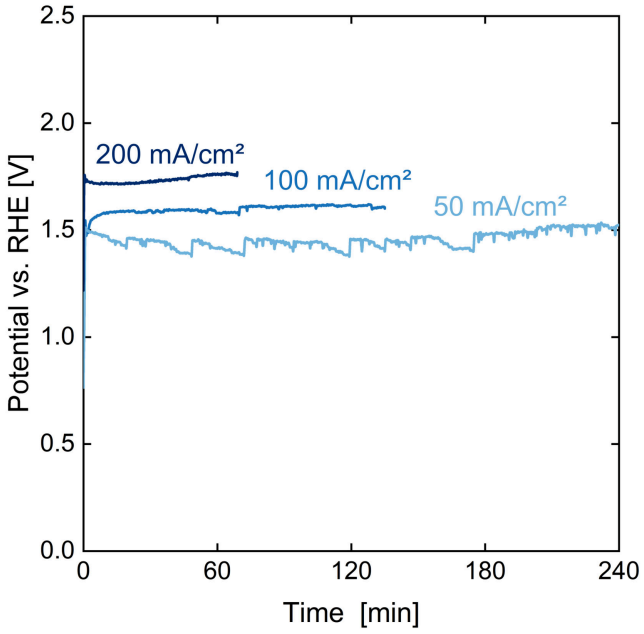

Figure A.2.: Chronopotentiometry curves of MOR at three different current densities. The methanol oxidation was conducted at 25 °C, 50 mL/min, 2 mol/L KOH, 1 mol/L methanol and with a BPM.

Crossover of formate and methanol to the catholyte

Samples of the catholyte were taken after the experiments with different membrane types. The samples were taken with a syringe and analyzed via High-Performance Liquid Chromatography (HPLC)(Agilent 1200) with an organic resin column (CS-Chromatographie Service GmbH). The measurements were conducted with a 5 mmol/L H_2SO_4 eluent with a flow rate of 0.5 mL/min at 40 °C using a refractive index detector and a variable wavelength detector. It should be noted that the catholyte measurements provide only qualitative information on the crossover, as the duration of the experiments varied and the catholyte was continuously exchanged.

Table A.1.: Catholyte concentrations after the experiments with different membrane types.

Membrane	Formate [mg/L]	Methanol [mg/L]
BPM	< 0.1	< 0.1
CEM	< 0.1	37.0
AEM	1.1	112.1

A.3. Feed and bleed operating mode

Model comparison: Ideal vs. non-ideal mixing

The ideally mixed model shown in Figure A.3a assumes ideal mixing for the total electrolyte volume within the system. As we will show, the ideally mixed model represents most aspects of the feed and bleed behavior correctly and has only a few limitations despite its simplicity. The non-ideally mixed model shown in Figure A.3b considers that a portion of the electrolyte volume is not ideally mixed and that the electrolyte flow is recirculated with a delay.

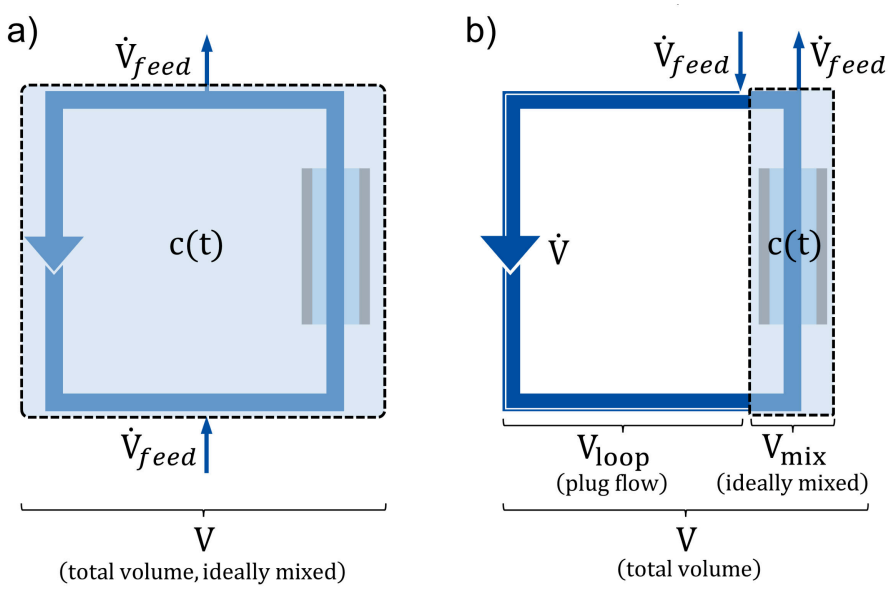

Figure A.3.: a) Model of the feed and bleed setup assuming ideal mixing for the total electrolyte volume in the system. b) Model of the feed and bleed setup considering non-ideal mixing by the delayed electrolyte recirculation in the loop.

The model equation for the non-ideally mixed feed and bleed setup is based on a mole balance of the ideally mixed part of the electrolyte volume within the setup. The non-ideally mixed part of the volume is considered by the recirculated stream, which reenters the volume delayed by the residence time in the loop volume. The balance described by Equation A.1 takes the form of a delayed differential equation. The balance can be reformulated in Equation A.2, which describes the change in product concen-

tration $c(t)$ in the ideally mixed volume V_{mix} depending on the feed $\dot{V}_{feed}$ and loop flow rate $\dot{V}$, the inlet concentration c_{feed}, the current density i, the geometric electrode area A, the faraday efficiency FE, the number of electrons transferred in the product forming reaction z, the Faraday constant F, and the residence time in the loop τ_{loop}, which is calculated according to Equation A.3.

$$\begin{aligned} V_{mix}\frac{dc(t)}{dt} =& \dot{V}\cdot\left(\frac{\dot{V}_{feed}}{\dot{V}}\cdot c_{feed}+\frac{\dot{V}-\dot{V}_{feed}}{\dot{V}}\cdot c(t-\tau_{loop})\right) \\ &+\frac{iA\cdot FE}{zF}-\dot{V}_{feed}\cdot c(t)-(\dot{V}-\dot{V}_{feed})\cdot c(t) \end{aligned} \tag{A.1}$$

$$\begin{aligned} V_{mix}\frac{dc(t)}{dt} =& \dot{V}_{feed}\cdot(c_{feed}-c(t)) \\ &+\frac{iA\cdot FE}{zF}+(\dot{V}-\dot{V}_{feed})\cdot(c(t-\tau_{loop})-c(t)) \end{aligned} \tag{A.2}$$

$$\tau_{loop} = \frac{V_{loop}}{\dot{V}} \tag{A.3}$$

Figure A.4 compares the results from the non-ideally mixed model with the ideally mixed model and illustrates the effect of different parameters on the system behavior. The product concentration curves calculated for the non-ideally mixed model align well with the ideally mixed model even if the feed flow rate $\dot{V}_{feed}$ or the electrolyte volume V is varied (see Figure A.4a-b). Decreasing the ideally mixed volume V_{mix} and the loop flow rate $\dot{V}$ can lead to non-ideal mixing as shown in Figure A.4c due to lack of back mixing and slow recirculation, respectively. This example highlights two aspects of non-ideal mixing: The product concentration increases step-wise due to the delayed feedback loop and the concentration increases slightly faster as the effective volume is reduced at low recirculation. The duration of the concentration steps corresponds to the residence time of the stream in the loop τ_{loop}. The concentration steps are more pronounced at low V_{mix} and high τ_{loop}.

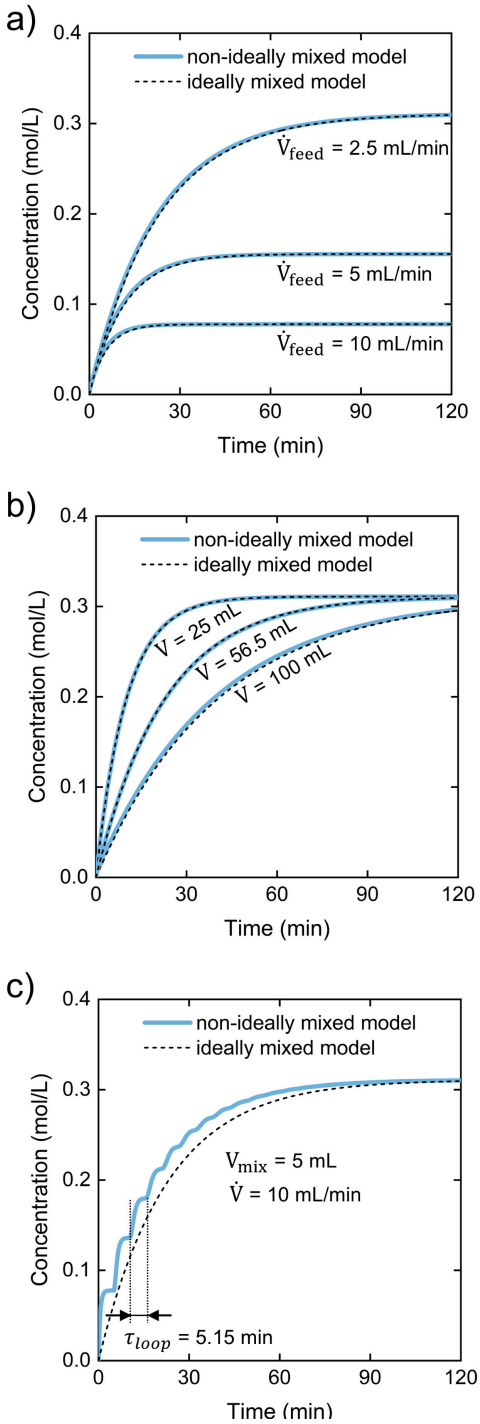

Figure A.4.: Product concentration curves of feed and bleed systems calculated with the non-ideally mixed model (blue, continuous line) and the ideally mixed model (black, dashed line), starting at t=0 when the current is switched on and a product-forming reaction begins. The plots show the influence of different parameters on the behavior of the feed and bleed system: a) volume flow of the feed, b) total electrolyte volume in the system, and c) provides an example of non-ideal behavior at insufficient mixing. The varied parameters are indicated in each plot, all other parameters remained unchanged at the values of our experimental setup ($\dot{V}_{feed}$ = 2.5 mL min^{-1}, V = 56.5 mL, V_{mix} = 20 mL, $\dot{V}$ = 50 mL min^{-1}, i = 200 mA cm^{-2}, A = 25 cm^2, FE = 100%, and z=4 electrons transferred per reaction).

The deviation from ideal behavior is less pronounced if the influence of V_{mix} and $\dot{V}$ is considered separately (see Figure A.5). The deviation from ideally mixed behavior at slow recirculation points out the limitations of the ideally mixed model. However, non-ideal behavior can be easily avoided by increasing the loop flow rate to ensure fast recirculation.

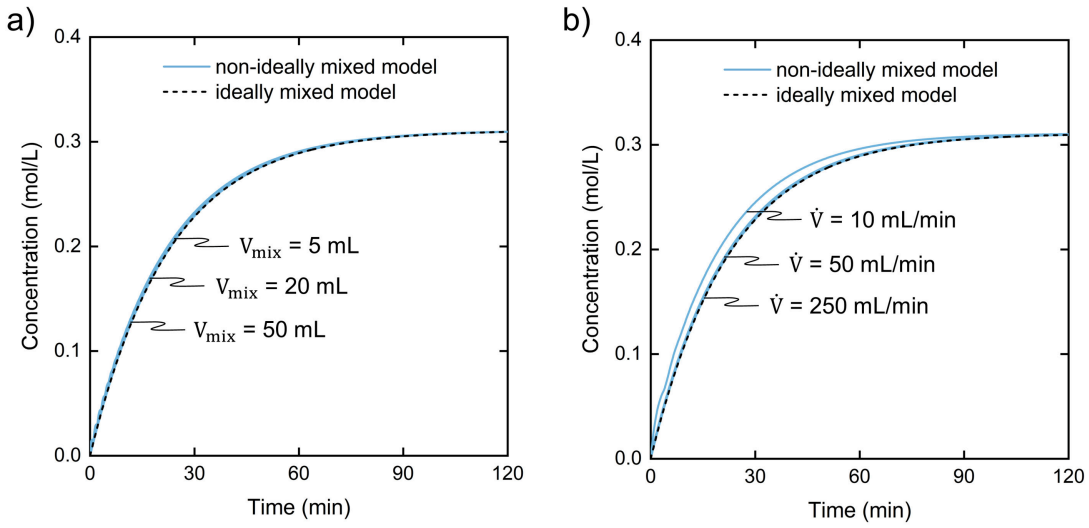

Figure A.5.: Influence on the concentration curve of the calculated feed & bleed setup with an ideal and non-ideal model, when changing a) the cell volume V_{mix} with constant system volume V of 56.5 mL or b) the cell flow rate $\dot{V}$ at a constant feed flow rate $\dot{V}_{feed}$ of 2.5 mL min^{-1}

Validating the approach of the FE calculation

The general approach for the FE calculation was to calculate an unknown variable (the FE) from a measured concentration curve by applying a discretized equation derived from the analytical solution of the ideally mixed model. The precise FE during an experiment is unknown, as the FE might change over time and between experiments. Therefore, direct experimental validation is difficult, as the FE must be known for comparison. Instead of the FE, we back-calculated the feed concentration from a measured concentration curve via online FTIR as described in Section 5.2 using the same mathematical approach as for the FE calculation. In contrast to the FE, the precise value of the feed concentration is known and can be compared to

the calculated feed concentration for validation. We conducted an experiment in which we changed the feed from a solution of 0 mol L^{-1} sulfate to a second solution of 0.5 mol L^{-1} sulfate, without any electrochemical reaction. Sulfate was chosen as tracer due to its distinct FTIR peak. The sudden change in the feed concentration represents a step function analog to the sudden start of an electrochemical reaction when the current is turned on. The attenuated response of the feed and bleed system is shown in the measured concentration curve in Figure A.6a.

In the absence of any chemical reaction, rearranging the equation used for FE calculation (Equation 5.7) yields Equation (A.4) with the feed concentration c_{feed} as a function of two measured concentration points (c_n and c_{n-1}):

$$c_{feed} = c_{n-1} + \frac{c_n - c_{n-1}}{1 - exp\left(-\frac{\dot{V}_{feed}}{V} \cdot (t_n - t_{n-1})\right)} \tag{A.4}$$

By applying Equation A.4, the feed concentration was calculated from the measured concentration curve, analog to the FE calculation.

Figure A.6b) compares the true and the calculated feed concentration. The calculated feed concentration curve shows good agreement with the true feed concentration after 10 min. During the first 10 min the calculation results overestimated the true feed concentration. The initial overshoot was likely an artifact caused by non-ideal mixing within the flow cell.

Calculating differences between concentration points (see Equation A.4) amplifies the noise of the measured concentration data, especially at fast sampling rates. Smoothing can reduce noise, however the settings should be chosen appropriately to avoid significantly altering the slope and shape of the concentration curve. Figures A.6 c) and d) show the effect of smoothing the measured concentration curves (weighted adjacent averaging with a window size of 20 points). The calculated feed concentration based on the smoothed concentration curve exhibited an improved match to the true concentration with less noise.

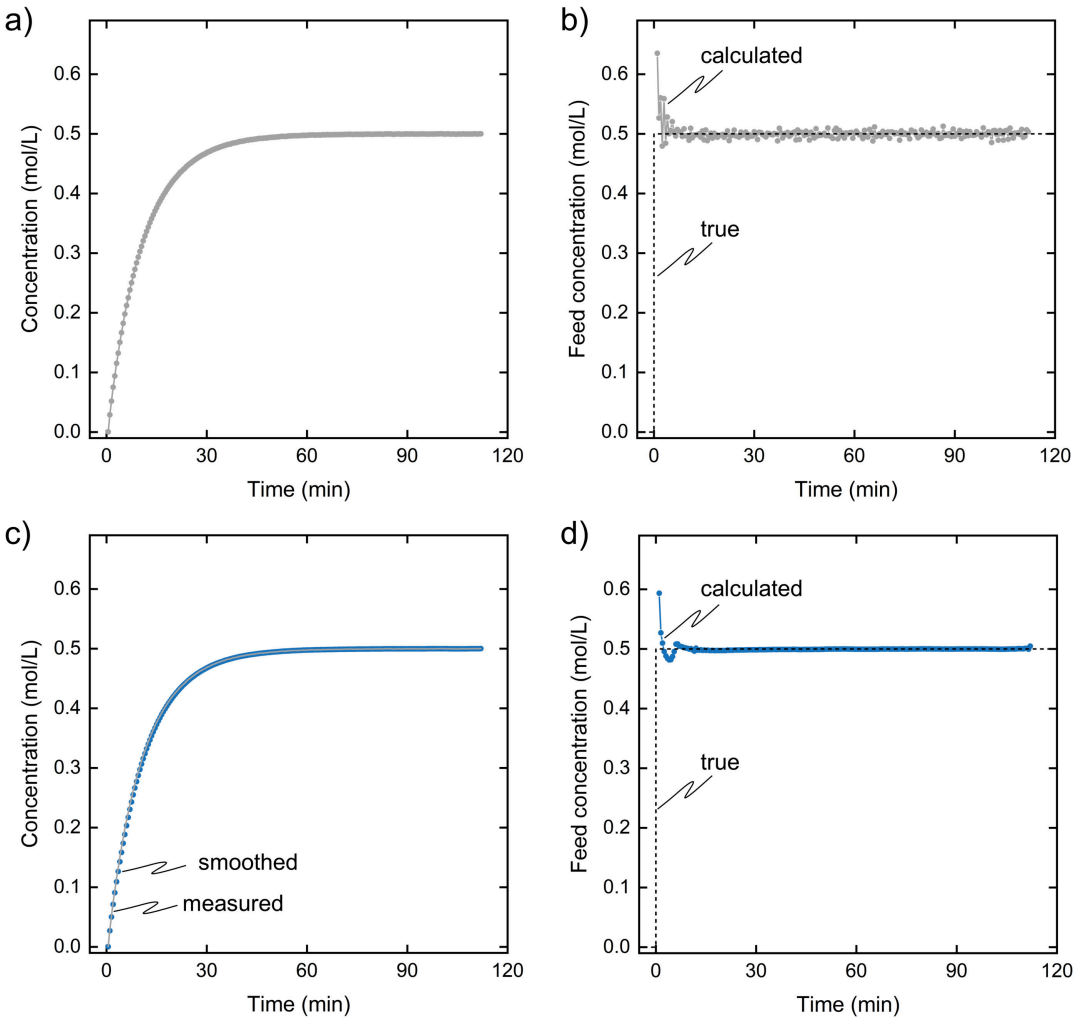

Figure A.6.: a) Measured sulfate concentration curve as response of the feed and bleed setup to a sudden change of the feed concentration from 0 mol L^{-1} to 0.5 mol L^{-1} at a feed flow rate of 5 mL min^{-1}. b) Calculated feed concentration compared to the true feed concentration (as prepared). The feed concentration was calculated from the measured sulfate concentration by equation A.4. c) The smoothed concentration curve (blue circles) closely aligns with the measured sulfate concentration curve (gray line). d) Feed concentration calculated from the smoothed concentration data by equation A.4.

Nomenclature

AEM	Anion exchange membrane
BPM	Bipolar membrane
CEM	Cation exchange membrane
CO2R	Carbon dioxide reduction
CSTR	Continuous stirred-tank reactor
DSA	Dimensionally stable anodes
DMFC	Direct methanol fuel cell
ECSA	Electrochemical active surface area
EDX	Energy dispersive X-ray spectroscopy
FE	Faraday efficiency
FEP	Fluorinated ethylene propylene
FTIR	Fourier-transform infrared spectroscopy
GDE	Gas diffusion electrode
HER	Hydrogen evolution reaction
HPLC	High-performance liquid chromatography
LSV	Linear sweep voltammetry
MMO	Mixed metal oxide
MOR	Methanol oxidation reaction
OER	Oxygen evolution reaction
PEM	Polymer electrolyte membrane
PFR	Plug flow reactor
PFSA	Perfluorosulfonic acid
RHE	Reversible hydrogen electrode
SHE	Standard hydrogen electrode
SEM	Scanning electron microscopy
XPS	X-ray photoelectron spectroscopy
XRD	X-ray diffraction analysis

Bibliography

[Ahme2011] M. Ahmed and I. Dincer. “A review on methanol crossover in direct methanol fuel cells: challenges and achievements”. *International Journal of Energy Research* 35.14 (2011). DOI: 10.1002/er.1889 (cit. on pp. 50, 51, 86).

[Ande2014] A. B. Anderson and H. A. Asiri. “Reversible potentials for steps in methanol and formic acid oxidation to CO2; adsorption energies of intermediates on the ideal electrocatalyst for methanol oxidation and CO2 reduction”. *Physical chemistry chemical physics : PCCP* 16.22 (2014). DOI: 10.1039/c3cp54837f (cit. on p. 27).

[Aren2020] L. F. Arenas, C. Ponce de León, and F. C. Walsh. “Critical Review—The Versatile Plane Parallel Electrode Geometry: An Illustrated Review”. *Journal of The Electrochemical Society* 167.2 (2020). DOI: 10.1149/1945-7111/ab64ba (cit. on p. 98).

[Aust2014] N. Aust and A. Kirste. “Paired Electrosynthesis”. In*Encyclopedia of Applied Electrochemistry*. Ed. by G. Kreysa, K.-i. Ota, and R. F. Savinell. Springer New York, 2014. Pp. 1505–1510. (Cit. on pp. 17, 22).

[Baes2023] J. Baessler, T. Oliveira, R. Keller, and M. Wessling. “Paired Electrosynthesis of Formic Acid from CO2 and Formaldehyde from Methanol”. *ACS Sustainable Chemistry & Engineering* 11.18 (2023). DOI: 10.1021/acssuschemeng.2c07523 (cit. on pp. 23, 25, 112).

[Baes2024] J. Baessler, N. Vollmert, J. Vehrenberg, M. Mineur, S. Schenke, L. Griesberg, P. M. Pineda, and R. Keller. “Reaction engineering for high yield electrosynthesis: Unraveling the impact of reaction conditions and conversion on methanol oxidation to formate”. *Chemical Engineering Journal* 495 (2024). DOI: 10.1016/j.cej.2024.153000 (cit. on pp. 23, 25, 112).

[Bago1977] V. S. Bagotzky, Y. Vassiliev, and O. A. Khazova. “Generalized scheme of chemisorption, electrooxidation and electroreduction of simple organic compounds on platinum group metals”. *Journal of Electroanalytical Chemistry and Interfacial Electrochemistry* 81.2 (1977). DOI: 10.1016/S0022-0728(77)80019-3 (cit. on pp. 27, 45).

[Bago2006] V. S. Bagotsky. *Fundamentals of electrochemistry*. 2. ed. The Electrochemical Society series. Hoboken, NJ: Wiley-Interscience, 2006. DOI: 10.1002/047174199X (cit. on p. 7).

[Bahm2016] A. M. Bahmanpour, A. Hoadley, S. H. Mushrif, and A. Tanksale. “Hydrogenation of Carbon Monoxide into Formaldehyde in Liquid Media”. *ACS Sustainable Chemistry & Engineering* 4.7 (2016). DOI: 10.1021/acssuschemeng.6b00837 (cit. on p. 32).

[Bake2012] R. W. Baker. *Membrane technology and applications*. 3rd ed. Chichester West Sussex and Hoboken: John Wiley & Sons, 2012 (cit. on p. 99).

[Bald1927] R. T. Baldwin. “History of the chlorine industry”. *Journal of Chemical Education* 4.3 (1927). DOI: 10.1021/ed004p313 (cit. on p. 17).

[Bals2007] J. Balster, R. Sumbharaju, S. Srikantharajah, I. Pünt, D. F. Stamatialis, V. Jordan, and M. Wessling. “Asymmetric bipolar membrane: A tool to improve product purity”. *Journal of Membrane Science* 287.2 (2007). DOI: 10.1016/j.memsci.2006.10.042 (cit. on p. 92).

[Bamb2010] V. Bambagioni, M. Bevilacqua, C. Bianchini, J. Filippi, A. Lavacchi, A. Marchionni, F. Vizza, and P. K. Shen. “Self-sustainable production of hydrogen, chemicals, and energy from renewable alcohols by electrocatalysis”. *ChemSusChem* 3.7 (2010). DOI: 10.1002/cssc.201000103 (cit. on p. 23).

[Bard2001] A. J. Bard and L. R. Faulkner. *Electrochemical methods: Fundamentals and applications*. 2. ed. Hoboken, NJ: Wiley, 2001 (cit. on pp. 7, 9–11, 13, 15).

[Bati2003] E. A. Batista, G. Malpass, A. J. Motheo, and T. Iwasita. “New insight into the pathways of methanol oxidation”. *Electrochemistry Communications* 5.10 (2003). DOI: 10.1016/j.elecom.2003.08.010 (cit. on pp. 2, 20, 25–28, 32, 33, 43, 48, 52).

[Bati2004] E. A. Batista, G. Malpass, A. J. Motheo, and T. Iwasita. “New mechanistic aspects of methanol oxidation”. *Journal of Electroanalytical Chemistry* 571.2 (2004). DOI: 10.1016/j.jelechem.2004.05.016 (cit. on p. 27).

[Bati2008] B. C. Batista, E. Sitta, M. Eiswirth, and H. Varela. “Autocatalysis in the open circuit interaction of alcohol molecules with oxidized Pt surfaces”. *Physical chemistry chemical physics : PCCP* 10.44 (2008). DOI: 10.1039/b811787j (cit. on p. 46).

[Beal2018] L. Beal, D. Hill, R. Martin, and J. Hedengren. “GEKKO Optimization Suite”. *Processes* 6.8 (2018). DOI: 10.3390/pr6080106 (cit. on p. 101).

[Béla1976] G. Bélanger. “Anodic Oxidation of Anhydrous Methanol”. *Journal of The Electrochemical Society* 123.6 (1976). DOI: 10.1149/1.2132939 (cit. on p. 48).

[Berg1982] D. Bergner. “Membrane cells for chlor-alkali electrolysis”. *Journal of Applied Electrochemistry* 12.6 (1982). DOI: 10.1007/BF00617483 (cit. on p. 98).

[Bevi2014] M. Bevilacqua, J. Filippi, A. Lavacchi, A. Marchionni, H. A. Miller, W. Oberhauser, E. Vesselli, and F. Vizza. “Energy Savings in the Conversion of CO 2 to Fuels using an Electrolytic Device”. *Energy Technology* 2.6 (2014). DOI: 10.1002/ente.201402014 (cit. on p. 23).

[Bhat1968] R. N. Bhatia, K. E. Gubbins, and R. D. Walker. “Mutual diffusion in concentrated aqueous potassium hydroxide solutions”. *Transactions of the Faraday Society* 64 (1968). DOI: 10.1039/TF9686402091 (cit. on p. 79).

[Bird2020] Y. Y. Birdja and J. Vaes. “Towards a Critical Evaluation of Electrocatalyst Stability for CO2 Electroreduction”. *ChemElectroChem* 7.23 (2020). DOI: 10.1002/celc.202001227 (cit. on p. 14).

[Boru2021] A. Boru and A. Wypych-Stasiewicz. “Conductivity studies of 1:1 electrolytes in water + methanol mixtures at 298.15K”. *Journal of Molecular Liquids* 344 (2021). DOI: 10.1016/j.molliq.2021.117695 (cit. on p. 87).

[Brow2018] W. R. Browne. *Electrochemistry*. Oxford chemistry primers. Oxford and New York, NY: Oxford University Press, 2018 (cit. on p. 13).

[Burd2019] T. Burdyny and W. A. Smith. “CO2 reduction on gas-diffusion electrodes and why catalytic performance must be assessed at commercially-relevant conditions”. *Energy & Environmental Science* 57 (2019). DOI: 10.1039/C8EE03134G (cit. on pp. 2, 98).

[Cao2005] D. Cao, G.-Q. Lu, A. Wieckowski, S. A. Wasileski, and M. Neurock. “Mechanisms of methanol decomposition on platinum: A combined experimental and ab initio approach”. *The journal of physical chemistry. B* 109.23 (2005). DOI: 10.1021/jp0501188 (cit. on p. 27).

[Carr2001] L. Carrette, K. A. Friedrich, and U. Stimming. “Fuel Cells - Fundamentals and Applications”. *Fuel Cells* 1.1 (2001). DOI: 10.1002/1615-6854(200105)1:1{\textless}5::AID-FUCE5{\textgreater}3.0.CO;2-G (cit. on p. 27).

[Chak2018] U. K. Chakraborty. “Reversible and Irreversible Potentials and an Inaccuracy in Popular Models in the Fuel Cell Literature”. *Energies* 11.7 (2018). DOI: 10.3390/en11071851 (cit. on p. 9).

[Chat2022] M. Chatenet, B. G. Pollet, D. R. Dekel, F. Dionigi, J. Deseure, P. Millet, R. D. Braatz, M. Z. Bazant, M. Eikerling, I. Staffell, P. Balcombe, Y. Shao-Horn, and H. Schäfer. “Water electrolysis: from textbook knowledge to the latest scientific strategies and industrial developments”. *Chemical Society Reviews* 51.11 (2022). DOI: 10.1039/D0CS01079K (cit. on p. 21).

[Chen2018] C. Chen, J. F. Khosrowabadi Kotyk, and S. W. Sheehan. “Progress toward Commercial Application of Electrochemical Carbon Dioxide Reduction”. *Chem* 4.11 (2018). DOI: 10.1016/j.chempr.2018.08.019 (cit. on p. 21).

[Chen2022] Z. Chen, W. Wei, L. Song, and B.-J. Ni. “Hybrid Water Electrolysis: A New Sustainable Avenue for Energy-Saving Hydrogen Production”. *Sustainable Horizons* 1 (2022). DOI: 10.1016/j.horiz.2021.100002 (cit. on p. 2).

[Chen2023] D. Chen, Y. Ding, X. Cao, L. Wang, H. Lee, G. Lin, W. Li, G. Ding, and L. Sun. “Highly Efficient Biomass Upgrading by a Ni−Cu Electrocatalyst Featuring Passivation of Water Oxidation Activity”. *Angewandte Chemie International Edition* 62.37 (2023). DOI: 10.1002/anie.202309478 (cit. on p. 21).

[Cher1998] M. Cheryan. *Ultrafiltration and microfiltration handbook*. Lancaster, Pa.: Technomic Pub. Co, 1998 (cit. on p. 99).

[Chil1999] C. L. Childers, H. Huang, and C. Korzeniewski. “Formaldehyde Yields from Methanol Electrochemical Oxidation on Carbon-Supported Platinum Catalysts”. *Langmuir* 15.3 (1999). DOI: 10.1021/la980798o (cit. on pp. 2, 20, 25, 26, 32, 33, 43, 52).

[Cogn1995] P. Cognet, J. Berlan, G. Lacoste, P.-L. Fabre, and J.-M. Jud. “Application of metallic foams in an electrochemical pulsed flow reactor Part I: Mass transfer performance”. *Journal of Applied Electrochemistry* 25.12 (1995). DOI: 10.1007/BF00242537 (cit. on p. 79).

[Corn2024] O. M. Cornejo, M. F. Murrieta, Z. G. Aguilar, J. F. Rodríguez, A. A. Márquez, M. I. León, and J. L. Nava. “Recent advances in electrochemical flow reactors used in advanced oxidation processes: A critical review”. *Chemical Engineering Journal* 496 (2024). DOI: 10.1016/j.cej.2024.153935 (cit. on p. 98).

[Cost2001] P. Costamagna. “Transport phenomena in polymeric membrane fuel cells”. *Chemical Engineering Science* 56.2 (2001). DOI: 10.1016/S0009-2509(00)00232-3 (cit. on p. 12).

[Cout2016] C. Coutanceau and S. Baranton. “Electrochemical conversion of alcohols for hydrogen production: a short overview”. *WIREs Energy and Environment* 5.4 (2016). DOI: 10.1002/wene.193 (cit. on pp. 22, 23).

[Danl1984] D. E. Danly. “Development and Commercialization of the Monsanto Electrochemical Adiponitrile Process”. *Journal of The Electrochemical Society* 131.10 (1984). DOI: 10.1149/1.2115324 (cit. on p. 99).

[Deng2024] Z. Deng, S. Xu, C. Liu, X. Zhang, M. Li, and Z. Zhao. “Stability of dimensionally stable anode for chlorine evolution reaction”. *Nano Research* 17.3 (2024). DOI: 10.1007/s12274-023-5965-7 (cit. on p. 21).

[Domi2013] A. Dominguez-Ramos and A. Irabien. “Analysis and Modeling of the Continuous Electro-oxidation Process for Organic Matter Removal in Urban Wastewater Treatment”. *Industrial & Engineering Chemistry Research* 52.22 (2013). DOI: 10.1021/ie303021v (cit. on p. 99).

[Drög2024] P. Drögemüller, T. Stobbe, and U. Schröder. “Closing the Gap: Towards a Fully Continuous and Self-Regulated Kolbe Electrosynthesis”. *ChemSusChem* 17.2 (2024). DOI: 10.1002/cssc.202300973 (cit. on p. 99).

[Du2023] X. Du, M. Tan, T. Wei, H. Kobayashi, J. Song, Z. Peng, H. Zhu, Z. Jin, R. Li, and W. Liu. “Highly efficient and robust nickel-iron bifunctional catalyst coupling selective methanol oxidation and freshwater/seawater hydrogen evolution via CO-free pathway”. *Chemical Engineering Journal* 452 (2023). DOI: 10.1016/j.cej.2022.139404 (cit. on pp. 2, 23, 25, 56, 74, 89, 112).

[Elia2019] N. Eliaz and E. Gileadi. *Physical electrochemistry: Fundamentals, techniques, and applications*. Second edition. Master. Weinheim: Wiley-VCH, 2019 (cit. on pp. 9, 10, 13).

[Endr2017] B. Endrdi, G. Bencsik, F. Darvas, R. Jones, K. Rajeshwar, and C. Janáky. “Continuous-flow electroreduction of carbon dioxide”. *Progress in Energy and Combustion Science* 62 (2017). DOI: https://doi.org/10.1016/j.pecs.2017.05.005 (cit. on p. 98).

[Fan2021] L. Fan, B. Liu, X. Liu, N. Senthilkumar, G. Wang, and Z. Wen. “Recent Progress in Electrocatalytic Glycerol Oxidation”. *Energy Technology* 9.2 (2021). DOI: 10.1002/ente.202000804 (cit. on p. 20).

[Ferr2008] P. Ferrin, A. U. Nilekar, J. Greeley, M. Mavrikakis, and J. Rossmeisl. “Reactivity descriptors for direct methanol fuel cell anode catalysts”. *Surface Science* 602.21 (2008). DOI: 10.1016/j.susc.2008.08.011 (cit. on p. 27).

[Flei1972] M. Fleischmann, K. Korinek, and D. Pletcher. “The kinetics and mechanism of the oxidation of amines and alcohols at oxide-covered nickel, silver, copper, and cobalt electrodes”. *Journal of the Chemical Society, Perkin Transactions 2* 10 (1972). DOI: 10.1039/p29720001396 (cit. on pp. 30, 76).

[Gawe2022] A. Gawel, T. Jaster, D. Siegmund, J. Holzmann, H. Lohmann, E. Klemm, and U.-P. Apfel. “Electrochemical CO2 reduction - The macroscopic world of electrode design, reactor concepts & economic aspects”. *iScience* 25.4 (2022). DOI: 10.1016/j.isci.2022.104011 (cit. on pp. 21, 22).

[Good1995] F. Goodridge and K. Scott. *Electrochemical Process Engineering*. 1995. DOI: 10.1007/978-1-4899-0224-5 (cit. on p. 99).

[Gree2015] R. A. Green, R. C. D. Brown, D. Pletcher, and B. Harji. “A Microflow Electrolysis Cell for Laboratory Synthesis on the Multigram Scale”. *Organic Process Research & Development* 19.10 (2015). DOI: 10.1021/acs.oprd.5b00260 (cit. on p. 98).

[Grig2020] S. A. Grigoriev, V. N. Fateev, D. G. Bessarabov, and P. Millet. “Current status, research trends, and challenges in water electrolysis science and technology”. *International Journal of Hydrogen Energy* 45.49 (2020). DOI: 10.1016/j.ijhydene.2020.03.109 (cit. on pp. 1, 18).

[Hais2019] T. Haisch, F. Kubannek, C. Haisch, D. W. Bahnemann, and U. Krewer. “Quantification of formaldehyde production during alkaline methanol electrooxidation”. *Electrochemistry Communications* 102 (2019). DOI: 10.1016/j.elecom.2019.03.013 (cit. on p. 25).

[Hayn2017] W. M. Haynes, ed. *CRC handbook of chemistry and physics: A ready-reference book of chemical and physical data*. 97th edition. Boca Raton, London, and New York: CRC Press, 2017, pp. 869–907 (cit. on pp. 9, 20, 32, 44, 46).

[Hein1999] A. Heinzel and V. M. Barragán. “A review of the state-of-the-art of the methanol crossover in direct methanol fuel cells”. *Journal of Power Sources* 84.1 (1999). DOI: 10.1016/S0378-7753(99)00302-X (cit. on p. 50).

[Heli2004] H. Heli, M. Jafarian, M. G. Mahjani, and F. Gobal. “Electro-oxidation of methanol on copper in alkaline solution”. *Electrochimica Acta* 49.27 (2004). DOI: 10.1016/j.electacta.2004.06.015 (cit. on pp. 25, 30, 76, 113).

[Hiet2010] J. Hietala, A. Vuori, P. Johnsson, I. Pollari, W. Reutemann, and H. Kieczka. “Formic Acid”. In *Ullmann’s encyclopedia of industrial chemistry*. Vol. 5. Chichester: Wiley, 2010. Pp. 1–22. (Cit. on pp. 56, 112).

[Hilt2024] G. Hilt. “Recent advances in paired electrolysis and their application in organic electrosynthesis”. *Current Opinion in Electrochemistry* 43 (2024). DOI: 10.1016/j.coelec.2023.101425 (cit. on p. 22).

[Huan2017a] T. N. Huan, G. Rousse, S. Zanna, I. T. Lucas, X. Xu, N. Menguy, V. Mougel, and M. Fontecave. “A Dendritic Nanostructured Copper Oxide Electrocatalyst for the Oxygen Evolution Reaction”. *Angewandte Chemie (International ed. in English)* 56.17 (2017). DOI: 10.1002/anie.201700388 (cit. on pp. 58, 72, 102).

[Huan2017b] T. N. Huan, P. Simon, G. Rousse, I. Génois, V. Artero, and M. Fontecave. “Porous dendritic copper: An electrocatalyst for highly selective CO2 reduction to formate in water/ionic liquid electrolyte”. *Chemical science* 8.1 (2017). DOI: 10.1039/c6sc03194c (cit. on p. 58).

[Huan2024a] H. Huang, M. Sun, S. Li, S. Zhang, Y. Lee, Z. Li, J. Fang, C. Chen, Y.-X. Zhang, Y. Wu, Y. Che, S. Qian, W. Zhu, C. Tang, Z. Zhuang, L. Zhang, and Z. Niu. “Enhancing H2O2 Electrosynthesis at Industrial-Relevant Current in Acidic Media on Diatomic Cobalt Sites”. *Journal of the American Chemical Society* 146.13 (2024). DOI: 10.1021/jacs.4c02031 (cit. on p. 98).

[Huan2024b] M. Huang, K. Lao, L. Ma, J. Tao, X. Zhuang, T. Hu, Y. Pan, H. Liu, L. Wen, S. Xu, X. Liu, Y. Wu, S. Li, H. B. Tao, and N. Zheng. “A Solid Electrolyte RHE for Electrode Diagnosis of Proton Exchange Membrane Water Electrolyzers”. *ACS Applied Materials & Interfaces* 16.30 (2024). DOI: 10.1021/acsami.4c07472 (cit. on pp. 20, 21).

[Iban2017] J. Ibanez, B. A. Frontana-Uribe, and R. Vasquez-Medrano. “Paired Electrochemical Processes: Overview, Systematization, Selection Criteria, Design Strategies, and Projection”. *Journal of the Mexican Chemical Society* 60.4 (2017). DOI: 10.29356/jmcs.v60i4.117 (cit. on pp. 17, 22).

[ICIS2007] ICIS. *Formaldehyde*. Accessed: 2021-02-01. 2007. URL: https://www.icis.com/explore/resources/news/2007/04/27/4502303/formaldehyde/ (cit. on pp. 2, 32).

[ICIS2010] ICIS. *Formaldehyde Uses and Market Data*. Accessed: 2021-02-01. 2010 (cit. on p. 32).

[Inte2022] International Energy Agency. *Global Hydrogen Review*. Paris, 2022 (cit. on p. 21).

[Intr2018a] Intratec Solutions LLC, ed. *Formic Acid Price*. Accessed: 09.10.2023. 2018 (cit. on pp. 2, 56).

[Intr2018b] Intratec Solutions LLC, ed. *Methanol Price*. Accessed: 09.10.2023. 2018 (cit. on pp. 2, 56).

[Inze2015] G. Inzelt. “Crossing the bridge between thermodynamics and electrochemistry. From the potential of the cell reaction to the electrode potential”. *ChemTexts* 1.1 (2015). DOI: 10.1007/s40828-014-0002-9 (cit. on p. 7).

[Iwas2002] T. Iwasita. “Electrocatalysis of methanol oxidation”. *Electrochimica Acta* 47.22-23 (2002). DOI: 10.1016/S0013-4686(02)00336-5 (cit. on p. 32).

[Iwas2003] T. Iwasita. “Chapter 41: Methanol and CO electrooxidation”. In*Handbook of Fuel Cells – Fundamentals, Technology and Applications*. Ed. by W. Vielstich, A. Lamm, and H. Gasteiger. Wiley, 2003. Pp. 603–624. (Cit. on p. 45).

[Jack2021] J. Jack, W. Zhu, J. L. Avalos, J. Gong, and Z. J. Ren. “Anode co-valorization for scalable and sustainable electrolysis”. *Green Chemistry* 23.20 (2021). DOI: 10.1039/D1GC02094C (cit. on p. 2).

[Jame2018] M.-I. Jamesh and X. Sun. “Recent progress on earth abundant electrocatalysts for oxygen evolution reaction (OER) in alkaline medium to achieve efficient water splitting – A review”. *Journal of Power Sources* 400 (2018). DOI: 10.1016/j.jpowsour.2018.07.125 (cit. on pp. 74, 91).

[Joun2018] M. Jouny, W. Luc, and F. Jiao. “General Techno-Economic Analysis of CO2 Electrolysis Systems”. *Industrial & Engineering Chemistry Research* 57.6 (2018). DOI: 10.1021/acs.iecr.7b03514 (cit. on pp. 1, 2, 21, 56).

[Jusy2003] Z. Jusys, J. Kaiser, and R. J. Behm. “Methanol Electrooxidation over Pt/C Fuel Cell Catalysts: Dependence of Product Yields on Catalyst Loading”. *Langmuir* 19.17 (2003). DOI: 10.1021/la020932b (cit. on pp. 20, 25).

[Kahl2023] T. Kahlstorf, J. N. Hausmann, T. Sontheimer, and P. W. Menezes. “Challenges for Hybrid Water Electrolysis to Replace the Oxygen Evolution Reaction on an Industrial Scale”. *Global challenges (Hoboken, NJ)* 7.7 (2023). DOI: 10.1002/gch2.202200242 (cit. on pp. 18–23).

[Kint2017] J. Kintrup, M. Millaruelo, V. Trieu, A. Bulan, and E. S. Mojica. “Gas Diffusion Electrodes for Efficient Manufacturing of Chlorine and Other Chemicals”. *The Electrochemical Society Interface* 26.2 (2017). DOI: 10.1149/2.F07172if (cit. on p. 21).

[Krey2014] G. Kreysa, K.-i. Ota, and R. F. Savinell. *Encyclopedia of applied electrochemistry*. Springer reference. New York, NY: Springer, 2014 (cit. on p. 15).

[Kuma2023] M. Kumar, B. Meena, A. Yu, C. Sun, and S. Challapalli. “Advancements in catalysts for glycerol oxidation via photo-/electrocatalysis: a comprehensive review of recent developments”. *Green Chemistry* 25.21 (2023). DOI: 10.1039/D3GC03094F (cit. on pp. 20, 22).

[Lang2024] H. Lange, A. Klose, L. Beisswenger, D. Erdmann, and L. Urbas. “Modularization approach for large-scale electrolysis systems: a review”. *Sustainable Energy & Fuels* 8.6 (2024). DOI: 10.1039/D3SE01588B (cit. on p. 98).

[Lee2002] J. Lee, C. Eickes, M. Eiswirth, and G. Ertl. “Electrochemical oscillations in the methanol oxidation on Pt”. *Electrochimica Acta* 47.13-14 (2002). DOI: 10.1016/S0013-4686(02)00075-0 (cit. on p. 45).

[Leon2020] M. E. Leonard, M. J. Orella, N. Aiello, Y. Román-Leshkov, A. Forner-Cuenca, and F. R. Brushett. “Editors’ Choice—Flooded by Success: On the Role of Electrode Wettability in CO2 Electrolyzers that Generate Liquid Products”. *Journal of The Electrochemical Society* 167.12 (2020). DOI: 10.1149/1945-7111/abaa1a (cit. on p. 50).

[Leon2024] G. Leonzio, A. Hankin, and N. Shah. “CO2 electrochemical reduction: A state-of-the-art review with economic and environmental analyses”. *Chemical Engineering Research and Design* 208 (2024). DOI: 10.1016/j.cherd.2024.07.014 (cit. on p. 22).

[Leve1999] O. Levenspiel. *Chemical reaction engineering*. 3. ed. Hoboken, NJ: Wiley, 1999 (cit. on p. 16).

[Li2008] L. Li, Z. Wei, X. Qi, C. Sun, and G. Yin. “Chemical oscillation in electrochemical oxidation of methanol on Pt surface”. *Science in China Series B: Chemistry* 51.4 (2008). DOI: 10.1007/s11426-007-0110-0 (cit. on p. 45).

[Li2017] T. Li, Y. Cao, J. He, and C. P. Berlinguette. “Electrolytic CO2 Reduction in Tandem with Oxidative Organic Chemistry”. *ACS Central Science* 3.7 (2017). DOI: 10.1021/acscentsci.7b00207 (cit. on p. 23).

[Li2018] Y. C. Li, Z. Yan, J. Hitt, R. Wycisk, P. N. Pintauro, and T. E. Mallouk. “Bipolar Membranes Inhibit Product Crossover in CO2 Electrolysis Cells”. *Advanced Sustainable Systems* 2.4 (2018). DOI: 10.1002/adsu.201700187 (cit. on pp. 51, 89).

[Li2020a] M. Li, X. Deng, Y. Liang, K. Xiang, D. Wu, B. Zhao, H. Yang, J.-L. Luo, and X.-Z. Fu. “Co_xP@NiCo-LDH heteronanosheet arrays as efficient bifunctional electrocatalysts for co-generation of value-added formate and hydrogen with less-energy consumption”. *Journal of Energy Chemistry* 50 (2020). DOI: 10.1016/j.jechem.2020.03.050 (cit. on pp. 2, 20, 56, 74, 89, 112).

[Li2020b] M. Li, X. Deng, K. Xiang, Y. Liang, B. Zhao, J. Hao, J.-L. Luo, and X.-Z. Fu. “Value-Added Formate Production from Selective Methanol Oxidation as Anodic Reaction to Enhance Electrochemical Hydrogen Cogeneration”. *ChemSusChem* 13.5 (2020). DOI: 10.1002/cssc.201902921 (cit. on pp. 2, 25, 29, 56, 74, 89).

[Li2020c] R. Li, J. Xu, R. Zeng, Q. Pan, T. Tang, and W. Luo. “Halides-assisted electrochemical synthesis of Cu/Cu2O/CuO core-shell electrocatalyst for oxygen evolution reaction”. *Journal of Power Sources* 457 (2020). DOI: 10.1016/j.jpowsour.2020.228058 (cit. on p. 64).

[Li2024] J. Li, H. Yu, J. Na, S. Jia, Y. Zhao, K. Lv, W. Zhang, J. Chi, and Z. Shao. “Recent advances in selective methanol oxidation electrocatalysts for the co-production of hydrogen and value-added formate”. *Catalysis Science & Technology* 14.19 (2024). DOI: 10.1039/D4CY00727A (cit. on p. 25).

[Liu2006] H. Liu, C. Song, L. Zhang, J. Zhang, H. Wang, and D. P. Wilkinson. “A review of anode catalysis in the direct methanol fuel cell”. *Journal of Power Sources* 155.2 (2006). DOI: 10.1016/j.jpowsour.2006.01.030 (cit. on pp. 24, 32).

[Luna2019] P. de Luna, C. Hahn, D. Higgins, S. A. Jaffer, T. F. Jaramillo, and E. H. Sargent. “What would it take for renewably powered electrosynthesis to displace petrochemical processes?” *Science (New York, N.Y.)* 364.6438 (2019). DOI: 10.1126/science.aav3506 (cit. on pp. 1, 18, 21, 22).

[Lund2001] H. Lund and O. Hammerich. *Organic electrochemistry*. 4. ed., rev. and expanded. New York, NY: Marcel Dekker, 2001 (cit. on p. 99).

[Luo2018] T. Luo, S. Abdu, and M. Wessling. “Selectivity of ion exchange membranes: A review”. *Journal of Membrane Science* 555 (2018). DOI: 10.1016/j.memsci.2018.03.051 (cit. on p. 9).

[Lyon2010] S. B. Lyon. “Corrosion of Noble Metals*”. In*Shreir’s Corrosion*. Elsevier, 2010. Pp. 2205–2223. (Cit. on pp. 43, 44).

[Mahm2018] N. Mahmood, Y. Yao, J.-.-W. Zhang, L. Pan, X. Zhang, and J.-.-J. Zou. “Electrocatalysts for Hydrogen Evolution in Alkaline Electrolytes: Mechanisms, Challenges, and Prospective Solutions”. *Ad-*

vanced Science 5.2 (2018). DOI: 10.1002/advs.201700464 (cit. on p. 21).

[Malj2020] S. Maljuric, W. Jud, C. O. Kappe, and D. Cantillo. “Translating batch electrochemistry to single-pass continuous flow conditions: an organic chemist’s guide”. *Journal of Flow Chemistry* 10.1 (2020). DOI: 10.1007/s41981-019-00050-z (cit. on p. 98).

[Mart2008] A. L. Martins, B. C. Batista, E. Sitta, and H. Varela. “Oscillatory instabilities during the electrocatalytic oxidation of methanol on platinum”. *Journal of the Brazilian Chemical Society* 19.4 (2008). DOI: 10.1590/S0103-50532008000400011 (cit. on p. 45).

[Mell2018] G. B. Melle, F. W. Hartl, H. Varela, and E. Sitta. “The effect of solution pH on the oscillatory electro-oxidation of methanol”. *Journal of Electroanalytical Chemistry* 826 (2018). DOI: 10.1016/j.jelechem.2018.08.033 (cit. on p. 45).

[Meye1972] D. Meyerstein, F. M. Hawkridge, and T. Kuwana. “On the spectroelectrochemical characterization of the electrocatalytic oxidation of Cu(II) ethylenediamine”. *Journal of Electroanalytical Chemistry and Interfacial Electrochemistry* 40.2 (1972). DOI: 10.1016/S0022-0728(72)80382-6 (cit. on p. 76).

[Mile1937] H. A. Miley. “Copper Oxide Films”. *Journal of the American Chemical Society* 59.12 (1937). DOI: 10.1021/ja01291a043 (cit. on p. 68).

[Mint1963] M. S. Mintz. “Electrodialysis - Principles of process design”. *Industrial & Engineering Chemistry* 55.6 (1963). DOI: 10.1021/ie50642a003 (cit. on p. 99).

[Möhl2018] S. Möhle, M. Zirbes, E. Rodrigo, T. Gieshoff, A. Wiebe, and S. R. Waldvogel. “Modern electrochemical aspects for the synthesis of value-added organic products”. *Angewandte Chemie International Edition* 57.21 (2018). (Cit. on p. 98).

[Mom2019] R. Mom, L. Frevel, J.-J. Velasco-Vélez, M. Plodinec, A. Knop-Gericke, and R. Schlögl. “The Oxidation of Platinum under Wet Conditions Observed by Electrochemical X-ray Photoelectron Spectroscopy”. *Journal of the American Chemical Society* 141.16 (2019). DOI: 10.1021/jacs.8b12284 (cit. on p. 41).

[Na2019] J. Na, B. Seo, J. Kim, C. W. Lee, H. Lee, Y. J. Hwang, B. K. Min, D. K. Lee, H.-S. Oh, and U. Lee. “General technoeconomic analysis for electrochemical coproduction coupling carbon dioxide reduction with organic oxidation”. *Nature communications* 10.1 (2019). DOI: 10.1038/s41467-019-12744-y (cit. on pp. 1, 2, 32, 56).

[Nebu2007] V. Neburchilov, J. Martin, H. Wang, and J. Zhang. “A review of polymer electrolyte membranes for direct methanol fuel cells”. *Journal of Power Sources* 169.2 (2007). DOI: 10.1016/j.jpowsour.2007.03.044 (cit. on p. 50).

[Nich2020] T. P. Nicholls, C. Schotten, and C. E. Willans. “Electrochemistry in continuous systems”. *Current Opinion in Green and Sustainable Chemistry* 26 (2020). DOI: 10.1016/j.cogsc.2020.100355 (cit. on p. 98).

[Noël2019] T. Noël, Y. Cao, and G. Laudadio. “The Fundamentals Behind the Use of Flow Reactors in Electrochemistry”. *Accounts of chemical research* 52.10 (2019). DOI: 10.1021/acs.accounts.9b00412 (cit. on p. 98).

[Oene2021] S. Z. Oener, L. P. Twight, G. A. Lindquist, and S. W. Boettcher. “Thin Cation-Exchange Layers Enable High-Current-Density Bipolar Membrane Electrolyzers via Improved Water Transport”. *ACS Energy Letters* 6.1 (2021). DOI: 10.1021/acsenergylett.0c02078 (cit. on p. 92).

[Olah2018] G. A. Olah, A. Goeppert, and G. K. S. Prakash. *Beyond oil and gas: The methanol economy*. 3rd ed. Weinheim: Wiley-VCH, 2018, pp. 205–210 (cit. on pp. 20, 32).

[Ota1984] K.-i. Ota, Y. Nakagawa, and M. Takahashi. “Reaction products of anodic oxidation of methanol in sulfuric acid solution”. *Journal of Electroanalytical Chemistry* 179.1-2 (1984). DOI: 10.1016/0368-1874(84)87017-3 (cit. on pp. 2, 20, 25, 26, 28, 32, 33, 43, 52).

[Oxle1964] J. E. Oxley, G. K. Johnson, and B. T. Buzalski. “The anodic oxidation of methanol: Open-circuit transient reactions”. *Electrochimica Acta* 9.7 (1964). DOI: 10.1016/0013-4686(64)85040-4 (cit. on p. 46).

[Pare2013] S. Parez, G. Guevara-Carrion, H. Hasse, and J. Vrabec. “Mutual diffusion in the ternary mixture of water + methanol + ethanol and its binary subsystems”. *Physical chemistry chemical physics : PCCP* 15.11 (2013). DOI: 10.1039/c3cp43785j (cit. on p. 79).

[Pärn2021] R. Pärnamäe, S. Mareev, V. Nikonenko, S. Melnikov, N. Sheldeshov, V. Zabolotskii, H. Hamelers, and M. Tedesco. “Bipolar membranes: A review on principles, latest developments, and applications”. *Journal of Membrane Science* 617 (2021). DOI: 10.1016/j.memsci.2020.118538 (cit. on pp. 90, 92).

[Pére2020] E. Pérez-Gallent, C. Sánchez-Martínez, L. F. G. Geers, S. Turk, R. Latsuzbaia, and E. L. V. Goetheer. “Overcoming Mass Transport Limitations in Electrochemical Reactors with a Pulsating Flow Electrolyzer”. *Industrial & Engineering Chemistry Research* 59.13 (2020). DOI: 10.1021/acs.iecr.9b06925 (cit. on p. 79).

[Perr2019] S. C. Perry, D. Pangotra, L. Vieira, L.-I. Csepei, V. Sieber, L. Wang, C. Ponce de León, and F. C. Walsh. “Electrochemical synthesis of hydrogen peroxide from water and oxygen”. *Nature Reviews Chemistry* 3.7 (2019). (Cit. on p. 98).

[Perr2020] S. C. Perry, C. Ponce de León, and F. C. Walsh. “Review—The Design, Performance and Continuing Development of Electrochemical Reactors for Clean Electrosynthesis”. *Journal of The Electrochemical Society* 167.15 (2020). DOI: 10.1149/1945-7111/abc58e (cit. on p. 98).

[Petr2021] S. Petrovic. *Electrochemistry Crash Course for Engineers*. Cham: Springer International Publishing, 2021. DOI: 10.1007/978-3-030-61562-8 (cit. on p. 9).

[Phan2024] V. T. T. Phan, Q. P. Nguyen, B. Wang, and I. J. Burgess. “Oxygen Vacancies Alter Methanol Oxidation Pathways on NiOOH”. *Journal of the American Chemical Society* 146.7 (2024). DOI: 10.1021/jacs.3c13222 (cit. on pp. 30, 76).

[Ping2020] J. M. Pingarrón, J. Labuda, J. Barek, C. M. A. Brett, M. F. Camões, M. Fojta, and D. B. Hibbert. “Terminology of electrochemical methods of analysis (IUPAC Recommendations 2019)”. *Pure and Applied Chemistry* 92.4 (2020). DOI: 10.1515/pac-2018-0109 (cit. on p. 9).

[Plet1993] D. Pletcher and F. C. Walsh. “Industrial Electrochemistry”. (1993). DOI: 10.1007/978-94-011-2154-5 (cit. on pp. 8, 99).

[Plet2018] D. Pletcher, R. A. Green, and R. C. D. Brown. “Flow Electrolysis Cells for the Synthetic Organic Chemistry Laboratory”. *Chemical reviews* 118.9 (2018). DOI: 10.1021/acs.chemrev.7b00360 (cit. on pp. 98, 117).

[Poll2020] D. Pollok and S. R. Waldvogel. “Electro-organic synthesis - a 21st century technique”. *Chemical science* 11.46 (2020). DOI: 10.1039/d0sc01848a (cit. on p. 22).

[Port2022] H.-O. Portner, D. Roberts, C. Trisos, and N. Simpson. “Summary for Policymakers: Climate Change 2022: Impacts, Adaptation, and Vulnerability. Contribution of Working Group II to the Sixth Assessment Report of the Intergovernmental Panel on Climate Change”. (2022). DOI: 10.1017/9781009325844.001 (cit. on p. 1).

[Quen2023] M. Quentmeier, B. Schmid, H. Tempel, H. Kungl, and R.-A. Eichel. “Toward a Stackable CO 2 -to-CO Electrolyzer Cell DesignImpact of Media Flow Optimization”. *ACS Sustainable Chemistry & Engineering* 11.2 (2023). DOI: 10.1021/acssuschemeng.2c05539 (cit. on p. 98).

[Raki1999] M. Rakib, P. Mocoteguy, P. Viers, E. Petit, and G. Durand. “Behaviour of Nafionő 350 membrane in sodium sulfate electrochemical splitting: continuous process modelling and pilot scale tests”. *Journal of Applied Electrochemistry* 29 (1999). (Cit. on p. 99).

[Ramd2019] M. Ramdin, A. R. T. Morrison, M. de Groen, R. van Haperen, R. de Kler, E. Irtem, A. T. Laitinen, L. J. P. van den Broeke, T. Breugelmans, J. P. M. Trusler, W. de Jong, and T. J. H. Vlugt. “High-Pressure Electrochemical Reduction of CO2 to Formic Acid/Formate: Effect of pH on the Downstream Separation Process and Economics”. *Industrial & Engineering Chemistry Research* 58.51 (2019). DOI: 10.1021/acs.iecr.9b03970 (cit. on p. 56).

[Regn2024] M. Regnier, C. Vega, D. I. Ioannou, and T. Noël. “Enhancing electrochemical reactions in organic synthesis: the impact of flow chemistry”. *Chemical Society reviews* 53.21 (2024). DOI: 10.1039/d4cs00539b (cit. on p. 98).

[Reus2010] G. Reuss, W. Disteldorf, A. O. Gamer, and A. Hilt. “Formaldehyde”. In*Ullmann’s encyclopedia of industrial chemistry*. Vol. 19. Chichester: Wiley, 2010. Pp. 1–34. (Cit. on pp. 2, 32).

[Riss2020] J. Rissman et al. “Technologies and policies to decarbonize global industry: Review and assessment of mitigation drivers through 2070”. *Applied Energy* 266 (2020). DOI: 10.1016/j.apenergy.2020.114848 (cit. on p. 1).

[Rive2015] F. F. Rivera, C. P. de León, J. L. Nava, and F. C. Walsh. “The filter-press FM01-LC laboratory flow reactor and its applications”. *Electrochimica Acta* 163 (2015). DOI: 10.1016/j.electacta.2015.02.179 (cit. on p. 98).

[Sako2017] S. Sakong and A. GroSS. “Methanol Oxidation on Pt(111) from First-Principles in Heterogeneous and Electrocatalysis”. *Electrocatalysis* 8.6 (2017). DOI: 10.1007/s12678-017-0370-1 (cit. on pp. 27, 48).

[Sass2023] M. Sassenburg, M. Kelly, S. Subramanian, W. A. Smith, and T. Burdyny. “Zero-Gap Electrochemical CO2 Reduction Cells: Challenges and Operational Strategies for Prevention of Salt Precipitation”. *ACS energy letters* 8.1 (2023). DOI: 10.1021/acsenergylett.2c01885 (cit. on p. 91).

[Schm2004] V. M. Schmidt. *Elektrochemische Verfahrenstechnik: Grundlagen, Reaktionstechnik, ProzeSSoptimierung*. Weinheim: Wiley-VCH, 2004. DOI: 10.1002/3527602143 (cit. on pp. 7, 8, 12, 13).

[Scho2020] C. Schotten, T. P. Nicholls, R. A. Bourne, N. Kapur, B. N. Nguyen, and C. E. Willans. “Making electrochemistry easily accessible to the synthetic chemist”. *Green Chemistry* 22.11 (2020). DOI: 10.1039/D0GC01247E (cit. on p. 14).

[Schw2024] F. Schwarz, E. Larenz, and A. K. Mechler. “Sustainable electrochemical synthesis of dry formaldehyde from anhydrous methanol”. *Green Chemistry* (2024). DOI: 10.1039/D3GC04978G (cit. on pp. 25, 112, 124).

[Seeb2015] R. Seeber, C. Zanardi, and G. Inzelt. “Links between electrochemical thermodynamics and kinetics”. *ChemTexts* 1.4 (2015). DOI: 10.1007/s40828-015-0018-9 (cit. on p. 9).

[Seze2025] N. Sezer, S. Bayhan, U. Fesli, and A. Sanfilippo. “A comprehensive review of the state-of-the-art of proton exchange membrane water electrolysis”. *Materials Science for Energy Technologies* 8 (2025). DOI: 10.1016/j.mset.2024.07.006 (cit. on pp. 19–21).

[Shih2022] A. J. Shih, M. C. O. Monteiro, F. Dattila, D. Pavesi, M. Philips, A. H. M. Da Silva, R. E. Vos, K. Ojha, S. Park, O. van der Heijden, G. Marcandalli, A. Goyal, M. Villalba, X. Chen, G. T. K. K. Gunasooriya, I. McCrum, R. Mom, N. López, and M. T. M. Koper. “Water electrolysis”. *Nature Reviews Methods Primers* 2.1 (2022). DOI: 10.1038/s43586-022-00164-0 (cit. on pp. 1, 21).

[Shin2023] H. Shin, S. Lee, and Y.-E. Sung. “Industrial-scale H2O2 electrosynthesis in practical electrochemical cell systems”. *Current Opinion in Electrochemistry* 38 (2023). (Cit. on p. 98).

[Siri2022] B. Siritanaratkul, M. Forster, F. Greenwell, P. K. Sharma, E. H. Yu, and A. J. Cowan. “Zero-Gap Bipolar Membrane Electrolyzer for Carbon Dioxide Reduction Using Acid-Tolerant Molecular Electrocatalysts”. *Journal of the American Chemical Society* 144.17 (2022). DOI: 10.1021/jacs.1c13024 (cit. on p. 89).

[Sitt2008] E. Sitta and H. Varela. “On the open-circuit interaction between methanol and oxidized platinum electrodes”. *Journal of Solid State Electrochemistry* 12.5 (2008). DOI: 10.1007/s10008-007-0349-6 (cit. on pp. 46, 48).

[Solb2023] S. B. Solberg, P. Zimmermann, Ø. Wilhelmsen, R. Bock, and O. S. Burheim. “Analytical treatment of ion-exchange permselectivity and transport number measurements for high accuracy”. *Journal of Membrane Science* 685 (2023). DOI: 10.1016/j.memsci.2023.121904 (cit. on p. 92).

[Tanb2020] N. Tanbouza, T. Ollevier, and K. Lam. “Bridging Lab and Industry with Flow Electrochemistry”. *iScience* 23.11 (2020). DOI: 10.1016/j.isci.2020.101720 (cit. on p. 98).

[This2024] N. Thissen, J. Hoffmann, S. Tigges, D. A. M. Vogel, J. J. Thoede, S. Khan, N. Schmitt, S. Heumann, B. J. M. Etzold, and A. K. Mechler. “Industrially Relevant Conditions in Lab–Scale Analysis for Alkaline Water Electrolysis”. *ChemElectroChem* 11.1 (2024). DOI: 10.1002/celc.202300432 (cit. on pp. 2, 98).

[Vass2021] Á. Vass, B. Endrdi, and C. Janáky. “Coupling electrochemical carbon dioxide conversion with value-added anode processes: An emerging paradigm”. *Current Opinion in Electrochemistry* 25 (2021). DOI: 10.1016/j.coelec.2020.08.003 (cit. on pp. 1, 2, 18–23, 32).

[Vehr2023] J. Vehrenberg, J. Baessler, A. Decker, R. Keller, and M. Wessling. “Paired Electrochemical Synthesis of Formate Via Oxidation of Glycerol and Reduction of Co2 in a Flow Cell Reactor”. (2023). DOI: 10.2139/ssrn.4423290 (cit. on pp. 2, 20).

[Venn2019] J.-B. Vennekoetter, R. Sengpiel, and M. Wessling. “Beyond the catalyst: How electrode and reactor design determine the product spectrum during electrochemical CO2 reduction”. *Chemical Engineering Journal* 364 (2019). DOI: 10.1016/j.cej.2019.01.045 (cit. on p. 98).

[Verm2019] S. Verma, S. Lu, and P. J. A. Kenis. “Co-electrolysis of CO2 and glycerol as a pathway to carbon chemicals with improved technoeconomics due to low electricity consumption”. *Nature Energy* 4 (2019). DOI: 10.1038/s41560-019-0374-6 (cit. on pp. 2, 20, 23).

[Viel2003] W. Vielstich, A. Lamm, and H. Gasteiger, eds. *Handbook of Fuel Cells – Fundamentals, Technology and Applications*. Wiley, 2003 (cit. on p. 24).

[Viel2014] W. Vielstich. “CO, Formic Acid, and Methanol Oxidation in Acid Electrolytes–Mechanisms and Electrocatalysis”. In*Encyclopedia of Electrochemistry*. John Wiley & Sons Ltd, 2014. Pp. 466–511. (Cit. on p. 45).

[Wals2018] F. C. Walsh and C. Ponce de León. “Progress in electrochemical flow reactors for laboratory and pilot scale processing”. *Electrochimica Acta* 280 (2018). DOI: 10.1016/j.electacta.2018.05.027 (cit. on pp. 28, 79).

[Wals2019] F. C. Walsh, L. F. Arenas, and C. Ponce de León. “Developments in plane parallel flow channel cells”. *Current Opinion in Electrochemistry* 16 (2019). DOI: 10.1016/j.coelec.2019.02.006 (cit. on p. 98).

[Wang2020] J. Wang, Y. Gao, H. Kong, J. Kim, S. Choi, F. Ciucci, Y. Hao, S. Yang, Z. Shao, and J. Lim. “Non-precious-metal catalysts for alkaline water electrolysis: operando characterizations, theoretical calculations, and recent advances”. *Chemical Society reviews* 49.24 (2020). DOI: 10.1039/d0cs00575d (cit. on pp. 74, 91).

[Wang2021] S. Wang, A. Lu, and C.-J. Zhong. “Hydrogen production from water electrolysis: role of catalysts”. *Nano convergence* 8.1 (2021). DOI: 10.1186/s40580-021-00254-x (cit. on p. 19).

[Wang2023] Y. Wang, M. Xu, X. Wang, R. Ge, Y.-Q. Zhu, A.-Z. Li, H. Zhou, F. Chen, L. Zheng, and H. Duan. “Unraveling the potential-dependent structure evolution in CuO for electrocatalytic biomass valorization”. *Science bulletin* 68.23 (2023). DOI: 10.1016/j.scib.2023.09.033 (cit. on p. 30).

[Wasm1999] S. Wasmus and A. Küver. “Methanol oxidation and direct methanol fuel cells: a selective review”. *Journal of Electroanalytical Chemistry* 461.1-2 (1999). DOI: 10.1016/S0022-0728(98)00197-1 (cit. on pp. 24, 32).

[Wei2021] X. Wei, Y. Li, L. Chen, and J. Shi. “Formic Acid Electro-Synthesis by Concurrent Cathodic CO2 Reduction and Anodic CH3OH Oxidation”. *Angewandte Chemie International Edition* 60.6 (2021). DOI: 10.1002/anie.202012066 (cit. on pp. 2, 20, 23, 25, 29, 56, 74, 76, 113).

[Wels1990] B. Wels and D. C. Johnson. “Electrocatalysis of Anodic Oxygen Transfer Reactions: Oxidation of Cyanide at Electrodeposited Copper Oxide Electrodes in Alkaline Media”. *Journal of The Electrochemical Society* 137.9 (1990). DOI: 10.1149/1.2087072 (cit. on pp. 30, 76).

[Wrob2023] M. Wrobel, S. Kriescher, T. Schiffer, R. Keller, and M. Wessling. “On the weeping of the GDE cathode during bipolar membrane-based electrochemical CO2 reduction reaction at high current densities”. *Chemical Engineering Journal* 474 (2023). DOI: 10.1016/j.cej.2023.145335 (cit. on p. 89).

[Wu2021] D. Wu, J. Hao, Z. Song, X.-Z. Fu, and J.-L. Luo. “All roads lead to Rome: An energy-saving integrated electrocatalytic CO2 reduction system for concurrent value-added formate production”. *Chemical Engineering Journal* 412 (2021). DOI: 10.1016/j.cej.2020.127893 (cit. on pp. 2, 20, 29, 56, 74).

[Wynd2021] J. Wyndorps, H. Ostovari, and N. von der Assen. “Is electrochemical CO2 reduction the future technology for power-to-chemicals? An environmental comparison with H2-based pathways”. *Sustainable Energy & Fuels* 5.22 (2021). DOI: 10.1039/D1SE00975C (cit. on pp. 1, 18, 21).

[Xi2024] W. Xi, P. Yang, M. Jiang, X. Wang, H. Zhou, J. Duan, M. Ratova, and D. Wu. “Electrochemical CO2 reduction coupled with alternative oxidation reactions: Electrocatalysts, electrolytes, and electrolyzers”. *Applied Catalysis B: Environmental* 341 (2024). DOI: 10.1016/j.apcatb.2023.123291 (cit. on pp. 22, 23).

[Xian2020] K. Xiang, D. Wu, X. Deng, M. Li, S. Chen, P. Hao, X. Guo, J.-.-L. Luo, and X.-.-Z. Fu. “Boosting H 2 Generation Coupled with Selective Oxidation of Methanol into Value–Added Chemical over Cobalt Hydroxide@Hydroxysulfide Nanosheets Electrocatalysts”. *Advanced Functional Materials* 30.10 (2020). DOI: 10.1002/adfm.201909610 (cit. on pp. 2, 20, 23, 25, 29, 56, 74, 89).

[Xian2021] K. Xiang, Z. Song, D. Wu, X. Deng, X. Wang, W. You, Z. Peng, L. Wang, J.-L. Luo, and X.-Z. Fu. “Bifunctional $PtCo_3O_4$ electrocatalysts for simultaneous generation of hydrogen and formate via energy-saving alkaline seawater/methanol co-electrolysis”. *Journal of Materials Chemistry A* 9.10 (2021). DOI: 10.1039/D0TA10501E (cit. on pp. 2, 56, 89, 112).

[Xie1995] G. Xie and T. Okada. “Water Transport Behavior in Nafion 117 Membranes”. *Journal of The Electrochemical Society* 142.9 (1995). DOI: 10.1149/1.2048686 (cit. on p. 92).

[Xie2022] K. Xie, R. K. Miao, A. Ozden, S. Liu, Z. Chen, C.-T. Dinh, J. E. Huang, Q. Xu, C. M. Gabardo, G. Lee, J. P. Edwards, C. P. O’Brien, S. W. Boettcher, D. Sinton, and E. H. Sargent. “Bipolar membrane electrolyzers enable high single-pass CO2 electroreduction to mul-

ticarbon products". *Nature communications* 13.1 (2022). DOI: 10.1038/s41467-022-31295-3 (cit. on p. 89).

[Xu2019] Y. Xu and B. Zhang. "Recent Advances in Electrochemical Hydrogen Production from Water Assisted by Alternative Oxidation Reactions". *ChemElectroChem* 6.13 (2019). DOI: 10.1002/celc.201900675 (cit. on pp. 1, 2, 22, 23).

[Xue2024] H. Xue, Z.-H. Zhao, M. Yuan, and G. Zhang. "Microfluidic reactors for paired electrosynthesis: Fundamentals, applications and future prospects". *Green Energy & Environment* (2024). DOI: 10.1016/j.gee.2024.06.006 (cit. on p. 22).

[Yeo2024] J. Yeo, J. Ho Jang, Y. in Jo, J. Woo Koo, and K. Tae Nam. "Paired Electrosynthesis of Formaldehyde Derivatives from CO2 Reduction and Methanol Oxidation". *Angewandte Chemie (International ed. in English)* 63.2 (2024). DOI: 10.1002/anie.202316020 (cit. on pp. 23, 25).

[You2016] B. You, X. Liu, N. Jiang, and Y. Sun. "A General Strategy for Decoupled Hydrogen Production from Water Splitting by Integrating Oxidative Biomass Valorization". *Journal of the American Chemical Society* 138.41 (2016). DOI: 10.1021/jacs.6b07127 (cit. on p. 23).

[Yuan2018] L. Yuan, M. Li, T. Yuan, Y. Fang, and W. Wang. "In operando imaging of self-catalyzed formaldehyde burst in methanol oxidation reactions under open circuit conditions". *Chemical Science* 9.13 (2018). DOI: 10.1039/c7sc05347a (cit. on pp. 25, 48, 124).

[Zhan2018] B. Zhang, G. Yang, C. Li, K. Huang, J. Wu, S. Hao, and Y. Huang. "Electrochemical behaviors of hierarchical copper nano-dendrites in alkaline media". *Nano Research* 11.8 (2018). DOI: 10.1007/s12274-018-2010-3 (cit. on p. 72).

[Zhao2007] T. Zhao, K.-D. Kreuer, and T. van Nguyen. *Advances in fuel cells*. Amsterdam, San Diego, CA, and Oxford: Elsevier, 2007, pp. 187–226 (cit. on pp. 50, 51).

[Zhou2023] H. Zhou, Y. Ren, B. Yao, Z. Li, M. Xu, L. Ma, X. Kong, L. Zheng, M. Shao, and H. Duan. "Scalable electrosynthesis of commodity chemicals from biomass by suppressing non-Faradaic transforma-

tions". *Nature communications* 14.1 (2023). DOI: 10.1038/s41467-023-41497-y (cit. on p. 2).

[Zlot2017] A. Zlotorowicz, R. V. Strand, O. S. Burheim, Ø. Wilhelmsen, and S. Kjelstrup. "The permselectivity and water transference number of ion exchange membranes in reverse electrodialysis". *Journal of Membrane Science* 523 (2017). DOI: 10.1016/j.memsci.2016.10.003 (cit. on p. 92).

[Zosk2007] C. G. Zoski. *Handbook of electrochemistry*. Amsterdam: Elsevier, 2007 (cit. on p. 10).